Paleogeography and 3D variability of a dynamically uplifted shelf: observations from seismic stratigraphy of the Paleocene East Shetland Platform

Lucas Valore[1], Tor Sømme[12], Stefano Patruno[3], Cecile Robin[4], François Guillocheau[4], Christian Eide[1]

1 – Department of Earth Science, University of Bergen, Bergen, Norway

2 – Equinor ASA, Oslo, Norway

3 – Department of Engineering, School of Sciences and Engineering, University of Nicosia, Nicosia, Cyprus

4 – Géosciences Rennes, Université de Rennes 1, Rennes, France

* Corresponding author: lucas.valore@uib.no, Realfagbygget, Allégaten 41, Postboks 7803, 5020 Bergen, Norway

keywords: Dynamic topography, PETM, along-strike variability, seismic geomorphology

Abstract

In the Paleocene North Sea, pulses in turbidite fan deposition and shelfal progradation have been correlated to episodes of regional uplift caused by a precursor of the Icelandic Plume. However, in the East Shetland Platform, the specific impacts of dynamic uplift on the regional paleogeographic evolution are less understood. Using new, high resolution 3D seismic data from an underexplored proximal area, we investigate the paleogeography of the East Shetland Platform in terms of the extent and timing of erosion *vs* deposition, focusing on how these can be used to reconstruct changes in relative sea-level along-strike. Using a combination of well data, clinoform-based seismic stratigraphy and seismic attribute analysis of >60 000 km² of 3D data, we have devised paleogeographic maps of multiple Paleocene to Early Eocene units, with high temporal resolution for the Late Paleocene – Early Eocene Moray Group. This includes six unconformity-bounded units marked by prograding clinoforms of the Dornoch Formation, which are covered by backstepping sequences of the Beauly Member (Balder Formation). Temporal and spatial changes in the distribution of downdip depocenters and updip unconformities indicate strong lateral variability in patterns of shelf accommodation/erosion and local sediment supply. This results from a complex interplay between laterally-uneven RSL fall, inherited topography, time-varied sediment entry point distribution and along-shore sediment transport regimes. Unconformities and paleogeographic maps suggest a first-order control on erosion and sediment distribution promoted by the transiently and differentially uplifted topography of Shetland, which is characterized by an anomalous erosive history in the Bressay High in the center of our study area, where the Lower Dornoch Formation has been eroded and marked fluvial incision is observed. Ultimately, results indicate shorter-wavelength and shorter-period variations in uplift than what is typically assumed for dynamic topography, perhaps as a result of additional modulation by lithospheric structures or influence of previous rift-related faults.

1. Introduction

Sequence and seismic stratigraphy have become increasingly powerful tools for the reconstruction of source-to-sink sedimentation dynamics in recent years. Notably, sequence and seismic stratigraphy have been used to investigate source-area dynamics in systems affected by mantle-related uplift/subsidence ("dynamic topography"), providing constraints for timing and magnitude of uplift, tectonic tilting, sediment fluxes and paleogeographic reorganization (Baby et al., 2018, 2020; Sømme et al., 2019; 2023). Dynamic topography anomalies have been commonly modelled as long-wavelength (~10^4 km) perturbations with "dome-like" uplift functions, especially in the ancient geological past (Jones and White, 2003; Barnett-Moore et al., 2017). These theoretically result in correspondingly large-scale and long-term surface and stratigraphic responses (Friedrich et al. 2018; Krob et al., 2020). However, evidence of fast transient uplift in plume-affected areas (Al-Hajri et al., 2009; Hartley et al., 2011) as well as shorter wavelength dynamic topography (Burov and Guillou-Frottier, 2005; Burov and Gerya, 2014; Hoggard et al., 2016) has shown that surface and stratigraphic responses are

likely more complex than what traditionally suggested (Petersen et al., 2010; Arnoud et al., 2018; Ding et al., 2019). Concomitantly, 3D sequence stratigraphic studies of both modern and ancient coastal environments have shown that variability in along-strike sequence stratigraphy can be commonplace (Martinsen and Helland-Hansen, 1995; Chiarella et al., 2019; Zecchin and Catuneanu, 2020). Lateral variability in coastal systems can be tied to the differential development of progradation/retrogradation and erosion/aggradation due to local effects of supply, sediment transport dynamics, accommodation and overall autogenic parameters. Critically, the prevalence of along-strike variability in plume affected shelf-margins is poorly constrained. These observations have important implications for source-to-sink reconstructions of dynamically uplifted areas and attempts to constrain plume signatures using the stratigraphic record. Furthermore, they indicate that both low-resolution/regional and high-resolution/local studies may fail to produce realistic models of mantle perturbations on surface processes, especially if not integrated in a cohesive paleogeographic framework.

Paleocene to Early Eocene deposits in the North Sea (Figures 1-3) include multiple episodes of shelfal to deep-water sand deposition, which have drawn attention due to their proposed connection to anomalous and episodic uplift events across the entire northwestern Europe (*e.g.* Knox, 1996; White and Lovell, 1997; Mudge and Jones, 2004; Patruno et al., 2022). These uplift events have been associated by many authors to fluctuations in dynamic topography caused by a precursor of the Icelandic Plume (White and McKenzie, 1989; White and Lovell, 1997; Nadin et al., 1997; Rainbird and Ernst, 2001), although some initial studies also discussed regular plate tectonics and eustasy as potential drivers for sedimentation (e.g., Stewart, 1987; Liu and Galloway, 1997; Mudge and Jones, 2004). Early Paleogene deposits in the North Sea have since proved favorable for investigations on the nature of dynamic topography/uplift and related source-to-sink responses, in particular due to the rare preservation of complete depositional profiles ranging from the aforementioned deep-water deposits to the buried erosional landscapes that potentially helped supply them (Underhill, 2001; Stucky de Quay et al., 2017; Stucky de Quay and Roberts, 2023; Conway-Jones and White, 2022). Additionally, superimposed on regional uplift, the most intense and distinguished *hyperthermal* of the pre-Holocene Cenozoic occurred - the Paleocene-Eocene Thermal Maximum or PETM (Jones et al., 2013). While it appears that this climatic event further modified sediment routing systems and sedimentation rates across the North Sea (Jin et al., 2022; Sømme et al., 2023), its contribution is still uncertain in Shetland.

Seismic and well-log stratigraphic studies have provided important observations on the paleogeography and development of unconformities, flooding surfaces and associated relative sea-level (RSL) curves during the Paleocene (Jones and Milton, 1994; Milton and Dyce, 1995; Neal, 1996; Mudge, 2015), laying the foundations for our current understanding of its stratigraphy (Figures 2, 3). Despite this, current paleogeographic reconstructions lack detailed insight into the clinoforms of the Late Paleocene, particularly in terms of the development of individual sequences and their depositional trends, the characteristics of proximal coastal environments and the distribution of unconformities (Figures 2, 3). Similarly, RSL curves derived from individual 2D sections in Shetland do not showcase the effects of along-strike variability,

something that may have strong impacts for reconstructions of external forcing parameters (*e.g.* uplift and subsidence).

Despite the large volumes of available data, reconstructions of the source-to-sink response of dynamic uplift in Shetland are currently hindered by an overall incomplete understanding of the area's paleogeographic evolution during the Paleocene. This particularly affects our comprehension of episodes of subaerial catchment/unconformity development (Figures 2 and 3) and their connections to traceable stratigraphic responses, such as sedimentation rate peaks and progradational pulses. In order to help insert these observations into a paleogeographic context, we provide a new seismic stratigraphic framework based on recently acquired, high-resolution 3D data covering proximal areas of the East Shetland Platform, combined with a review of existing bio- and lithostratigraphy. The goals of this paper are threefold: 1) create a unified stratigraphic framework for the Late Paleocene – Early Eocene of the ESP by integrating seismic interpretation in a total area of 250 x 370 km and analysis of 45 borehole datasets, 2) elucidate the paleogeographic evolution in the area by examining sedimentary environments in seismic and well data, investigating changing sediment routing systems along-strike 3) determine patterns of erosion throughout the Paleocene, exploring their influences on paleogeographic evolution and reconstructions of external forcing factors.

2. Geological setting

The North Sea is the offshore area between Scandinavia, the United Kingdom and Northwest Europe that hosts several subbasins with a complex geological history (e.g. Underhill and Richardson, 2022; Patruno et al. 2022). This started with the collapse of the Caledonian mountains during the Devonian, which controlled post-orogenic deposition across the modern-day North Atlantic (Fossen, 2010; Rotevatn et al., 2018). Broad continental rifting succeeded in the Late Permian - Early Triassic, following the structural framework inherited from the Caledonian deformation and resulting in a N-S oriented rift basin (Ziegler, 1992; Faerseth, 1996; Phillips et al., 2019). After an "inter-rift" phase of thermal doming in the Middle Jurassic, another extensional episode occurred in the Late Jurassic, responsible for focused tripartite faulting in the Viking, Witch Ground and Central grabens (Coward et al., 2003; Phillips et al., 2019; Figure 1B). After cessation of rifting during the Early Cretaceous, a 1-3 km thick post-rift succession accumulated, being punctuated by the final opening of the North Atlantic in the Paleogene (Mudge, 2015; Stoker et al., 2018).

The East Shetland Platform (Figure 1) behaved as a structural high during most of the Mesozoic, when rifting was focused on adjacent areas such as the Moray Firth Basin to the south, the East Shetland Basin to the north and the Viking Graben to the east (Platt and Cartwright, 1998; Ahmadi *et al*., 2003). Rift-related structures (in particular the Shetland Platform – Viking Graben boundary faults) are marked by steep slopes that are also observed in the post-rift succession (Figures 1A, 2), which appear to have further conditioned deposition during post-rift times (Mudge, 2015; Stoker et al., 2018).

During the Late Cretaceous, post-rift thermal subsidence was accompanied by widespread deposition of carbonate/chalk of the Chalk Group (Southern North Sea) and mudstones of the Shetland Group (Northern North Sea). During this "quiescent" tectonic setting, the present-day Shetland Platform was potentially completely flooded (Surlyk et al., 2003; Coward et al., 2003; Hall, 2021).

The Paleocene – Early Eocene succession

After the Cretaceous high relative sea-level, hinterland rejuvenation and siliciclastic input initiated in the Early Paleocene, possibly already during the Danian (Ahmadi et al., 2003). These have been widely attributed to plume-induced thermal doming and uplift in southern Greenland, southwestern Norway and the United Kingdom (White and Lovell, 1997; Coward et al., 2003; Shaw Champion et al., 2008). Conversely, a less explored cause for regional uplift would be rift-shoulder uplift during the North Atlantic opening (Anell et al., 2009; Mudge, 2015; Stoker et al., 2018; Foulger et al., 2020). Regardless of origin, uplift inverted the topography in proximal areas, promoting reworking of late Mesozoic deposits and intensified hinterland denudation (Shaw Champion et al., 2008; Wilkinson, 2017), followed by a debated amount of extensional subsidence in the North Sea and the Faroe-Shetland Basin (Fletcher et al., 2013; Mudge, 2015; Stoker et al., 2018; Foulger et al., 2020). This setting favored the deposition of the Montrose and Moray groups (Figures 2 - 3).

Deep-water channel and fan systems of the Montrose Group replaced previous chalk and carbonate deposition During the Early Paleocene (Danian to Selandian). Initial mass-wasting was potentially caused by gravitational instability across the North Sea (Ahmadi *et al*., 2003; Kilhams et al., 2015; Soutter et al., 2018). The basinal sandstones and shales of the Våle (T20 in BP scheme) and Lista (T30) formations were deposited in this scenario, and their proximal counterparts in East Shetland are now likely eroded (Figure 2).

The overlying Thanetian-Ypresian Moray Group includes marine and non-marine sediments deposited in a prominent episode of shelf progradation, better observed in the Outer Moray Firth, the East Shetland Platform and the East Shetland Basin (Figures 1 - 3). Although a relatively thick portion of sediments were trapped in the shelf (>200 m in UK well 9/12b-4), significant input of sediment (including sand) in basin-floor fans also occurred in the Forties, Hermod, Flugga, Teal and Skadan systems, which comprise important Paleocene reservoirs (Underhill and Richardson, 2022; Patruno et al., 2022). Shelfal deposition was accompanied by prominent base-level fall during the Dornoch progradation (Jones and Milton, 1994; Neal, 1996), punctuated by an Early Eocene flooding event (the boundary between T40 and T45 in Jones and Milton, 1994; Dixon and Pearce, 1995). This marks the maximum shallowing of the entire Paleocene-Early Eocene succession (Figure 2).

Base-level fall during the Dornoch progradation resulted in traceable, landward offlap advance and catchment erosion of older Lista deposits, with vertical incision of >300 m in areas such as the Bressay Channel (Underhill, 2001; Stucky de Quay et al., 2017). This fast episode of erosion has been correlated to a

simultaneous event at the Faroe-Shetland basin, widely attributed to a transient fluctuation in dynamic topography during the Paleocene-Eocene transition (Shaw Champion et al., 2008; Hartley et al., 2011). Shortly after, at ~55-53 Ma (Ypresian), volcanism and tectonic activity culminated in continental breakup in the Norwegian Sea and in the Faroe-Shetland Basin (Gernigon et al., 2012; Abdelmalak et al., 2016; Foulger et al., 2020). This was concomitant with the deposition of the Balder Formation, which includes subaerial and subaqueous ash-fallout deposits and reworked volcaniclastics (Mudge, 2015; Watson et al., 2017), as well as backstepping, shallow marine siliciclastic deposits developed on top of the Dornoch shelf (Knox and Holloway, 1992; Brunstad et al., 2013; Figures 2 and 3). Breakup and volcanic activity were followed by subsidence and RSL-rise, possibly enhanced by an Early Eocene eustatic highstand (Miller et al., 2005; 2020; Pujalte et al., 2014).

Paleocene-Eocene Thermal Maximum

Progradation of Dornoch Formation sediments partly occurred during the Paleocene-Eocene Thermal Maximum (PETM). Its origin has been ascribed to different processes, including greenhouse gas release promoted by magma-sediment interaction (Svensen et al., 2004; Berndt et al., 2023) or simply large-scale, explosive LIP volcanism (Gutjahr et al., 2017; Gernon et al., 2022). Discrete paleoenvironmental modifications associated to the PETM include increased global denudation and sedimentation rates (Dunkley Jones et al., 2018; Pogge von Strandmann et al., 2021; Vimpere et al., 2023). In the Forties turbidite system in the Central Graben, a five-fold increase in sediment supply has been attributed to the PETM (Jin et al., 2022), while equivalent deposits do not appear to include similar increases in the Norwegian North Sea, in the Horda Platform (Sømme et al., 2019). A two-to-tenfold increase in sediment flux is otherwise observed in the Froan Basin in the Norwegian Sea (Sømme et al., 2023), where the PETM also modified deep-water sediment distribution by promoting increased transport and bypass of mud in wide and erosive slope-channel complexes.

3. Methods

3.1 Seismic stratigraphic interpretation

Seismic interpretation was carried out using two high-resolution PGS Geostreamer surveys, one covering the East Shetland Platform in quadrants 8 and 9 (PGS15004) and one in the Bressay area, in quadrants 9 and 3 (PGS15010, Figure 1C). Deposits in the basinal Viking Graben were interpreted using the PGS Megamerge and CGG North Viking Graben surveys. Proximal areas of quadrants 7 and 8 were also interpreted using high-resolution 2D data acquired by PGS, available by the UK Oil and Gas Authority (Figure 1C). Total coverage of 3D data is around 160 x 370 km or 59200 km², with an additional 150 x 250 km proximal area covered with 2D data only. Acquisition and processing data for each of these surveys can be found in the Supplementary Material. Seismic interpretation itself was carried out using combinations of horizon picking

techniques, ranging from 3D autotracking to manual interpretation with no snapping, depending on the continuity of reflectors.

Late Paleocene to Early Eocene sedimentary units were initially divided based on the identification of stratal terminations (onlaps, offlaps, truncations and downlaps), patterns of stratal stacking and overall seismic facies characteristics. These are all useful for the recognition of unconformities (truncations), shifts in onlap/offlap and changes in clinoform geometries, which are in turn indicative of changes in accommodation/supply ratios (Catuneanu, 2019 and references therein). Clinoform and shoreline rollover trajectories can also be used to reconstruct depositional trends and relative sea-level curves after depth-conversion and decompaction (Helland-Hansen and Hampson, 2009). Here, we use overburden-removed sections to calculate rollover trajectories of key seismic transects. In the paper, we show these transects in two-way-time, while their decompacted equivalents and the parameters used for depth-conversion and decompaction can be found in the Supplementary Material.

3.2 Well-log interpretation and biostratigraphic ties

Queries were conducted to select around 60 wells with available biostratigraphic data in the study area. After quality control and revision of individual biostratigraphic reports, this was narrowed down to 45 wells (Figure 1B), which were used for biostratigraphic ties and stratigraphic interpretations. Utilized biostratigraphic datums (dinocysts and foraminifera) are summarized in Figure 3 and described in the Results chapter. Further explanations for the stratigraphic frameworks showcased in Figure 3 can be found in the supplementary material. Checkshot data and revised lithostratigraphic/chronostratigraphic picks were used in conjunction with measured or calculated velocity data for the construction of synthetic seismograms and calibration of well-seismic ties. Overall, differences between pre and post well-tie tops are small (<10-30 m).

3.3 Paleogeographic reconstruction

In the absence of a good coverage by cores in proximal settings, the distinction between gross depositional environments of each mapped unit was primarily based on seismic stratigraphy and geomorphology, which was complemented by well data and calibrated by other paleogeographic reconstructions, in particular the sequence-specific facies maps produced by TGS (FMB database). Seismic geomorphology was based on the assessment of several sedimentary geometries in attribute maps, extracted from multiple time-horizons and slices of each unit (Figures 4-6). We mapped in detail the areas corresponding to individual depositional environments and their characteristic seismic facies for each unit, cross-checking and referencing seismic lines in 3D to determine their extent. To avoid mixing closely stacked or overlying incisional features in the thinner portions of individual units, they were cropped at their minimum resolvable thickness thresholds, which are related to survey-dependent vertical resolutions and minimum reflector

thicknesses (~10 to 20 ms). Examples of the criteria used for interpretation and inferred modern analogues for sedimentary geometries and environments can be found in Figures 4 and 5.

4. Results - Seismic stratigraphic framework

The studied interval encompasses Danian to Ypresian sediments of the Montrose and Moray groups (Figure 2), which can be summarized as one largely "deeper-water" unit (Montrose Gp.) succeeded by one complete non-marine to basin-floor fan system (Moray Gp., Deegan and Scull, 1977). The latter allows for a greater number of paleogeographical inferences based on seismic stratigraphy and clinoform analysis, being the main focus of this study. In this section, we present overall stratigraphic and paleogeographic aspects of all our mapped units, including the defining characteristics of new subunits of the Moray Group and their correlation to previous stratigraphic schemes (Figures 2, 3).

4.1 Montrose Group

Våle Formation

Above the Intra-Danian Unconformity, incision is observed in prominent, km-wide channelized features, which are filled by Våle Formation deposits (Figure 7A). Våle Formation sediments are restricted in the platform, occurring as patches around channelized depositional systems, and being almost completely absent or eroded updip of the ESP-Viking Graben fault north of the Beryl transect area (Figures 7A, 8-11). Downdip in the Viking Graben, a seemingly conformable Cretaceous – Paleocene transition is observed. where the Våle Formation is marked by apparent aggradation and underfilling (Figures 10, 12). Depocenters are observed in the Beryl Embayment, in the central and southern Viking Graben and close to the Piper Shelf (Figure 7A).

In terms of depositional environments, larger channels observed in the East Shetland Platform are here interpreted to be submarine, consistent with core-data from the Mariner field area (Silcock et al., 2020) and their km-wide, sinuous configuration (Figure 6B), which differs considerably from narrower fluvial systems observed in the overlying Moray Group, for example (Figures 4A, 6A). This interpretation largely follows other paleogeographic reconstitutions for the time (Ahmadi et al., 2003, Mudge, 2015). Lastly, Våle Formation sediments have been shown to consist of a lower unit of reworked carbonate/chalk and an upper unit of predominant submarine sands (V1 and V2 units in Brunstad et al., 2013 and this paper, Figures 8-12).

Lista Formation

Sediments of the Lista Formation include thick (up to 600 ms in Figure 7B, or >500 m in Norwegian well 25/4-1) successions of slope/basin deposits, which can be considerably sandy (average of >30% sand in the Viking Graben in the wells in this study). Lista Formation sediments are well-distributed across the study area, but depocenters in the Dutch Bank Basin, the Viking Graben and northeast Bressay are noted (Figure

7B). These depocenter were formed where pre-existing depressions/basins and grabens were present, suggesting a pattern of relative basin underfill. Similarly to Våle, prominent and isolated submarine channels can be observed in the East Shetland Platform, while more dispersed channel-lobe systems are verified downdip in the Viking Graben (Figures 5C, 7B). This downdip change is also verified by the increase in injectite proportion to the east, where soft-sediment remobilization is ubiquitous, leading to chaotic to transparent seismic facies (*e.g.* Figures 5, 8). These facies hinder unambiguous seismic stratigraphic subdivision of Lista, and as such it was regionally mapped as a single unit in this unit.

Comparable observations of the Lista Formation have led authors to consider that the East Shetland Platform and Viking Graben correspond to slope and basin-floor areas, similarly to the Våle Formation (Ahmadi et al., 2003), essentially following the structural distinction between platform highs and basinal areas (*e.g.* the ESP and the Viking Graben). The real nature and gradient of the original depositional profile are difficult to constrain by seismic stratigraphy, however, and depositional environments of Lista were simply mapped in this work as undifferentiated slope/basin with channels and channel-lobe systems.

Correlation to other biostratigraphic and chronostratigraphic schemes

Although several subdivisions and sequences of the Montrose Group have been described in the literature (Figure 3), the available biostratigraphic framework and the obscuring effects of soft-sediment remobilization render systematic division challenging in the East Shetland Platform. In other studies, the most readily recognizable stratigraphic markers associated to the Montrose Group are (1) the "intra-Danian unconformity" (Mudge and Jones, 2004, Mudge 2015) which marks a gap between Late Cretaceous to Danian chalk/mudstones of the Shetland/Chalk Group and the Danian base of the Våle Fm.; (2) "the near-top Danian unconformity" (Mudge and Bujak 2001, Mudge and Jones 2004; Mudge, 2015), which divides the Våle Fm in a lower calciclastic member and an upper sandy member (Mudge and Jones, 2004, Brunstad et al., 2013; Mudge, 2015); (3) the "top Våle flooding surface", which overall marks the transition between Våle Formation sandstones and Lista Fm. shales (Mudge and Bujak, 2001; Mudge and Jones, 2004, Mudge, 2015) and (4) the "mid-Paleocene" or "top Selandian" unconformity in the middle of the Lista Formation, which in the ESP is evidenced by the reworking of dinocyst flora and marks the base of the heavily remobilized and injected Heimdal Member sandstones (Mudge and Jones, 2004; Brunstad et al., 2013; Mudge, 2015). Biostratigraphic markers for these surfaces can be seen in Figure 3. However, because these are often difficult to trace in seismic, only the base and top of the Våle Fm were mapped regionally in this study.

4.2 Moray Group

Dornoch Formation

In the ESP, Dornoch Formation sediments include stacked clinoforms sets developed conformably above the Montrose succession in the Late Paleocene (Figures 2, 8-12). In this study, the Dornoch Fm was

divided in six new subunits (D1-D6) based on the combined recognition of basinward shifts in offlap, truncated topsets and downstepping clinoform rollovers - in other words, five subaerial unconformities or sequence boundaries between them, which mark the end of forced regression (Van Wagoner et al., 1988; Hunt and Tucker, 1992; Helland-Hansen and Gjelberg, 1994). A regional distinction is summarized in Figures 2 and 3. However, significant lateral variability is observed in the expression of sequence stratigraphic surfaces and clinoform geometries, including in their rollover trajectories (Figure 13). This will be explained in detail in Section 5.

In general, Dornoch subunits are comprised by alternating normal regressive and forced regressive systems tracts, toe-of-clinoform fans (proximal) and basinal channel-lobe and turbidite fan systems, although their relative proportions vary significantly along strike and dip, with the complete absence of individual systems tracts in some areas (Figures 8-12, see further in Section 5). Importantly, Dornoch subunits were grouped into two major domains in this study. D1 and D2 both form a partially preserved, narrow highstand shelf (in lower-order/higher-rank sense, Figure 2) developed in the proximal part of Quadrant 8, which is only partially covered by 3D seismic (Figures 1C, 8-10). There is currently no well-data coverage for this highstand shelf. To the east, a distinct lowstand system comprised of D3 to D6 deposits is observed (Figures 2, 8-12). Both groups also include associated slope/basin, submarine channel-lobe and basin-floor/turbidite fan deposits. All further references to highstand and lowstand Dornoch pertain to this higher-rank division.

The Dornoch lowstand (D3-D6) includes delta-scale to shelf-edge-scale clinoforms that built out a new shelf after RSL fall from the D1-D2 highstand (Figures 8-10). We interpret a subaerial or transitional coastal plain/deltaic origin for most Dornoch lowstand topsets, as suggested in several paleogeographic reconstructions (Milton et al., 1990; Milton and Dyce, 1995; Dixon and Pearce, 1995; Underhill, 2001). Various incision features in this lowstand shelf have also been interpreted as fluvial based on data from cores (Underhill, 2001; Stucky de Quay et al, 2017; Figure 14), and coal beds or lignite traces are common throughout the Moray Group (Milton et al., 1990; Figure 14). These observations indicate that lowstand clinoforms rollovers are located in or near shorelines (Figure 8).

Balder Formation – Beauly Member

Balder Formation deposits include progradational clinoforms sets intercalated with thin transgressive tracts (B1-B3 subunits in this study), which are part of an overall backstepping succession (Figures 2, 8-9). Coastal depositional systems are all part of the Beauly Member (Knox and Holloway, 1992; Brunstad et al., 2013; Mudge, 2015). Distribution of clinoforms varies strongly along-strike within the Beauly Mbr., with relative thicknening towards the south of the study area where a progradational lowstand tract is observed (B1 LST, Figures 8, 16A). This progradational systems tract is covered by transgressive deposits (B2 TST) and widely distributed progradational highstand deposits (B2 HST, Figures 8, 16B). An additional transgressive unit is locally resolvable above the B2 highstand (B3 TST, Figure 8). Balder/Beauly deposits are condensed

to the north and to the east of the study areas, where internal units cannot be resolved. Some slope/basin-floor systems of the Odin Member are also recognized locally (Brunstad et al., 2013; Mudge, 2015). Finally, the Balder Fm. includes widespread ash fallout in various environments, responsible for distinct wireline and seismic responses (Brunstad et al., 2013).

Correlation to other biostratigraphic and chronostratigraphic schemes

In this study, the basal surface of Dornoch Formation differs in character from many well-based schemes that correlate it to an unconformity (Mudge and Bujak, 2001; Mudge and Jones, 2004; Mudge 2015), as it is actually interpreted as a conformable flooding/condensation surface observed between the early D1-D2 shelf and underlying Lista deposits (Figures 8-10). However, a marked erosional unconformity between Lista and later Dornoch - Beauly deposits is indeed observed **updip** in seismic data, and results in a complete gap from the Lista Fm to D5-B2 (T45-T50 equivalent) in areas such as the west of the Beryl and Bressay transects (Figures 10-11). This unconformity also caps the first subunit D1, and so it must have developed **during** the Dornoch progradation and not entirely before it (Figure 9).

In different schemes and industry biozonations, the base of Dornoch Formation has been correlated to multiple different datums and ages, ranging from the last occurrence of *Alisocysta margarita* at ~57.6 Ma (Dixon and Pearce, 1995; Jolley et al., 2021 - age adjusted to Speijer et al., 2020) to *Apectodinium* related datums at ≤56 Ma, already in the Ypresian (Brunstad et al., 2013). Based on correlation of our own units to biostratigraphic markers, it appears that the base of Dornoch maximum flooding surface predates the first stratigraphic occurrence of *Apectodinium sp.* and *Apectodinium augustum* (Figure 3). It is then adequate to position the surface inside the interval of the "impoverished agglutinated assemblage" of Mudge and Jones (2004), at some time between the top of *A. Margarita* and base of *Apectodinium sp.* Here, we use the top of *A. Margarita* as an estimate of Dornoch's oldest possible age at 57.6 Ma (Figure 3).

If the base of Dornoch predates *Apectodinium sp*, then some confident chronostratigraphic subdivisions of Dornoch are possible using the same datum. These correspond to a Late Thanetian interval below between the top of *A. Margarita* and the base of *A. augustum* (D1-D3), one "Earliest" Ypresian part between the first and last occurences of *Apectodinium sp.* or *A. augustum* (D4) and one Early Ypresian part (D5-D6) below the acme of *Cerodinium wardanense* and the corresponding Balder Formation. Importantly, this subdivision also coincides with **pre-PETM, syn-PETM and post-PETM Dornoch Formation**. The subdivision in two major progradational sequences in several schemes also follows usage of *A. Augustum* and therefore the PETM as a major datum (*e.g. "*Forties" and "Dornoch" units in Mudge, 2015; T40 and T45 in the BP scheme, Figure 3). Critically, however, the **higher-rank highstand and lowstand domains** defined in our study on the basis of seismic stratigraphy do not directly correspond to these, as syn-PETM Dornoch (D4) rather occurs in the middle of the lowstand succession (Figures 2, 3). Moreover, the absence of robust 1 biozonations for pre-PETM deposits (D1-D3) means they are not internally constrained by palynological data (Figure 3).

The base of the Balder Formation/Beauly Mbr. or its correlated sequences (*e.g.* T50) is typically picked at a maximum flooding surface above the prograding Upper Dornoch Fm, close to an acme or top of *C. wardanense* (Figure 3). In this study, a high amplitude reflector observed at the base of Beauly Member clinoforms possibly represents this maximum flooding surface (Figure 8) and its associated coal-rich coastal plain deposits (Milton et al., 1990; Jones and Milton, 1994; Brunstad et. al, 2013, Figure 14). However, we note that an **underlying transgressive surface** associated with this basal flooding serves better as the boundary between Upper Dornoch Fm. and Beauly Mbr. deposits (Figures 2, 8-12; a tentative correlation to other schemes is shown in Figure 3). In the south of our study area, normal regressive Dornoch and Beauly clinoforms are separated by clinoform rollover backstepping with no locally discernible transgressive deposits, which is locally expressed as **a maximum flooding surface** as outlined previously (Figures 8, 9). However, this is accompanied by upstepping of the marine onlap in cogenetic bottomsets downdip (Figures 8, 9), which possibly represent a toe-of-clinoform apron deposited during shoreline transgression ("regraded slope apron" in Galloway, 1989; "healing phase" in Posamentier and Allen, 1993). The base of this toe-of-clinoform apron (B1 TST) is hence better delimited by **a transgressive surface** that is in fact amalgamated with the overlying maximum flooding surface updip, where an equivalent transgressive systems tract is not recognizable (Figures 8, 9). In some areas towards the north, the entire Balder/Beauly interval is rather characterized by an extensive and undifferentiated B1-B3 TST covering much of the underlying Dornoch Fm. shelf (Figures 10, 12). This is part of the marked along-strike variability in the Beauly Member, which will be further detailed in Section 5.

The biostratigraphic character of the top of the Balder Formation/Beauly Mbr. also varies considerably in different schemes, being assigned to the base of *Wetzeliella astra* or the various tops of *H. tubiferum, Fenestrela antiqua* and *D. oebisfeldensis* (Figure 3). However, the relative ages of *H. tubiferum* and *D. oebisfeldensis* biozones vary across schemes and depend significantly on individual semiquantitative analyses and top identification. In seismic, the top of Balder age deposits is more readily correlated to the maximum flooding surface below the Mousa Formation progradational deposits (Mudge and Bujak, 1996; Patruno and Reid, 2016), which is a regionally developed surface (Figures 2, 8-12). The age of this MFS is tentatively tied to the base of *W. astra* and tops of *H. tubiferum* and *Fenestrela antiqua* at ~55.4 Ma (Brunstad et al., 2013; Speijer et al., 2020; Jolley et al., 2021).

5. Results – Along-strike stratigraphy of the Moray Group

In this section, we provide a detailed description of the along-strike variability of Moray Group units. Individual seismic transects, sediment entry points, deltas and RSL curves are described first, while a lateral comparison of their key aspects is presented in Section 5.6. The names utilized for specific transect areas are shown in Figure 1A and are based on nearby fields, onshore geographic features or features observed in our dataset (*e.g.* Botanist), as explained further below.

5.1 South ESP transect area

In the southern ESP, the Dornoch highstand units D1 and D2 include partially preserved delta-scale clinoforms (sensu Patruno and Helland-Hansen, 2018) and slope/basin deposits to the east (Figures 8 and 15A). Between D2 and D3 in the key transect in Figure 8, significant basinward translation (~30 km) and downstepping (500 m) of the clinoform rollover are observed, most of it during non-accretionary forced regression (*sensu* Helland-Hansen and Gjelberg, 1994). The total extent of rollover advance was then matched by topset aggradation during the deposition of the D3 to D5 lowstand units. In the same seismic line, further downstepping of the rollover and distinguishable forced regressive wedges are not clear inside the Dornoch Fm. lowstand (D3 to D5), but topset truncation and stacking of distinct clinoforms sets are nevertheless observed (unconformities between D3, D4 and D5, Figure 8). Topset truncation surfaces at the top of D3 and D4 can be mapped and correlated laterally to better expressed unconformities (*e.g.* in Botanist, where clinoform downstepping is also observed, Figure 9). Lastly, downdip of D3-D5 clinoforms, distinct "mound-like" fans accumulated close to the Crawford Spur and South Viking Gaben boundary (Figures 8, 14 – well UK 16/1-2 – Figures 15C-E).

Above D5 topsets, a strong amplitude reflector is linked to a flooding surface and coal-rich coastal plain deposits characteristic of the Beauly Member (Brunstad et al., 2013, Figure 14). This is associated to an underlying transgressive toe-of-clinoform apron interpreted to precede coastal plain flooding (Figure 8). A prominent but localized unit lying above this transgressive tract was interpreted here as a Beauly-age lowstand systems tract (Figures 8, 16A), which includes delta to shelf-edge-scale clinoforms (Figure 8). The Beauly Mbr. lowstand clinoforms extend from the south ESP to the south of the Beryl Embayment (Figures 6A, 16A).

5.2 Botanist transect area

From the Botanist to Beryl transect areas, a thicker (150-200 ms, up to 220 m) succession of D1-D2 deposits forming a partially eroded escarpment is observed (Figures 9, 15A-B), representing the best-preserved portion of the D1-D2 highstand shelf in the entire study area. An up to 100 ms (~120 m) thick channel is observed stemming from this region from Lista to early Dornoch times, which we here term the Sandwick channel (Figures 7B, 9, 15A-B). Due to its position in a slope/basin environment during this interval, it was interpreted as a relatively long-lived sandy submarine channel associated to a small lobe/fan in the South Viking Graben to the east (Figures 15A-B).

The lowstand shelf (D3-5) developed after strong clinoform rollover downstepping and RSL fall during D2, which is estimated around 390 m by trajectory analysis after overburden removal (Figure 9). A prominent fluvial channel is observed in the D3 coastal plain, situated close to thick, normal regressive D3 foresets (Figures 4A, 6A, 15C). In attribute maps, these clinoforms are interpreted as a progradational wave-dominated shore/strandplain(?) connected to a sediment point source in a local depocenter (**Botanist Delta**, Figures 6A,

15C). A regionally recognized D3 toe-of-clinoform fan is also thickest (~150 ms or 160 m) in the Botanist transect area (Figures 9, 15C). It is not possible to clearly distinguish associated falling-stage clinoforms, and the toe-of-clinoform fan are seen offlapping against previous normal regressive foresets and underfilling this inner shelf area. Conversely, subsequent D4 forced regression in the Botanist area accompanies topset truncation and observable clinoform downstepping (Figure 9). This forced regressive wedge can be followed from this region to the Beryl embayment in the north (Figure 15D).

A shift towards more expressive topset aggradation and onlap recovery occurred during D5 (Figure 9). Fluvial channel-like features above D4 and D5 topsets are more pervasive than in D3, as observed in Figures 15C-E. No unconformity is observed above D5 topsets here, only the amalgamated transgressive and flooding surfaces of overlying Beauly units (Figure 9).

During deposition of the Beauly Member, a distinct system of canyons and drainage-like systems was developed, which we here term the Botanist system after its distinctive "leaf-like" features (Figure 17B). The main Botanist Canyon (after which this transect is named) is located immediately to the north of the Sandwick channel, and involves further incision above the Dornoch lowstand shelf (Figures 1, 4C, 16B, 18A). Due to a connection to TSTs within Beauly and likely continued incision during times of RSL-rise, these features are interpreted to be caused by tidal reworking of abandoned fluvial channels and delta lobes.

5.3 Beryl transect area

In the Dornoch highstand escarpment around the Beryl transect, D1 continues to show proximal delta-scale clinoforms (<100 ms high) passing eastwards to forced regressive or truncated shelf-edge-scale clinoforms (> 200 ms high in Figure 10). Interestingly, D2 is absent in this area and the highstand shelf is clearly partially eroded when compared to Botanist (Figure 9). This is highlighted by the smaller rollover downstepping observed between D1 and D3 (~160 m), which is only a minimum estimate due to truncation of D1 clinoforms (Figures 10, 13).

A critical observation is that downdip, in the area immediately to the north of the Sandwick channel and the Botanist canyon, D3 clinoforms are absent and lowstand deposits are remarkably thin (Figures 15C, 18A). Individual unconformities are difficult to recognize here, but it appears that D5 topsets are directly onlapping against remnants of D2 slope/basin deposits (Figure 18A). Further north, closer to the area of Figure 10, a restricted, flat-topped delta-like system is observed in D3 (**Beryl Delta** in Figures 6A, 15C, UK 8/15-1 in Figure 14). This system is potentially fed by a fluvial point source, but distinct curvi-linear features in attribute maps point to a spit-like, wave-reworked environment (Figure 6A). To the southwest, channel-like features leading downdip to areas of flat, subaqueous and thin D3 deposits could be the result of tidal-reworking and sediment starvation (Figures 6A, 15C).

Similarly to Botanist, a D3 toe-of-clinoform apron is observed to the east of normal regressive D3 (Figures 6A, 10). No shoreline-like features appear to be preserved in this area, and an eastward translation in the clinoform rollover is observed at the onset of D4 (Figure 10). Further east, D4 and D5 normal regressive clinoforms are separated by localized canyon incision, which corresponds to an eroded area of 4x10 km (Figure 10, red polygon in Figures 6A, 15D). This incision was developed during D4 forced regression, which involved up to 140 m of local rollover downstepping in the Beryl Embayment (Figures 10, 18D) and the deposition of another falling-stage toe-of-clinoform apron (Figures 10, 15D, 18D). Erosion was responsible for almost complete removal of D4 in the center of this area, creating physical disconnection between normal and forced regressive D4 (Figure 10). This area was then filled by coastal plain topsets during D5 and Beauly (Figure 10).

To the south of this incised valley, curvi-linear strandplain-like shorelines and small deltas are observed in D4 (Figure 6A, 15D). This curved shoreline extends further until the Beryl Embayment, where progradation directions shift towards the south, and a wide strandplain accumulated also during D5 and D6 (Figures 6A, 15E-F). The geometry of this system appears to be influenced by an underlying Lista to early-Dornoch-age sandy channel complex similar to the Sandwick channel in Botanist (Figures 6A, 6C, 7B, 15A). D4-D5 clinoforms are observed in the Beryl Embayment onlapping against a subtle mound created by this channel complex and underlying basement highs (Figure 18B).

5.4 Bressay transect area

The Beryl and Bressay transect areas are divided by a deep canyon incised above Moray Group strata (Figures 1A, 17A). This is interpreted as an Eocene submarine canyon responsible for sediment routing from the younger Mousa delta updip to the Frigg fan downdip (not shown in Figure 1A). Northwards of the Frigg canyon, D1 to normal regressive D3 are truncated and eroded, and an area where Dornoch is completely absent is found in the western Bressay High (Figures 11, 15A-C). In this region, Montrose group units are also thinner and eroded (Figure 7A-B). Here, a remarkable erosional landscape can be observed (Figures 17A, C). This 30 x 40 km region represents a newly described subaerial catchment akin to the Flett and Judd landscapes in Faroe (Shaw Champion et al., 2008; Walker et al., 2022), with characteristic mountainous hillslopes and >300 meters of relief. Sinuous, 5 km wide channel-belts and terrace-like surfaces are observed, as well as smaller-scale, axial meandering river in a central alluvial plain (Figure 17C). This catchment is only partially imaged by 3D seismic and likely extends further westward, where only 2D data is available. Its eastern termination is marked by drainage outflow into the flatter area of a D4-age coastal plain, south of the Bressay transect (Figure 15D). Further discussions on the nature and age of this catchment are presented in Section 6.

Syn-PETM Dornoch (D4) is here characterized by expanded coastal plain aggradation and fluvial fill in incised valleys (Figures 11, 15D). These fluvial valleys are part of the Bressay Channel as described in Underhill (2001) and Stucky de Quay et al. (2017), corresponding to 200-300 meters of pre-PETM incision

and syn-PETM fluvial fill, as also suggested by cores of Dornoch Formation in well 3/28a-4 (Figures 11, 14 15D, 17A). To the east, closer to the fault-boundary with the Central Viking Graben, post-PETM D5 clinoforms are observed, with thin to absent topsets updip (Figures 11, 15E). On the absence of clear indications of forced regression during D4 and D5, marked topset thinning in D5 is better linked to transgressive erosion, as showcased by topset truncation by overlying Beauly deposits (Figures 11, 15E). Below D4 and D5, a thin, poorly preserved section of pre-PETM Dornoch deposits can also be observed (D3?, Figures 11, 15C). Additionally, in northern Bressay, several incisions are observed above D4 and D5 (Figures 15D-E, 18C, see also Stucky de Quay and Roberts, 2022). These also appear to be filled by Mousa Formation strata, being interpreted as highstand submarine canyons with potential previous fluvial erosion during the Dornoch lowstand.

In the Central Viking Graben, a region of long-lived, sandy basin-floor fan deposition is observed, comprising Lista (Heimdal Member), Dornoch (Hermod Member), Beauly (Odin Member) and Frigg-age deposits (Figure 11). The pre-PETM part of Hermod is included in our map of D3 (Figures 11, 15C). However, considering a D1-D3 gap in the Bressay High, it is possible that pre-D3 deposits reworked from the shelf during RSL fall are present in the area, but are simply unresolved (Figures 15A-B). Indeed, ≤D3-D4 deposits in the Hermod fan appear to be connected to a slope channel stemming from the Bressay Channel incision updip (Figures 15C-D).

Lastly, we observe 25-50 km of shoreline retreat from Dornoch to the westernmost seismically resolvable Beauly highstand, where shallow marine deposits form well-preserved beach-ridge-like features (Figures 4B, 11, 16B). These reach as far as the Bressay catchment, where they are directly covering eroded Lista Fm sediments (Figure 11).

5.5 East Shetland Basin (ESB) transect area

The best distinguished Dornoch subunits at the ESB are D3-D5 sets of shelf-edge-scale clinoforms with flat to ascending rollover trajectories, rather continuous forestepping and apparently little downstepping (Figure 12). These clinoforms show wide, concave and curvi-linear geometries in map view (Figure 15C) suggestive of wave-dominated transport. Evidence of fluvial and coastal plain environments is not unequivocal in map view or seismic lines, and it is likely that clinoform rollovers here are subaqueous rather than shorelines, as opposed to clinoforms in the southern transects.

D3 appears to include a better developed unconformity than subsequent sequences, with significant deposition in a toe-of-clinoform fan (Figures 12, 15C). Onlap then recovered significantly during D4, and while D5 topsets appear to be restricted, upstepping clinoforms suggest this restriction is either related to topset erosion during the Beauly transgression or poorer seismic imaging (Figure 12). D5 also appears to thin gradually to the north, which in turn indicates a supply-controlled pinch-out and non-deposition rather than

erosion. However, the absence of significant downstepping during D4 and D5 is also consistent with their shelf-edge scale and likewise suggestive that rollovers are subaqueous (Figure 12, 13).

The ESB succession also includes less developed delta-scale clinoforms preceding D3 (Figure 12). This includes deposits that are not regionally divisible in two (i.e. D1 and D2 in other areas), although signs of an unconformity are seen locally (D1-D2 boundary, Figure 12). It is similarly likely that this succession includes D1-D2-equivalent deposits due to its pronounced thickness, which is shown in the isopach map for D2 in Figure 15B.

5.6 Along-strike comparisons

Despite following similar overall trends in deposition, Moray Gp. subunits show important distinctions in the expression of specific stratigraphic features and surfaces, in particular the development of depocenters, forced regressive wedges and transgressive successions. These are summarized in Figures 13 and 19, while some key examples are described in the following section.

Along-strike variability of the pre-PETM Dornoch (D1-3)

The clearest variation along-strike for Dornoch highstand units (D1-2) is their near complete absence in the Bressay transect area (Figure 11), which coincides with the development of the West Bressay catchment and the Bressay Channel (Figures 15C, 17A, 17C). Important differences in the geometries of initial deposits of the Dornoch lowstand are also noted, particularly when comparing the South ESP and Botanist areas (Figures 8-9, 12C). In the **Botanist Delta**, D3 foresets are much thicker at 175 ms (~185 m), versus only 60 ms (65 m) in the South ESP (Figures 8-9). These thick foresets are observed in a local depocenter to the north of a fluvial point source, which could have favored a locally higher sediment supply (Figures 9, 15C). However, strandplain-like systems observed in the South ESP and Botanist (Figure 6A) evidence wave-dominated deposition, which appears to have prevailed during the Dornoch lowstand. Wave-dominated settings favor enhanced along-shore transport and bypass, possibly strongly conditioning local sediment supply rates (Figures 15C-D). In the Botanist Delta, the development of a depocenter may be related to the local accumulation of laterally transported sediments in addition to direct fluvial input (see Section 6.2).

A lateral distinction in the expression of forced regression is also observed during later D3. In the South ESP, topset erosion can be inferred by reflector truncation and development of fluvial incision above normal regressive D3 (Figures 8, 13, 15C), but no specific falling-stage systems tract appears to be developed. In Botanist and Beryl, a distinct toe-of-clinoform apron is observed after D3 normal regression, but direct evidence of RSL fall such as downstepping clinoforms is also unclear (Figures 9-10, 13). In Bressay, however, D3 deposits are interpreted as almost entirely subaerially eroded (Figures 11, 15C), suggesting variability in the development of unconformities and timing of peak RSL-fall, which occurs during D2 in the southern areas and during D3 in the Bressay High (Figure 19).

Syn-to-post PETM Dornoch lowstand (D4-D6) – Beryl Embayment succession

In the Beryl Embayment, a D4-D6 depocenter is characterized by the progradation of a local strandplain-like system associated to mounded bottomsets (Figures 6A, 15D-F). This depocenter is also marked by fluvial incision and forced regression. Local incision in a 4 x 10 km area (red polygon in Figure 15D) can be connected to prominent (~140 m) clinoform rollover downstepping during D4 (Figure 10), which was succeeded by the development of a restricted forced regressive wedge during D5 (Figures 10, 18B). This contrasts with what is seen around Botanist and the South ESP, where a maximum 90 m of clinoform downstepping (Figure 8) or only upstepping are observed during D4 (Figure 9), while D5 is entirely normal regressive (Figure 13). D5 forced regression and the consequent distinction of D6 clinoforms is in fact only observed in the Beryl Embayment (Figures 10, 13, 15E-F, 18B).

Fluvial incision and reworking may have supplied some sediments to the forced regressive D4 clinoforms and fans found downdip in the Beryl Embayment (Figures 15D-F). However, the absence of a major delta at the mouth of the incised valley outlined in Figures 6A and 15D (red polygon) and the wider geometry of the D4 forced regressive wedge in Beryl suggest strong lateral sediment transport by longshore currents. Better preserved sediment entry points at this time include a D4-D5 age system of smaller fluvial channels and deltas observed 5-20 km to the southwest of the incised valley, which could have supplied sediments transported laterally to the Beryl Embayment (Figures 6A, 15D), conditioning sedimentation in a local depocenter.

Laterally variable expression of the backstepping Beauly Member

The development of individual systems tracts and stratigraphic surfaces during deposition of the Beauly Mbr. is markedly variable along-strike (Figures 13, 19). South of the Botanist canyon, well-developed, clinoform sets with beach-ridges alternate with thinner transgressive deposits marked by 20-30 km of landward shoreline retreat, characterizing a longer-term backstepping trend (Figures 8, 9, 13, 16A-B). Here, three pairs of seismically resolvable transgressive and maximum flooding surfaces are identified (B1-B3, Figure 19). The along-strike synchronicity of these internal stratigraphic surfaces is currently unknown. In Beryl and in the ESB, the Beauly Mbr. is characterized by thinner, undifferentiated transgressive deposits spanning B1 to B3. This implies strong amalgamation of stratigraphic surfaces laterally, as only a basal transgressive surface and an upper maximum flooding surface can be identified (Figure 19).

6. Discussion

6.1 Non-unique stratigraphy and possible solution sets

Coastal systems are formed by complex and superimposed controls, acting both upstream (*e.g.* sediment supply, climate) and downstream (*e.g.* relative sea-level and marine transport) (Castelltort and Van Den Driessche, 2003; Burgess and Prince, 2015; Zhang et al., 2019). These controls combine over time and

space to simultaneously determine the depositional patterns that are ultimately recorded in stratigraphy. Several depositional patterns are characteristically "non-unique", since they can be generated by more than one type of forcing parameter (*e.g.* flooding surfaces created by overpowering RSL rise *versus* decrease in supply with fixed rates of RSL rise). However, specific stratal geometries and features can be used to minimize ambiguity in the interpretation of forcing controls, a necessary step before further hypotheses on coastal evolution along-strike can be construed. This is done by enumerating possible causes behind non-unique sequence stratigraphic responses, their respective diagnostic features and the likelihood of their occurrence in the record (Heller et al., 1993; Burgess and Prince, 2015; Hampson, 2016). Stratigraphic features and their likely solution sets are summarized in Table 1.

The development and nature of unconformities can be better constrained by the observation of vertical clinoform rollover or shoreline shifts (Burgess and Prince, 2015; Hampson, 2016; Zhang et al., 2019). In the study area, strong, higher-rank rollover downstepping is observed during the initial development of the Dornoch lowstand shelf, corresponding to 200-500 meters of RSL fall (Figures 8-11). This most likely outpaces the rate and magnitude of eustatic fluctuations at the time (Figure 19), indicating a tectonic origin (Figures 20A-B). Most lower-rank (higher frequency) rollover fluctuations in this dataset are up to one order of magnitude smaller than this, and could be consistent with eustatic-control or modulation (Figures 13, 19). Lastly, the development of upstream-controlled erosion and bypass in areas with no direct evidence of RSL fall is also possible for individual systems tracts, such as in the D3 toe-of-clinoform aprons south of Bressay (Figures 9 and 10, Table 1).

Several controls can also simultaneously affect the development of flooding surfaces (Hampson, 2016). Overall, higher-rank flooding and landward shoreline retreat during Beauly are readily correlated to eustatic and subsidence related RSL-rise (Pujalte et al., 2014; Stucky de Quay et al., 2017; Hardman et al., 2018). Shoreline retreat during fixed RSL-rise and supply rates due to increased extent of the flooded coastal plain (autoretreat) may have occurred locally during the Beauly HST progradation, as constrained by estimates of maximum possible depositional lengths (in the sense of Muto, 2001 - see Supp. Material).

In summary, longer-term trends and major unconformities/flooding surfaces associated to larger-magnitude rollover shifts (100-500 m vertically, 10's km horizontally) are interpreted as allogenic and accommodation-induced, with increasing likelihood of autogenic or supply-driven overprint for shorter-term trends and systems tracts with smaller or unresolved clinoform rollover shifts. Importantly, these are also more likely to be affected by differential compaction and overall deformation.

Table 1 – Non-unique stratigraphic responses, possible diagnostic features and their examples in East Shetland

Seq. strat. response	Possible causes	Relation of forcing parameter to system	Possible diagnostic features	Examples in East Shetland
Flooding surface	Increase in rate of RSL rise > rate of sediment supply	Allogenic: RSL-rise due to subsidence or eustasy	• Basin-wide, large-scale flooding in longer-term retrogradation trend (systems with varied along-strike uplift can be more complex). • No observable change in supply rates	• Very likely: overall flooding between D4 and D5, associated to an increase in D5 topset aggradation; overall flooding during Beauly. • Likely: internal Beauly Mbr. flooding surfaces in the South ESP and Botanist. Similar development of internal flooding surfaces is noted (homogeneous downstream controls in a wave-dominated/tide-influenced environment).
	Decrease in sediment supply with fixed rate of RSL-rise	Allogenic: external change in supply (climate, erodibility of source area, drainage reorganization)	• Temporally connected to measured source-area controls on supply (decrease in sed. flux in respect to accommodation).	• Plausible: internal Beauly Mbr. flooding surfaces in the South ESP and Botanist. Abrupt switching to retrogradation after high supply rates: abrupt change in sediment supply?
		Autogenic: caused by internal changes in supply (avulsion, interim storage)	• Measured decrease in flux with no apparent external cause. • Individual sediment supply systems along-strike may exhibit independent autogenic "clocks" (e.g. two deltas with different avulsion times).	• Unlikely: internal Beauly Mbr. flooding surfaces in the South ESP and Botanist. Laterally variable autogenic timing is less likely to fit scale of observed flooding.
	Increase in extent of flooded coastal plain with fixed rates of RSL-rise and sediment supply (autoretreat)	Autogenic: direct consequence to shelf progradation, no external changes in RSL or supply	• Distinguished by concave landward shoreline trajectories (Muto et al. 2007) and characteristic depositional lengths (D = S/A)	• Likely: a component of flooding during the B2 HST in the South ESP (Table S2). • Unlikely: other Beauly Mbr. flooding surfaces. High overall supply means autoretreat was not favored.
Unconformity	RSL fall and topset degradation	Allogenic: RSL fall due to uplift or eustasy	• Shoreline and clinoform downstepping are verified. • More easily recognized when of broader scale. Actual scale and timing depend on forcing mechanisms and coastal/basin physiography.	• Very likely: clinoform downstepping between highstand and lowstand Dornoch; focused erosion and shoreline downstepping in the Beryl Embayment and southeast Bressay during D4 and D5. • Possible: subtle downstepping observed in other forced regressive wedges (D4 in Botanist, D2 and D3 in ESB).
	Topset degradation or bypass with no RSL fall	Allogenic or autogenic: degradation /bypass controlled by variations in discharge and supply ratios (supply-dominated sequences, Zhang et al., 2019)	• Flat-trajectory clinoforms, with indications of topset bypass or erosion (Zhang et al., 2019). • Concomitant climate-enhanced erosion can be constrained by other proxies.	• Likely: forced-regressive-like tracts with no clear clinoform downstepping. (D3 toe-of-clinoform fan in Botanist and the south ESP); additional upstream controlled topset erosion across multiple units, regardless of RSL forcing. • Plausible: flat-trajectory clinoforms (normal regressive D3 in Beryl, D2 and D3 in ESB, D4 in Botanist, B1 lowstand).

6.2 Trends in depositional patterns and sediment routing systems along strike

Along-strike sediment supply, wave-dominated transport and inherited topographic controls in the Dornoch lowstand (D3-D6)

During deposition of the lowstand Dornoch, wave-dominated conditions appear to have prevailed, as suggested by the geometries of strandplain systems developed across the entire study area (Figures 4, 6, 15C-E). Variations in fluvial sediment input can also be inferred by changes in the distribution and quantity of fluvial channels, observed in seismic attribute maps and represented in Figure 15. Interestingly, these may be a manifestation of time-varied upstream conditions of fluvial supply affecting drainage and alluvial plain organization (see section 6.3). However, enhanced along-shore sediment transport in wave-dominated shores is expected to strongly condition local sediment supply and determine "final" coastal depositional geometries (*e.g.* Dominguez et al., 1992; Bittencourt et al., 2005; Hampson and Howell, 2005), which will also be influenced by the pre-existing coastal physiography and its active littoral cells (Sanderson and Eliot, 1999; del Río et al., 2013). This has some important implications for the wave-dominated lowstand Dornoch shelf.

In the ESP, we note the development of individual depocenters of the Dornoch lowstand characterized by locally thicker strandplain systems (Section 5.6, Figures 15C-F). In the Botanist transect area, a D3-D5 depocenter was formed immediately to the south of a mound created by the **Sandwick submarine channel and its surrounding D1-D2 slope** (Figures 4, 9, 15C, 18A). In the Beryl Embayment, a D4-D6 strandplain is observed onlapping against a mound created by **another Lista-Dornoch age channel complex and a local structural high** (Figures 6A, 6C, 7B, 18B). In both areas, different deltas and sediment entry points of the lowstand coast appear to be segmented by these mounded features. Interestingly, drainage-like incisions are observed above the Sandwick channel and its surrounding highstand slope (Figure 4, 17A), suggesting that a positive and emergent topography was already established during the Dornoch lowstand. Therefore, while this mounded topography was likely enhanced by subsequent differential compaction, it was possibly initially created by locally thicker deposits of the Lista Fm/Dornoch highstand, since differential compaction would have to occur very quickly to create local topography already during the following Dornoch lowstand.

Critically, the formation of depocenters near shelf-perpendicular areas of emergent or positive topography suggests that these areas acted as barriers to sediment transported along-shore from south to north, forcing the accumulation of locally thicker wave-dominated systems during lowstand progradation. On the other hand, immediately to the north of the possibly emergent Sandwick channel and highstand slope, deposit thinness and absence of clinoforms suggest **sediment starvation** in the first lowstand unit D3, in the south of the Beryl transect area (Figures 6A, 15C, 18A). Simultaneously, local sediment input in the area was likely focused around small rivers further north, closer to the small delta/spit system seen in the Beryl transect (D3 in Figure 10, **Beryl Delta** in Figures 6A, 15C), which pinches out to the south (Figure 18A). Therefore, in

addition to hindered along-shore sediment supply from the south, direct fluvial supply also appears to have been limited in the Beryl transect area during D3 (Figure 20B).

In D5 and in the B1 LST, thickening in the Piper Shelf to the southwest (Figures 15E, 16A), possibly due to increased sediment derivation through the Moray-Firth and local accumulation, although the characteristics of the local fluvial supply are unclear due to absence of 3D data. Furthermore, Beauly deposits, which were deposited during basin-wide RSL rise, varied from transgressive and depositional in the south of the study area to transgressive and erosive in the north (Figure 13, 19). Because accommodation was likely similar along-strike for this interval (as verified in RSL-trends, Figure 19), this is most likely due to a difference in sediment supply, as observed in other transgressive or backstepping systems with distinct development of internal sequences along-shore (Catuneanu and Zecchin, 2016; Catuneanu, 2019). Akin to the Dornoch Fm., this was also influenced by wave-dominated deposition, as attested by the beach-ridges and strandplain systems that are also observed in the Beauly Member (Figures 4B-C, 16A-B).

North-to-south tilting of the shelf and impacts on lowstand sediment routing

The Dornoch highstand shelf constitutes an escarpment that was likely subaerially exposed during all of the subsequent lowstand progradation after the D2-D3 RSL fall event. This is attested by the widespread development of drainage and catchment-like features above both the highstand and lowstand shelves, as well as stratigraphic evidence of coastal to non-marine deposition in the lowstand (Figures 6A, 14, 17). Importantly, this escarpment's relief also appears to be different along-strike. This is suggested by the angular truncation developed above it towards the Bressay transect area, where the escarpment is apparently cut by a "peneplain" (Figure 17A). This angular truncation entails gradual increase in the eroded thickness of the highstand shelf towards the north, culminating in its complete removal below the West Bressay catchment, where deeper incision reaches Lista Fm. deposits (Figures 11, 17A). Critically, this gradient is suggestive of **N-S tilting of the ESP after D2 (Figure 20B)**. This is also illustrated by the fact that in most of the Beryl and south Bressay areas, the emergent highstand shelf is only covered by a thin Beauly-age reflector, marking the first shift from degradation to aggradation above the escarpment (meaning that the escarpment must have remained emergent until then - Figure 10). On the other hand, in the south ESP, topset aggradation above a lower-relief highstand escarpment potentially started already in D3 and increased until D5, when the lowstand coastal plain reached a more complete coverage of the previously exposed area (Figures 8, 15C-E). This difference in the age and magnitude of flooding above the highstand escarpment and the general increase in accommodation towards the south (Figures 13, 18A, 19) are also notably consistent with N-S tilting of the ESP.

Interestingly, N-S tilting and along-strike differences in escarpment relief may also have impacted lowstand sediment routing. In the previous section, we discussed how shelf-perpendicular features such as the Sandwick channel could have acted as barriers for along-shore sediment distribution in the Dornoch lowstand. We also noted that limited fluvial input might have occurred in the D3 Beryl Delta. Critically, restricted fluvial

supply is observed close to where the preserved topography of the Dornoch highstand escarpment is highest (Figures 15C, 17A). Furthermore, lowstand drainage networks incised in the Beryl transect area appear to be limited to the west by the highstand escarpment itself, while in the south these lowstand drainages probably extend further west in a lower-lying coastal plain (Figure 17A). It is reasonable then to think that the highstand escarpment itself acted as a partial barrier to sediment transport **along dip** in Beryl, disconnecting the main source-area to the west and newly incised D3-D6 (lowstand) drainages in the east (Figures 4, 17A, 20B), while this effect is not observed to the south. In other words, N-S tilting and RSL-fall may have resulted in a partial topographic barrier affecting the distribution of sediments in the transfer zone, leading to local disconnection of the lowstand coastal plain to a main western drainage. With continued erosion of the highstand shelf during D3-D4 and RSL rise during D5 - Beauly, coastal plain sediment transport systems could eventually have been reconnected along dip in Beryl (Figure 20C). During D5, shoreline progradation and RSL rise likely also surpassed the topographic barrier created by the Sandwick channel to the south, leading to more efficient along-shore sediment transport (Figure 13). The reconnection of both along-shore and downdip sediment routing systems hence explains the increase in sediment thickness from D3 to D5 in south Beryl and the relatively more even distribution of D5 clinoforms in the ESP overall.

6.3 Expression of the Paleocene-Eocene Thermal Maximum - PETM

Syn-PETM deposits are evidenced by intervals of *A. Augustum*, found for the most part in basinal areas where their thickness often is poorly constrained (Figures 8-10). One exception to this is the Bressay channel, where syn-PETM strata (D4) correspond to part or the entirety of a >250 m thick, localized fluvial fill (Figure 10, 14). In other proximal areas, even if D4 could be mapped on the basis of seismic stratigraphy, its exact correspondence to the PETM is ambiguous due to absence of sampled *A. Augustum* in wells.

Areas of higher confidence PETM identification include deeper basinal deposits restricted to three areas. One includes the confined area of the Beryl Embayment in quadrant 9, where falling-stage strata built considerable mounded bottomsets (Figures 10, 18B), meaning that the impact of the PETM on sedimentation is blurred by concomitant RSL-fall unrelated to the hyperthermal. The second is the area near the South ESP, where similar mounded fans appear, although their correlation with specific clinosets is more uncertain due to their disconnection to proximal equivalents (Figure 8). It is nevertheless noteworthy that the quantity of imaged fluvial channels appears to increase in the assumedly syn-PETM coastal plain in the south ESP (Figure 15D), which could fit other similar observations on the effects of the PETM for fluvial channel mobility (Barefoot et al., 2022; Prieur et al., 2023).

Finally, syn-PETM fan deposits are found in the Central Viking Graben east of Bressay, where they can be tied to specific wells in a relatively restricted area (Figures 11, 15D). In this area, it is possible that syn-PETM fans are in fact less extensive than pre and post-PETM systems, contrasting with other areas where the PETM appears to have enhanced sediment delivery to the basin floor (Pogge von Strandman et al., 2021,

Vimpere et al., 2023). This includes the Froan Basin in the Norwegian Sea, where PETM fans prograded further than before due to climate-enhanced bypass in slope-channels (Sømme et al., 2023). However, the stratigraphic succession in Bressay is characterized by prominent proximal erosion and distal redeposition predating the PETM (D1-D3), followed by RSL-driven increase in accommodation and sediment storage in the shelf during and after the hyperthermal (D4 - Beauly). This denotes a **strong tectonic signal** that likely predominates over the PETM in terms of sediment routing reorganization, hindering a simple evaluation of PETM *vs* "background" sedimentation. This has important implications for studies on sedimentation rates across the North Atlantic (*e.g.* Jin et al., 2022; Jolley et al., 2023; Sømme et al., 2023), as uplift-driven erosion still needs to be disentangled from the climatic signal for a clearer understanding of their impacts on sediment fluxes.

6.4 Late Paleocene – Early Eocene erosional surfaces and comparison with previous literature

Several works have discussed Thanetian to Ypresian unconformities in east and west of Shetland, pointing to the presence of one to two net erosive events at the time (Stucky du Quay et al., 2017; Hardman et al., 2018; Jolley et al., 2021; Conway-Jones and White, 2022). In this work, we identify at least 5 unconformities (D1-D5) of variable extent, magnitude and expression (Figure 19). These 5 unconformities cannot, however, be instantly connected to broad and regional tectonic events.

The best-preserved evidence of base-level fall in the studied succession is the clinoform rollover downstepping associated to the development of the lowstand D3-D5 shelf, circa 200-500 meters below D1-D2 in the southern transects (Figures 8-10, 13). Direct evidence of base-level fall before this time is partially obscured, as the original D1-D2 topsets and onlap/offlaps were likely altered by continuous erosion during the subsequential development of the Dornoch lowstand. Nevertheless, the heightened extent and rate of shoreline migration during the Lista to early Dornoch transition most likely involved some amount of RSL fall (Figure 13), similarly to what is observed in the Froan Basin (Sømme et al., 2023) and the Outer Moray Firth (Jones and Milton, 1994).

Relative sea-level fall and unconformity development from D2 to D3 in the southern transects is broadly consistent with the erosional history of the Bressay High (Figures 15C, 19). In Bressay, however, erosion in a broader area dominated from D1-D3 until D4, when an "abrupt" shift towards dominant aggradation occurred (Figures 11, 13, 19). In other words, forced regression is not observed at all during the Eocene (D4 onwards) in Bressay. This marks a significant contrast in depositional and erosional regimes when compared to all other areas, which are marked by alternating topset degradation and aggradation during the Dornoch Progradation (see Figure 19). A complete D1-D3 gap in Bressay suggests that either: (1) the area remained above the depositional base-level during all of that time, due to a distinct initial topography/longer-term uplift curve or (2) erosion advanced further and deeper than in other areas only during D3, due to a differential uplift event.

Differential uplift in the Bressay High is suggested by evidence of north-to-south tilting, as mentioned in Section 6.2, and is also relatively consistent with previous observations in the area made by Milton and Dyce (1995) and Underhill (2001). These authors suggest that the deep and localized incised valleys observed north of the Beryl Embayment (Figure 15D, red polygon) and in central Bressay (*e.g.* the Bressay Channel, Figures 11, 15C) were formed by a local uplift event, which would also have promoted overall erosion and sediment reworking in most of the Bressay High (see Figure 2 in Milton and Dyce, 1995). Erosion would have occurred at the edges of the differentially uplifted Bressay Granite (Milton and Dyce, 1995; Underhill, 2001; Parkes et al., 2020), a rejuvenated Devonian intrusive body delimited by a gravity anomaly (Donato and Tully, 1982). However, this anomaly has been later reinterpreted to be in great part caused by a local, remnant Devonian basin below the Cenozoic (observed in Figure 11, see also Patruno et al., 2019; Karstens et al., 2019), and as such the actual extent of the Bressay granite remains somewhat unclear (Holloway et al., 1991).

We contend that the proposed rejuvenation of the small Bressay granite cannot single-handedly explain broader erosion in the region. It appears more likely that the same event that caused RSL fall between the highstand and lowstand shelves in the south also led to erosion in Bressay. However, we do observe different magnitudes and timings of RSL fluctuations along-strike, as RSL fall in the south was already interrupted during the initial aggradation of normal regressive D3 (pre-PETM), while in Bressay erosion continued until just before D4 (syn-PETM, Figures 19, 20).

Interestingly, a complete pre-PETM (D1-D3) gap in the Bressay High is also consistent with the description of Stucky de Quay et al. (2017) for the relative age of the Bressay Channel unconformity. However, we argue that the occurrence of PETM deposits in the Bressay Channel should constrain its upper age at 56 Ma, rather than 55 (Figure 19). Along with an adjusted GTS2020 age of 57.6 Ma for *A. Margarita* as the oldest possible for the unconformity, we arrive at maximum duration of ~1.6 Myr, almost half of what is described in Stucky de Quay et al. (2017).

It is also noteworthy that the number of unconformity-bounded units missing in the Bressay Channel constrained independently in this paper (D1-D3) is equivalent to the number of knickpoints and steps of uplift increase described in Stucky de Quay et al. (2017). This could imply that the D1-D3 unconformities are also merged in the area, which would require subaerial exposure during all of D1-D3 as opposed to only D3, as currently shown in our paleogeographic reconstruction (Figures 15A-C, 19, 20). Despite this, some care must be taken before direct comparisons can be made. For instance, Stucky de Quay et al. (2017) argue that the geometries of observed knickzones are not affected by topographic inheritance or substrate lithologies. However, curvi-linear NE-SW features and incisions observed next to the Bressay Channel are markedly coincidental with the trends of soft-sediment polygonal faults observed in underlying Lista deposits (Figures 6C, 17A). Soft-sediment faults on the other hand appear to follow the NE-SW strikes of underlying, folded Devonian deposits, as also observed in Figure 3 in Stucky de Quay et al. (2017) - see also Karstens et al. (2019) and Parkes et al. (2020). Therefore, structural inheritance controlled by this Devonian fabric likely

influenced soft-sediment fault development in Lista, which in turn had an impact on Dornoch-age coastal plain channels (interpreted in Stucky de Quay et al., 2017 as NE-SW beach ridges). This suggests a strong relationship between fluvial geomorphology and inherited topography close to the Bressay Channel, meaning that any corresponding effects on knickpoint generation or propagation should not be dismissed.

The "abrupt" shift towards aggradation during D4 (syn-PETM) matches the post-"Bressay Unconformity" switch to subsidence suggested by Stucky de Quay et al. (2017), although post-uplift RSL-rise in our reconstruction appears to have been more incremental, with a first phase during D4-D5 (~100 m) and up to c. 200 m until ~55.4-54.7 Ma, during the deposition of the Beauly highstand (Figures 13, 19). In Faroe, subsidence rates calculated from paleoshorelines provide a similar constraint, suggesting the onset of subsidence is coeval with breakup and perhaps removal of regional dynamic support (Hardman et al., 2018).

In the south, differently from Bressay, intermittent topset erosion is observed during most of the Dornoch progradation, including in the syn to post-PETM D4 and D5 (Figure 19). D4 downstepping in Botanist is at most 90 m, significantly smaller than the 390 m of base-level fall from D2 to D3 in the same area (Figure 9). In Beryl, more significant downstepping during D4 (140 m) and the local development of D5 forced regression suggests a change in erosion/uplift mechanism to something less broad and potentially more fault-bounded (Figures 13, 15D-E, 19), characterizing prominent but areally focused syn-PETM to post-PETM erosion in the study area.

In several areas updip of the lowstand Dornoch shorelines, pre-PETM and post-PETM unconformities are merged (*e.g* in West Bressay, in the area above the Dornoch highstand escarpment and in the overall proximal part of the study area imaged only by 2D data). As a particularly well-imaged compound surface, the Western Bressay landscape is interpreted to be an area of dominant degradation that remained above the depositional base-level throughout most or all of the Dornoch progradation (Figure 17C, 19). It corresponds to an area updip of the local D4 and D5 onlap, and can be interpreted as part of a slightly longer-lived catchment (≥57.6-55.4 Ma) sitting 100-300 meters above the D5 shoreline (Sup. Material, Figures 17A, 17C, 20). It is likely that this feature is only formed and preserved due to the relatively fast fluctuations in onlap of ~30 km throughout the evolution of the Moray Group (cf. Shaw Champion et al., 2008; Hardman et al., 2018).

Lastly, in the ESB, differently from the southern transects, progressive offlap advance or clinoform downstepping during Dornoch are less significant, which is consistent with the longer-term buildout of a shelf-edge. However, continuous erosion in the footwall block *updip* of the ESB can be inferred from the absence of Dornoch clinoforms and a thin cover of likely Beauly age above an unconformity of uncertain age (Figures 12, 18D). This highlights a regime of predominant degradation in the higher platform and more continuous accommodation in the basin, akin to fault-scarp degradation and hanging wall deposition, suggesting a different subsidence and uplift history compared to areas like Beryl and the Bressay high (Figure 19).

Implications for tectonic evolution of the East Shetland Platform

Across the North Atlantic, dynamic topography has been suggested as a main driver for Late Paleocene – Early Eocene uplift (*e.g.* Hartley et al., 2011; Stucky de Quay et al., 2017). This study shows that fast and laterally variable RSL fall is recorded by variably expressed forced regressive wedges during the Dornoch progradation. Observed spatial and temporal patterns of RSL fall (Figures 19, 20) point to shorter-wavelength and shorter period variations in uplift than what has traditionally been related to dynamic topography (*e.g.* Jones and White, 2002; Barnett-Moore et al., 2017). Similar observations have led authors to argue that transient uplift phases could be generated by fast, laterally spreading thermal anomalies stemming from the Icelandic Plume and travelling through the asthenosphere (Rudge et al., 2008; Stucky de Quay and Roberts, 2022). Others have since suggested a stronger contribution of rift-related uplift in the North Atlantic domain in general (Fletcher et al., 2013; Stoker et al., 2018; Foulger et al., 2020). While it is not our aim to solve this debate here, our observations indicate potential north-to-south tilting and short-wavelength differential uplift, as well as some additional coincidence between the spatial expression of forced regressive wedges and tectonic elements (faults) in Shetland. It is important to consider that the distinction of individual vertical motion phases induced by dynamic topography might be affected by other local controls, as suggested by comparisons of uplift curves and unconformities across the North Atlantic (*e.g.* Sømme et al., 2023). This could include not just sediment supply and local subsidence, but also their interplay with a previously faulted inherited topography (*e.g.* how it may react to differential loading or compaction, Bertram and Milton, 1988).

6.5 Summary of paleogeographic evolution

In East Shetland, preserved deposits are seemingly entirely deep-marine until the progradation of Dornoch Formation clinoforms (Figures 7A-B). No unambiguous evidence of subaerial erosion could be distinguished in deposits of the Montrose Group (Figure 19). The ensuing geological evolution is illustrated in Figure 20:

- **Stage 1**: after deposition of the Montrose Group, an initial shift of the offlap towards the basin was recorded in the D1-D2 highstand shelf, during the Late Thanetian (Early T40).
- **Stage 2**: the D1-D2 shelf was then exposed subaerially during regional RSL fall around 300-500 meters, becoming part of a longer-term source area during basinward translation of the coastal plain onlap. In the south, RSL fall was already interrupted during lowstand topset aggradation in D3. Conversely, erosion peaked at the same time in the Bressay High to the north, where the Bressay Channel was incised. It is unknown whether the Bressay Channel was connected to a larger catchment updip (*e.g.* West Bressay Catchment?). This might have been caused by N-S tilting and/or a short-wavelength (100 km) difference in uplift or isostatic/compactional load between the areas. At the same time, wave-dominated deposition favored the outbuilding of strandplain systems in the new lowstand Dornoch,

potentially enhanced by the inherited topography of the previous highstand shelf and slope. Multiple fan systems were deposited in the Viking Graben.

- **Stage 3**: after regional RSL fall, a shift to coastal plain aggradation occurred in the Bressay High. Although timings are not certain, erosion and unroofing in the source area eventually completely erased the Dornoch HST shelf updip of the aggrading coastal plain in Bressay, while it remained partially preserved further south. In the south, coastal plain aggradation and degradation alternate during D4-D5, with more pronounced RSL fall close to the Beryl Embayment (up to 140 m during D4, when valley incision similar to the Bressay Channel is also noticed, and another 50 m of clinoform downstepping during D5). This suggests local controls on RSL fall. Topography-influenced wave-dominated deposition appears to continue in the Beryl Embayment, where another depocenter characterized by strandplain progradation is observed.

- **Stage 4**: during regional RSL rise, a progradational system developed in the south (the Beauly lowstand unit), while only transgression was recorded north of the Beryl Embayment. This could be due to an along-strike difference in sediment supply.

- **Stage 5**: during continued RSL rise and after one (or more) episode of broad transgression, another HST system prograded above the previous Dornoch shelf, recording extensive strandplain-like ridges (Figures 5B-C). This system was probably gradually flooded, with the development of potential tidal canyons being remarked (Figures 5C, 17B).

- **Stage 6**: after eventual full transgression of the Dornoch and Beauly shorelines, a new, higher-rank highstand was established during the Ypresian. This marked a significant landward migration of the transfer zone and coastal onlap. At this point, RSL rise (eustasy+subsidence?) and reduction in hinterland uplift both resulted in a lower relief.

7. Conclusions

After analysis of a large amount of new, high-resolution data inserted in a coherent, regional paleogeographic context, we draw the following major conclusions:

- New high resolution paleogeographic maps for the Middle Thanetian to Early Ypresian show that progressive offlap advance is consistent with a longer trend of base-level fall, which is highlighted in the abrupt highstand to lowstand RSL fall event of D2-D3. Regionally, this longer-term trend was also marked by intermittent onlap recovery (shelf accommodation) during D1-D4 and D5-D6 and marked onlap recovery from D5-D6 to B1-B3. Progradation was accompanied by significant lateral variability in depositional trends, which was modulated by a complex interplay of topographic inheritance, time-varied sediment entry points, along-shore sediment transport and shelf accommodation/erosion.

- The development of subaerial drainages in intermittently exposed areas is remarked, being connected to the vertical stacking of erosional surfaces in a coastal plain environment. Overall, unconformities mark

the variation through time in the extent of source-to-sink catchment and transfer zone areas, which tended to advance seaward during base-level fall and development of a lowstand shelf (*e.g.* West Bressay catchment). Submarine fan sedimentation was enhanced during offlap advance and catchment incision on the shelf. It nevertheless occurred during both normal and forced regression in the Dornoch lowstand and also followed highstand deposition during Beauly, potentially influenced by tidal reworking of the shelf.

- The uneven distribution of eroded/exposed areas and their differential, fast transient advance and retreat in some regions (*e.g.* Bressay High) during the Late Paleocene suggest shorter wavelength uplift than what is assumed for larger dynamic topography anomalies. It should be noted that this broadly follows the distribution of structural elements and the rift-related lithospheric configuration of the North Sea. Smaller amplitude fluctuations in shelf accommodation are probably more heavily affected by additional eustatic and climatic modulation.

- Reconstructed uplift curves might vary significantly depending on which erosional landscapes are used for inversion, due to the uneven development of unconformities along-strike and dip and their often complex juxtaposition.

- A strong tectonic signal during the Paleocene-Eocene transition likely predominates over the PETM in terms of sediment routing. Its impact for sedimentation rates in Shetland is currently unclear, and should be tested in similar forward stratigraphic models for more effective signal disentangling.
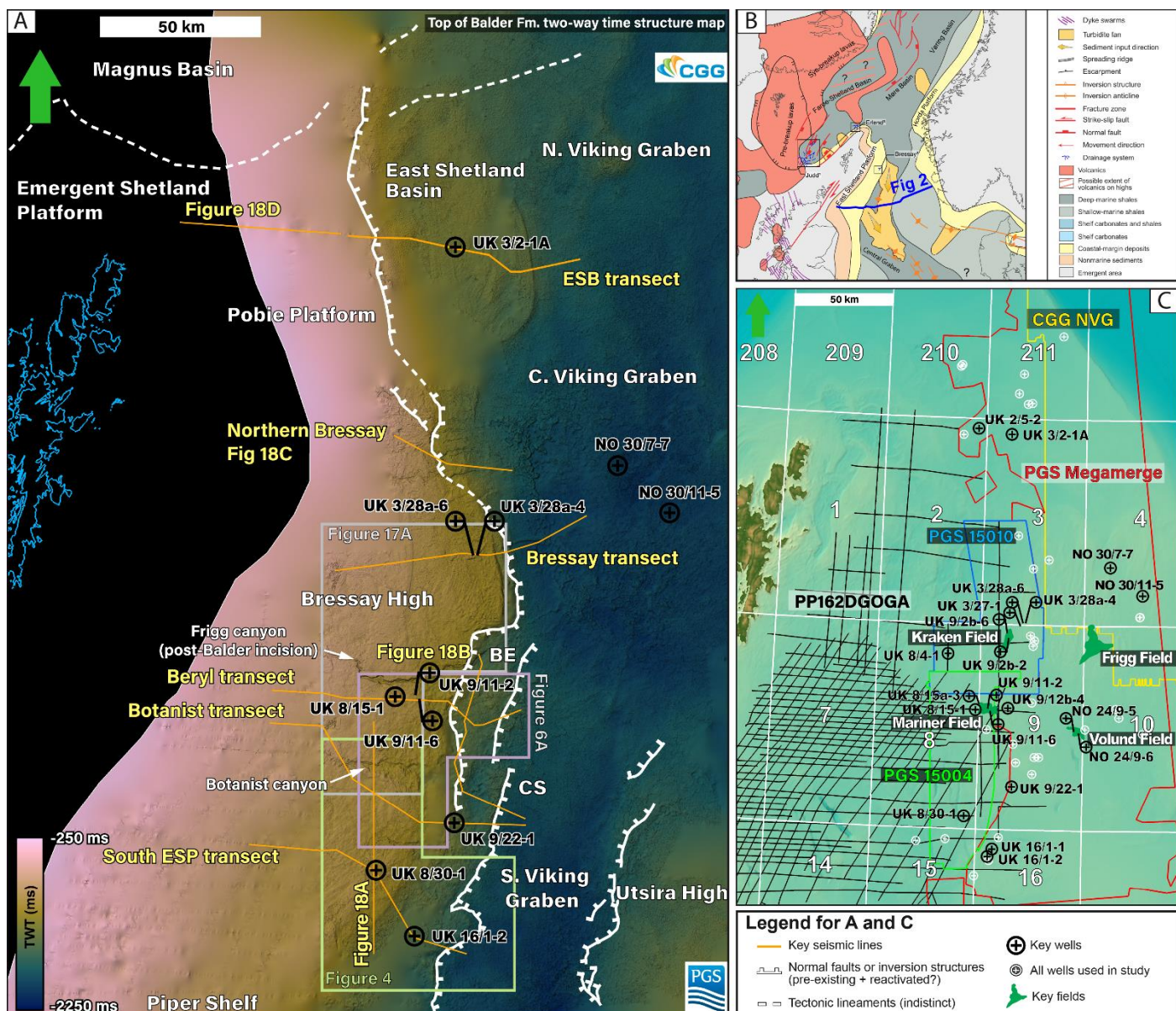
8. Acknowledgements

9. Figures

Figure 1: Location of the study area and dataset. A) Top of Balder Fm. structure map in time. Orange lines are seismic lines referred throughout the paper. Structural elements are based on the Norwegian Petroleum Directorate (NPD) structural element map, Mudge (2015) and own mapping. BE – Beryl Embayment; CS – Crawford Spur. B) Tectonic reconstruction of the Paleocene, modified from Coward et al. (2003). CG – Central Graben; ESP – East Shetland Platform; FSB – Faroe Shetland Basin; MB – Møre Basin; MF - Moray Firth; VB – Vøring Basin. – Witch Ground Graben. C) Dataset utilized in this study. White circles are wells with revised biostratigraphic and lithostratigraphic picks. Bathymetry from GEBCO. Grid refers to UK exploration quadrants.
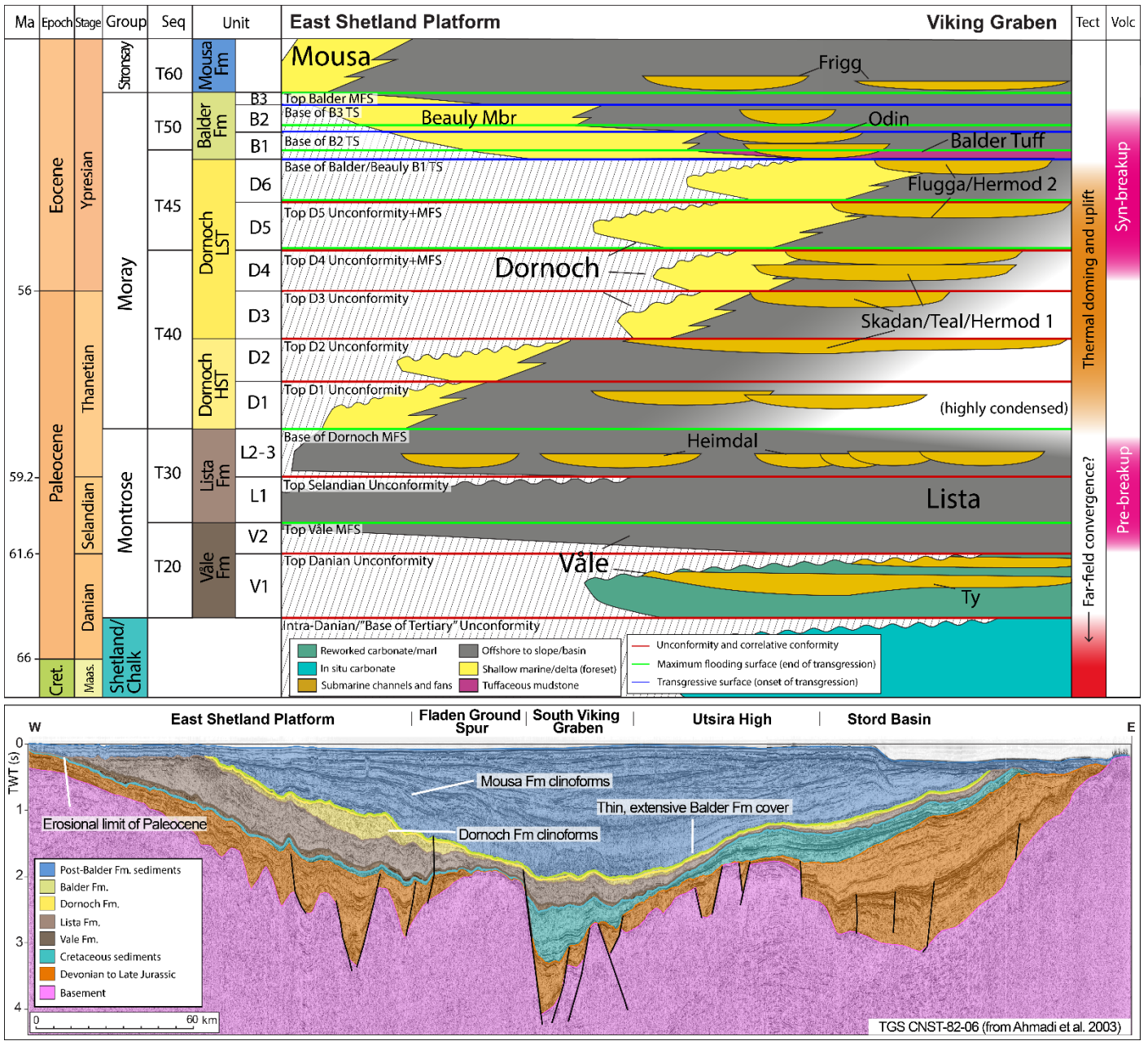
Figure 2: Simplified stratigraphic chart of the study area and regional seismic line from TGS CNST-82 survey, modified from Ahmadi et al. (2003). Location shown in Figure 1B. Tectonic and volcanic events after Gernigon et al. (2012), Foulger et al. (2020) and Jolley et al. (2021). Sequences from BP, after the correlation in Figure 3 with Jones and Milton (1994) and Dixon and Pearce (1995).
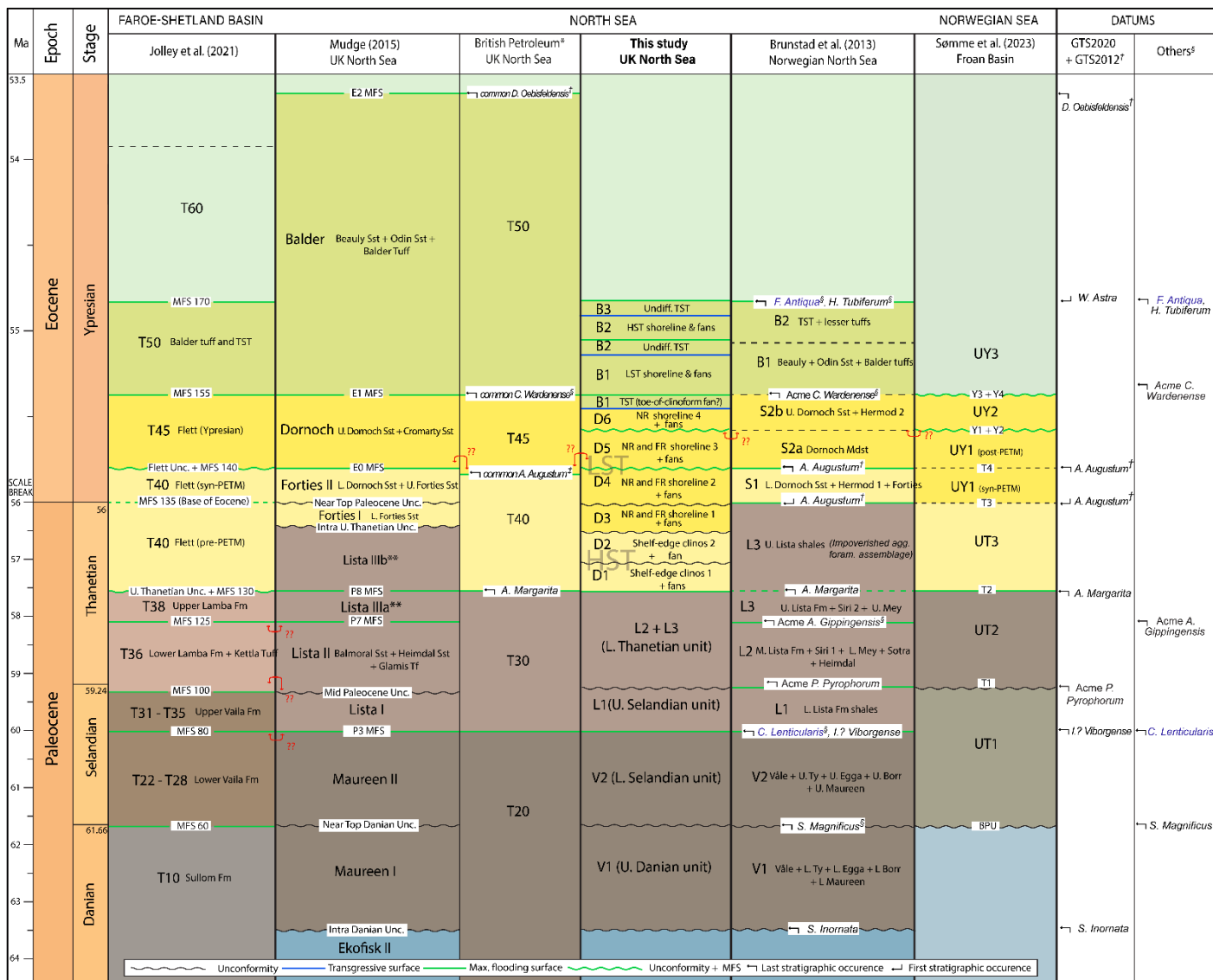
Figure 3: Stratigraphic chart showing the comparison between litho, chrono and biostratigraphic significance of multiple schemes and our study. Nomenclature in this study is based in Knox and Holloway (1992) and Brunstad et al. (2013), with added subdivisions of Dornoch Formation based on our own work (D1-D6). While we correlate the base of Balder Fm. and the Beauly Mbr. with other works that choose a flooding surface as a stratigraphic marker, the character of this surface varies laterally between a flooding surface with no resolvable transgressive tract (below the Beauly lowstand) to a transgressive surface below a condensed transgressive tract. Dashed black lines indicate lithological limits with no definite sequence stratigraphic significance in other works (these can be tentatively correlated to surfaces in this study). Blue names are microfossils, while black names refer to palynological datums. Ages adjusted to GTS 2020 (Speijer et al., 2020), except for datums marked with †, which use GTS 2012 (Vandenberghe et al., 2012), and with §, which are based on correlation of datums and surfaces in Mudge and Bujak (2001) and Brunstad et al. (2013) to ages in Mudge (2015), Speijer et al. (2020) and Jolley et al. (2021). The only exception is the base of A. augustum, which is adjusted to the base of the Eocene (Jolley et al., 2021; Jin et al., 2022). These schemes use sequence stratigraphic surfaces (flooding surfaces, unconformities) for initial division, which are then correlated to biostratigraphic datums or biozonations. This chart is primarily a comparison of chrono and sequence stratigraphic frameworks rather than biostratigraphy. Further explanations can be found in the supplementary material. * - BP stratigraphic sequences are based on Jones and Milton (1994), with the addition of the biozonation of Dixon and Pearce (1995). While several reproductions of this chart include the lowermost T10 sequence, it was not originally defined in the referred studies. ** - Subdivisions of Lista III based on Mudge and Jones (2004). ‡ - Usage of A. Augustum in Dixon and Pearce (1995) differs slightly from other works shown here, since it includes two tops of A. augustum, the uppermost one already inside T45. This has been omitted or modified in later reproductions of this same scheme.

Seismic geomorphology and depositional environments

RMS amplitude + variance of Dornoch Fm., D4 unit base merged updip with subcropping units

- D3 below
- D1-2 below
- 2. Fluvial channels and delta
- 2. Lowstand drainages incised on highstand shelf/slope
- Sandwick Channel
- Dornoch HST slope
- 2. Fluvial Incisions on lowstand coastal plain
- 1. Coastal plain (undiff.)
- 3. Strandplain/wave-dominated delta
- 7. Slope/submarine channels
- 5. Toe-of-clinoform apron w/ small, shore-perpendicular ridges/lobes
- D4 Shoreline
- 6. Polygonal faults in muddy outer shelf/slope

2 km

PGS 15004

Examples throughout Dornoch and Beauly units

A 2. Fluvial channels — 2 km
Fluvial channel in D3 topsets
PGS 15004 — Dornoch D3 RMS amplitude

2 km — Fluvial channel above older coastal plain
Metomode River, Mozambique

B 3. Strandplains
W. Bressay catchment partially covered
Beach ridges
Older Lista submarine channel
Beauly B2 RMS amplitude + variance — 5 km
PGS 15010
Caravelas strandplain, NE Brazil — 2 km

C 3. Strandplains and 4. tidal channels
Beach ridges
Botanist canyon
Sandwick channel below
Beauly B2 RMS amplitude + variance — 4 km
PGS 15004
Guaraqueçaba bay, S Brazil — 2 km

7. Submarine channel-lobe complex

8. Undiff. turbidite fan

PGS Megasurvey

D 3. Spit/wave-dominated shore and 4. tidal channels — 2 km
Spit
Tidal channels?
PGS 15004 — Isoslice Dornoch, instant. amplitude
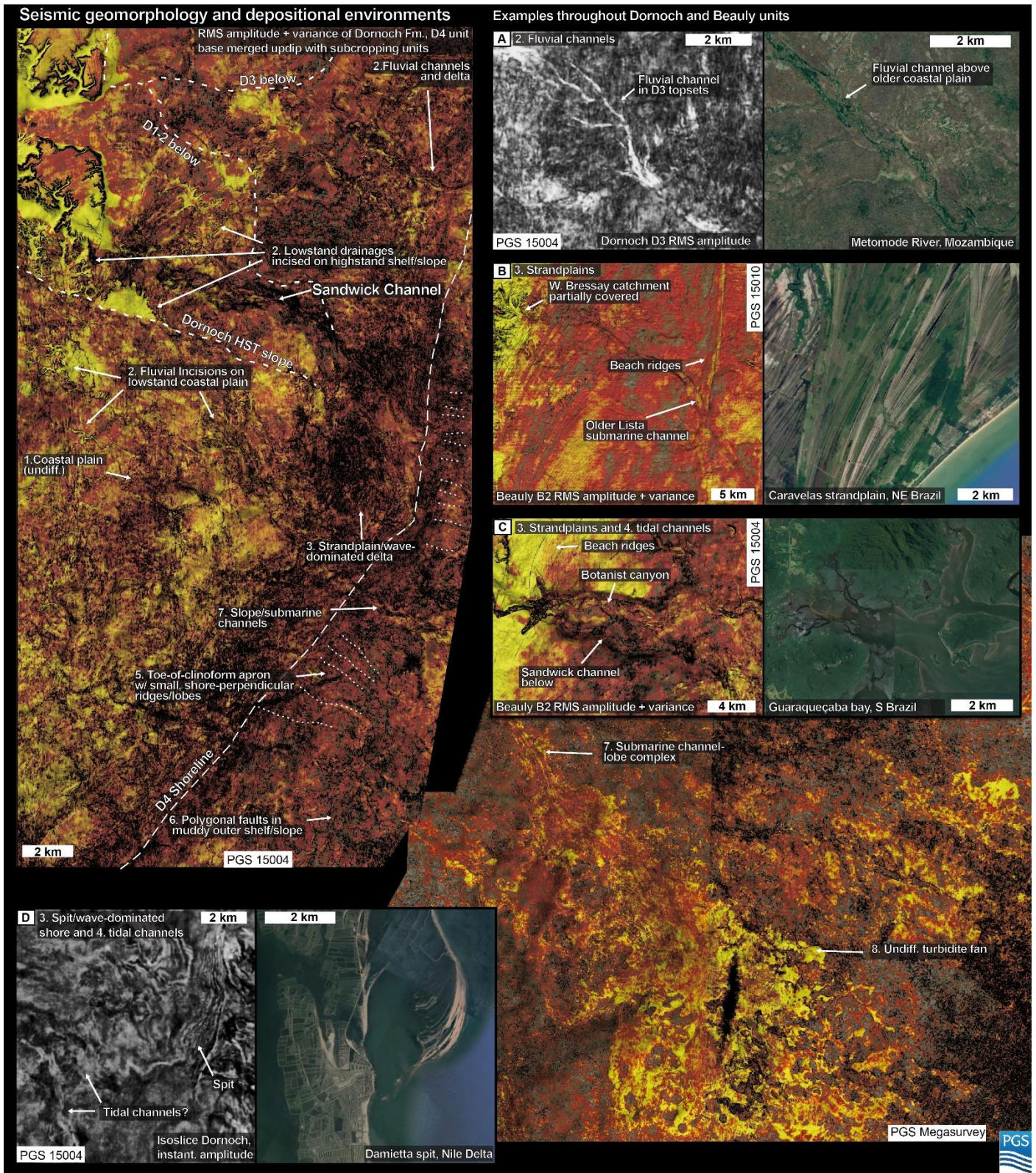2 km — Damietta spit, Nile Delta

Figure 4: Examples of features and depositional environments from seismic geomorphology and various attribute maps. All seismic data in image from PGS.
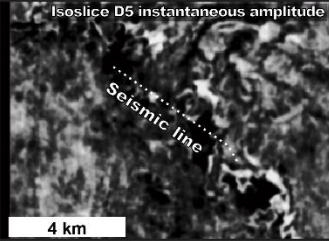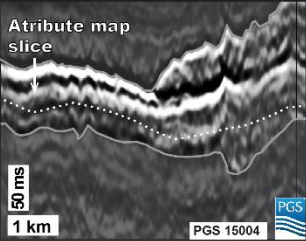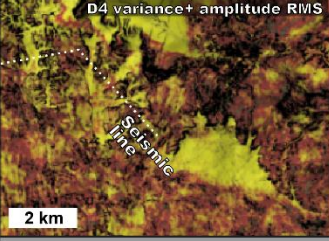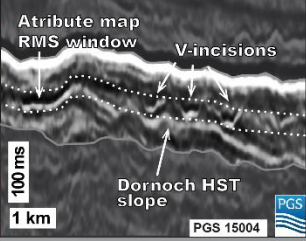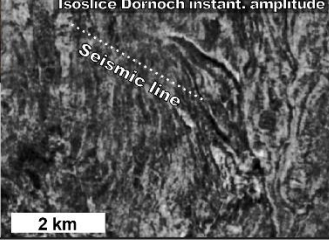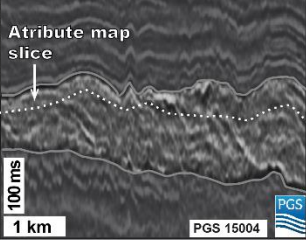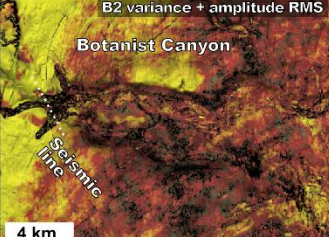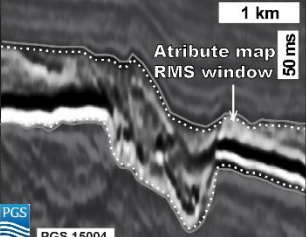
Map view	Line view	Occurence	Description	Observations
1. Undifferentiated coastal plain				
Isoslice D5 instantaneous amplitude · Seismic line · 4 km	Atribute map slice · 50 ms · 1 km · PGS 15004	Dornoch Balder	Map view: dendritic, chaotic or mottled patterns Line view: common high amplitude, continuous reflectors in clinoform topsets, w/ small channel-like forms, truncations	Associated to: Coals (Fig. 14); Smaller, 10-100's m wide channels and incised valleys (fluvial+tidal?); Drainage networks and areas of likely subaerial erosion (Underhill, 2001; Stucky de Quay et al., 2017)
2. Fluvial channel/channel-belt and drainage networks				
D4 variance+ amplitude RMS · Seismic line · 2 km	Atribute map RMS window · V-incisions · 100 ms · Dornoch HST slope · 1 km · PGS 15004	Dornoch Balder	Map view: distinct, linear, meandering or dentritic channels, 10-100's meters wide; Line view: commonly v-shaped incisions, 10's ms deep	Developed above eroded, truncated lowstand clinoform topsets (or HST escarpment); Channels (Fig 4A) connected to updip drainage networks (shown here); Associated to terrigenous organic material in the Bressay Channel (Fig. 14, Stucky de Quay et al., 2017)
3. Wave-dominated shore/strandplain				
Isoslice Dornoch instant. amplitude · Seismic line · 2 km	Atribute map slice · 100 ms · 1 km · PGS 15004	Dornoch Balder	Map view: 100's m wide, 1-5 km long curvi-linear and convex ridges in anastomosing/cross-cutting patterns Line view: delta-scale (10's ms) clinoforms, w/ some lateral variability in thickness and progradation direction	Developed above delta-scale clinoforms; Associated to other coastal plain features; Characteristic shoreface signature in well-logs (UK 8/15-1, 8/30-1, Fig. 14)
4. Tidal channel				
B2 variance + amplitude RMS · Botanist Canyon · Seismic line · 4 km	1 km · Atribute map RMS window · 50 ms · PGS 15004	Dornoch Balder	Map view: 100's m to km wide, 1-30 km long incisions, some in areas of previous delta progradation Line view: incised-valley-like systems, sometimes w/ amplitude anomalies	Developed in sediment starved areas in the Dornoch lowstand (Figs. 6A); Associated to overall transgressive or backstepping trend of the Beauly Mbr (Botanist system, shown here)

Figure 5: Chart showcasing common depositional environments and facies associations referred to in the text and their features in map and line view.

Map view	Line view	Occurence	Description	Observations
5. Toe-of-clinoform apron/fan				
		Dornoch Balder	Map view: <2 km long, shore-perpendicular ridges and lobe-like forms Line view: mound and lobe-like, semi-discontinuous to transparent reflectors	Developed immediatelly downdip of shoreline or shelf-edge; Observed mainly during lowstand progradation and shelf outbuilding with intermittent forced regression or topset bypass
6. Undifferentiated outer shelf to slope/basin				
		Våle Lista Dornoch Balder	Map view: varied, often indistict and low amplitude/variance, polygonal faults easier to recognize Line view: often transparent, sometimes more continuous and low amplitude reflectors w/ soft-sediment faulting	Main environment/bathymetry for Våle and Lista Fm., subdivided where submarine channels and fans are observed (7 and 8 in this table); Bottomsets in Dornoch clinoforms, division between shelf and slope simply based on position of ESP - Viking Graben boundary
7. Submarine channel/channel-lobe system				
		Våle Lista Dornoch Balder	Map view: usually 5-30 km long, 1-5 km-wide meandering channels to lobes, stacked in downdip fans Line view: mound and lobe-like often outlined by amplitude anomalies, internally can be more transparent	Includes individual submarine channels, channel-lobes and complexes; Widely recognized in Paleocene North Sea (Ahmadi et al., 2003; Mudge, 2015)
8. Undifferentiated turbidite fan				
		Våle Lista Dornoch Balder	Map view: 10's km wide and long fan-like areas, individual elements hard to distinguish Line view: similar to item 7, but lengthier (10-40 km) mound or lobe-like forms	Used for areas or intervals where distinction of individual depositional elements is harder

Figure 5: Chart showcasing common depositional environments and facies associations referred to in the text and their features in map and line view.
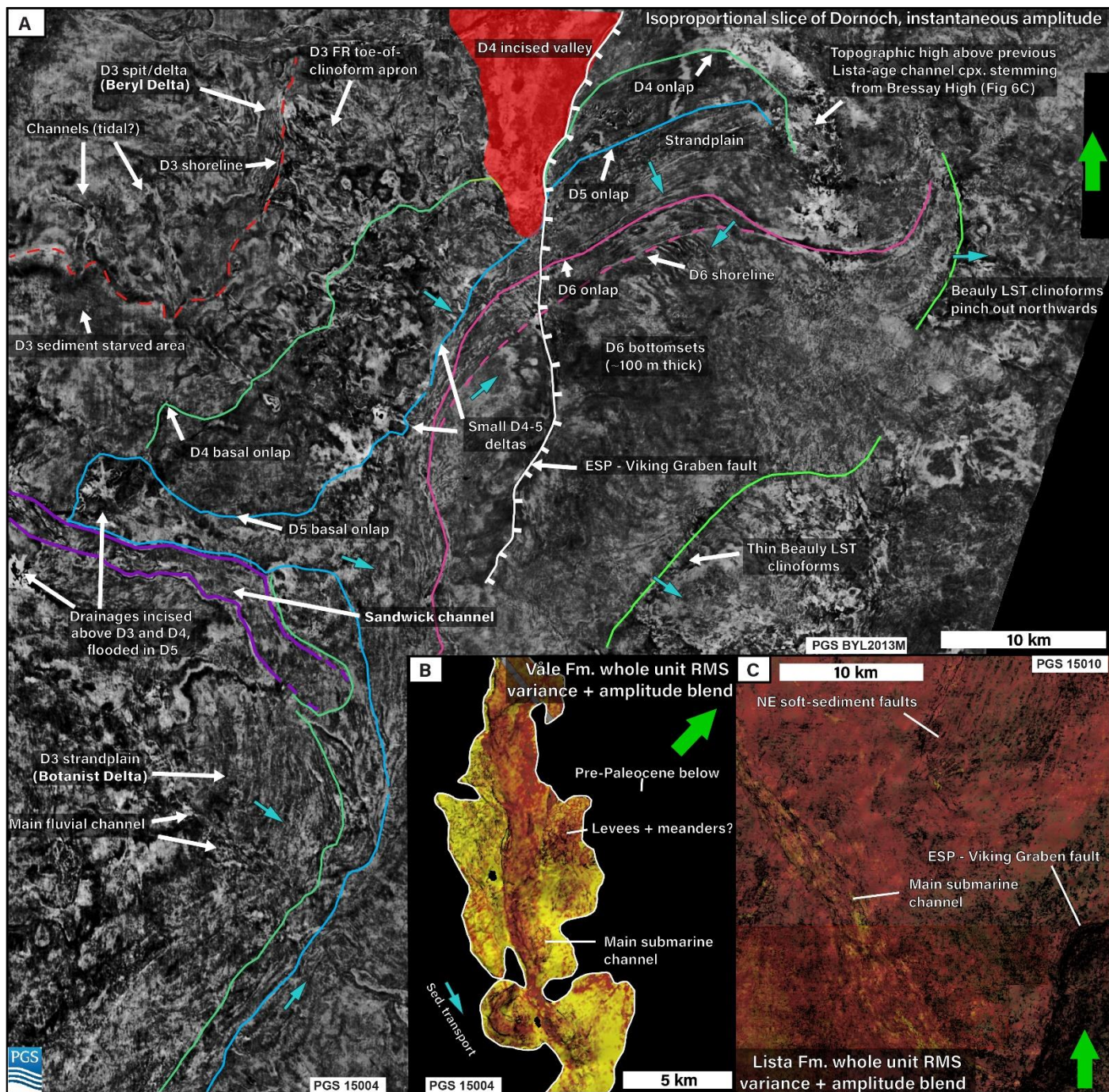
Figure 6: Attribute maps of Paleocene to Early Eocene units. A) Isoproportional slice inside Dornoch, showcasing various depositional environments of D3-D6 close to the Beryl transect and the Beryl Embayment. Blue arrows indicate sediment transport directions. Composite including attribute map of BYL2013M survey, courtesy of PGS. B) Sinuous submarine channel of the Våle Formation above the East Shetland Platform. C) Submarine channel complex inside the Lista Fm in south Bressay. This Lista Fm. channel complex is the same under the topographic high in Figure 6A and 18B. The NE trending features are soft-sediment faults that follow a local Devonian tectonic fabric in the basement (Figure 11).
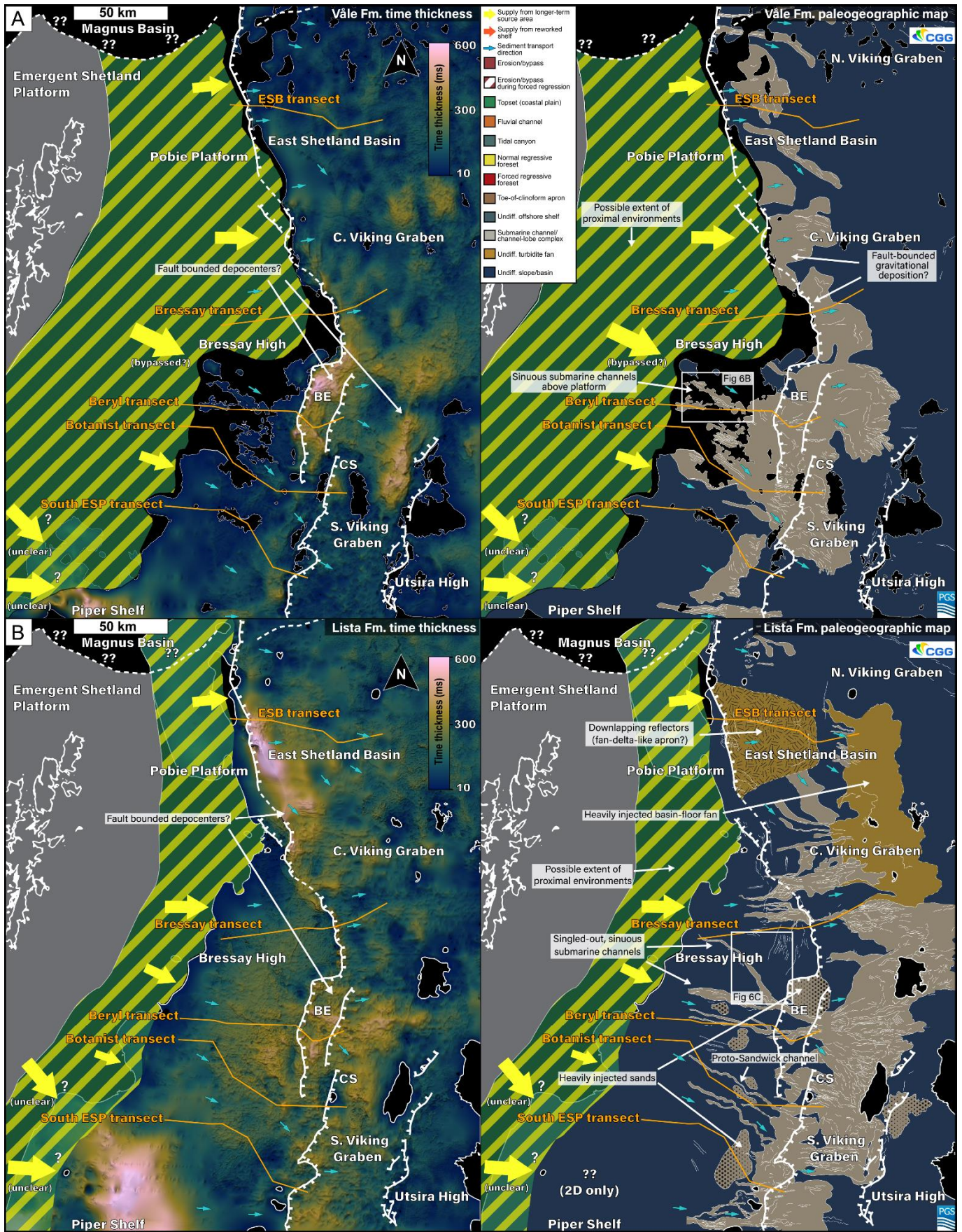
Figure 7: A) Time thickness and paleogeography of Våle Formation. Possible extent of proximal environments is based on the assumption of initially retreated shorelines (Lovell, 2010; Gale and Lovell, 2018) and the overall absence of shoreline/proximal environments where the unit is mapped. Reworked carbonates in Danian V1 unit are not differentiated in this map. B) Time thickness and paleogeography of Lista Formation. Extent of proximal environments is based on the Dornoch shelf width, and is a higher confidence extrapolation than

Våle Fm. However, subaerial exposure or unconformities are not clearly observed in our dataset, and were potentially precluded. Some areas of prominent sediment remobilization are highlighted (stippled polygons), but sand injection and soft-sediment deformation (including polygonal faulting in muddy areas) are ubiquitous inside Lista. BE – Beryl Embayment; CS – Crawford Spur.
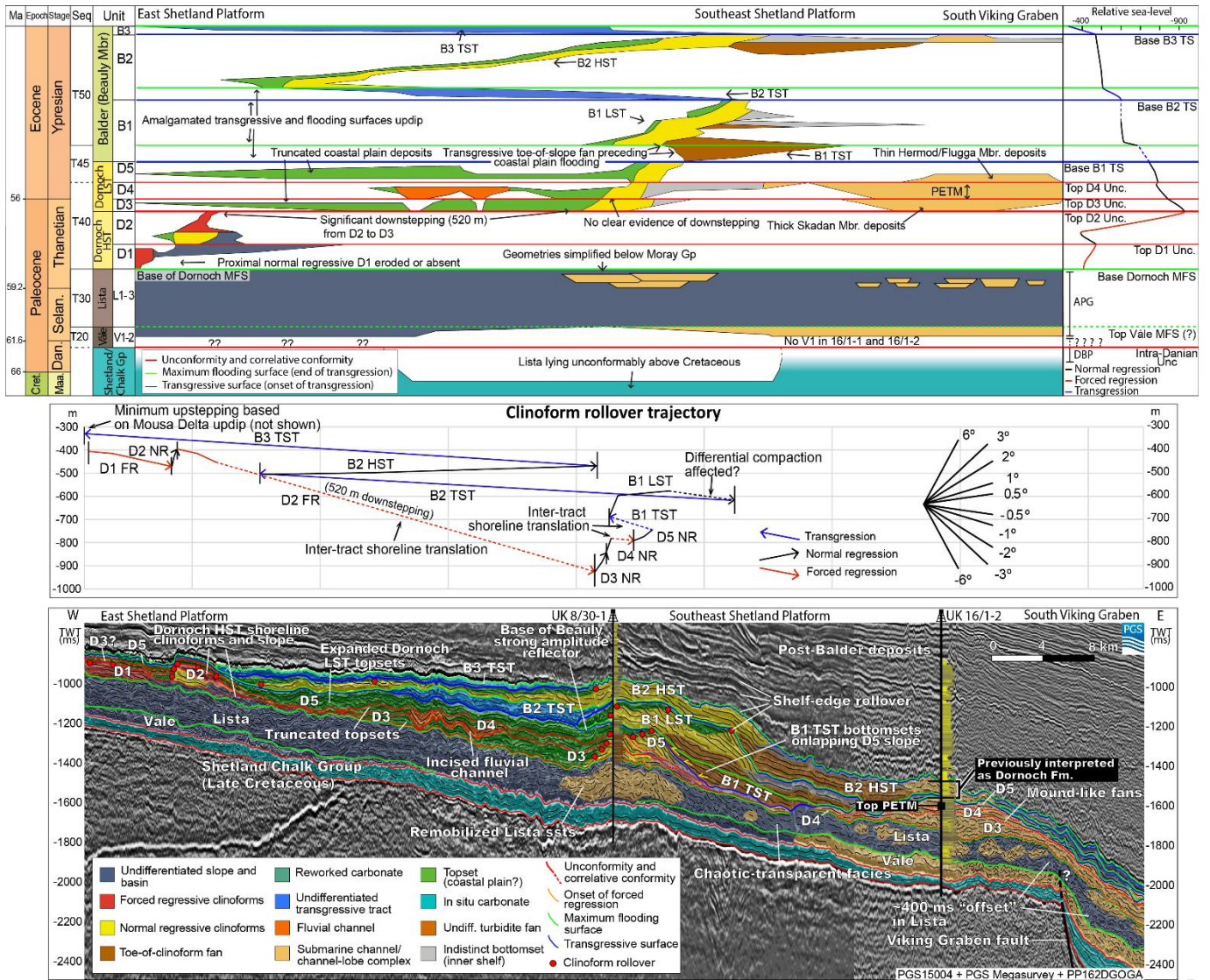
Figure 8: Wheeler chart elaborated in the southern part of the East Shetland Platform. Clinoform rollover trajectories for Figs 8-12 measured in overburden-removed equivalents of same sections (Supp. Material). RSL curve was drawn based on vertical component of rollover trajectory. Absolute values in RSL curve refer to the uncorrected bathymetries obtained from overburden backstripping (see Supp. Material). Geometries shown in Wheeler chart are directly based on reflector geometries and extents observed in seimic. Reflectors were flattened and then used to draw polygons representative of unit and facies belt disposition (matching mapped depositional environments). Trangressive surfaces are only represented where resolvable transgressive tracts are observed (*e.g.* below B1 TST). A characteristic amplitude anomaly is traditionally recognized as the base of the Beauly Member, and can be seen here below the B1 LST. This amplitude anomaly has often been associated with a flooding surface in coal-rich coastal plain deposits (Milton et al., 1990; Brunstad et al., 2013). The interval marked with ticks in well 16/1-2 has been previously interpreted as part of Dornoch Fm. in this and other well reports, but biostratigraphic sampling typically resulted in very poor recovery (sandy interval). Here, it is interpreted as part of the Beauly Mbr based on correlation with its updip counterpart. Finally, the extent of active faulting or compactional folding in Viking Graben fault during the Paleocene is unknown, and offset could be partially or entirely pre-existing. The same is true for all transects in Figures 8-12. APG – Accommodation in platform and graben. DBP – Degradation or bypass in platform.
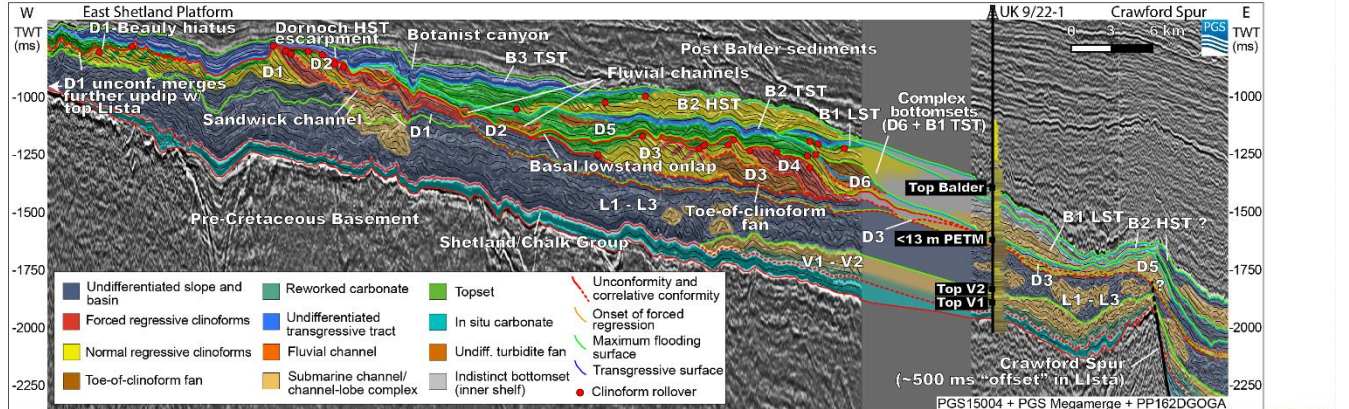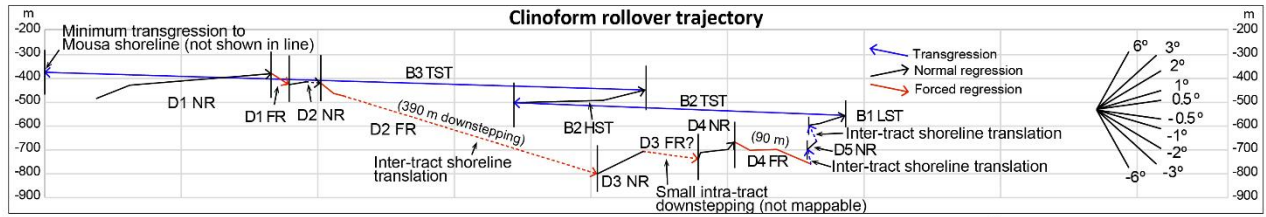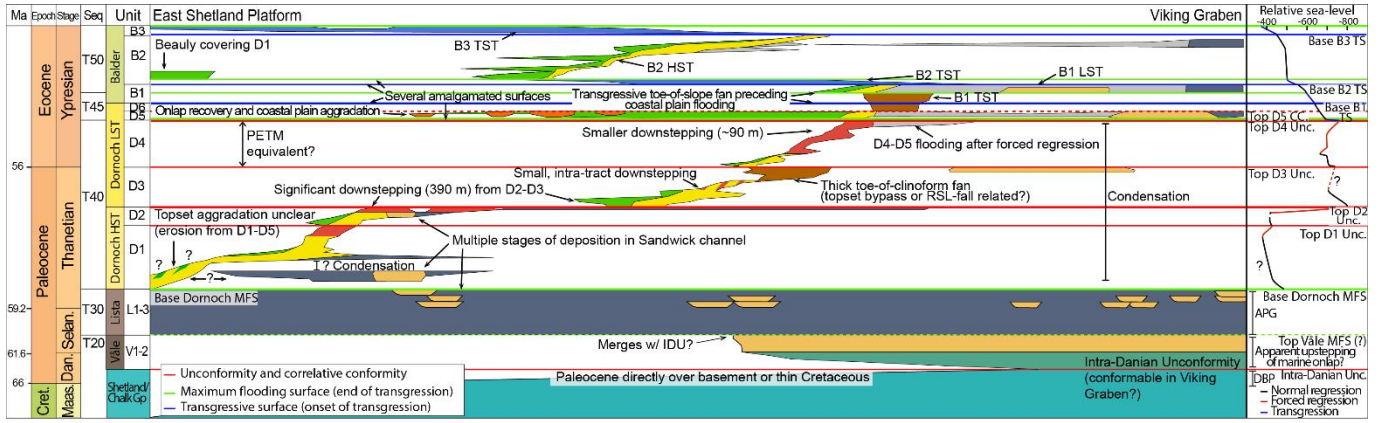
Figure 9: Wheeler chart elaborated on the southern end of the Botanist canyon. Distally, <13 m thick interval with A Augustum (syn-PETM) in well 9/22-1, which is not seismically resolvable in the immediate vicinity or to the east at the Viking Graben. Base of D6 correlative conformity in bottomsets based on mapping and correlation to D6 in the Beryl Embayment (Figure 10). APG – Accommodation in platform and graben. DBP – Degradation or bypass in platform
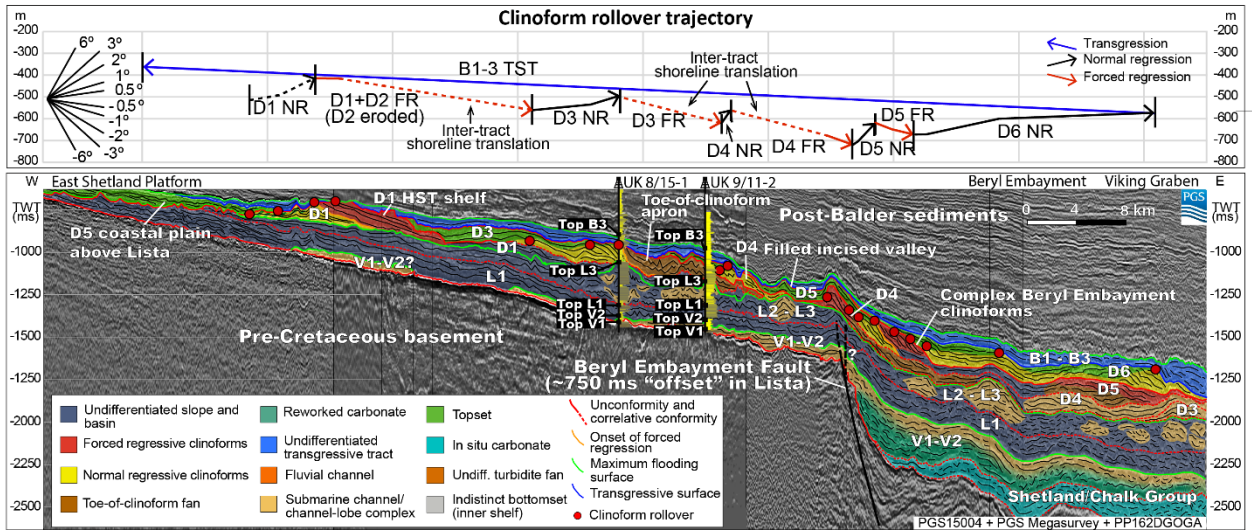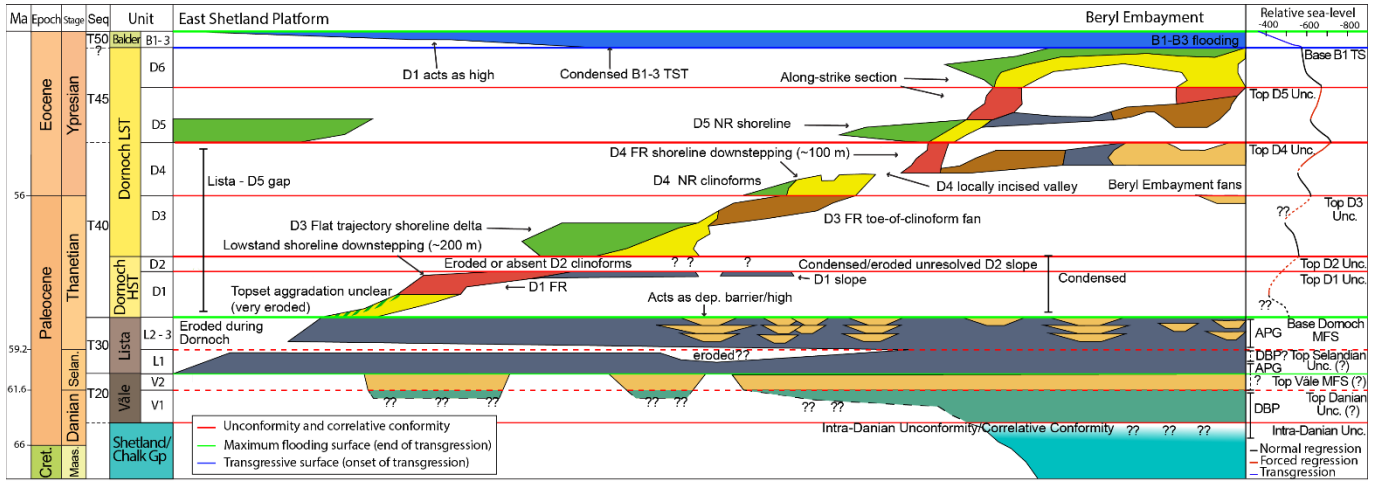
Figure 10: Wheeler chart elaborated north of the Botanist Canyon and south of the Frigg Canyon, encompassing the East Shetland Platform and the Beryl Embayment. Restricted incision during D4 and development of a locally more prominent forced regressive wedge (D4-D5) is noted. A similar interpretation can be seen in Milton and Dyce (1995). B1-B3 here is simply represented as an undifferentiated transgressive tract. Fragmentary evidence of "Top Danian" and "top Selandian" unconformities is indicated by related biostratigraphic gaps in wells in this transect, as well as missing sections or truncations in seismic. APG – Accommodation in platform and graben. DBP – Degradation or bypass in platform.
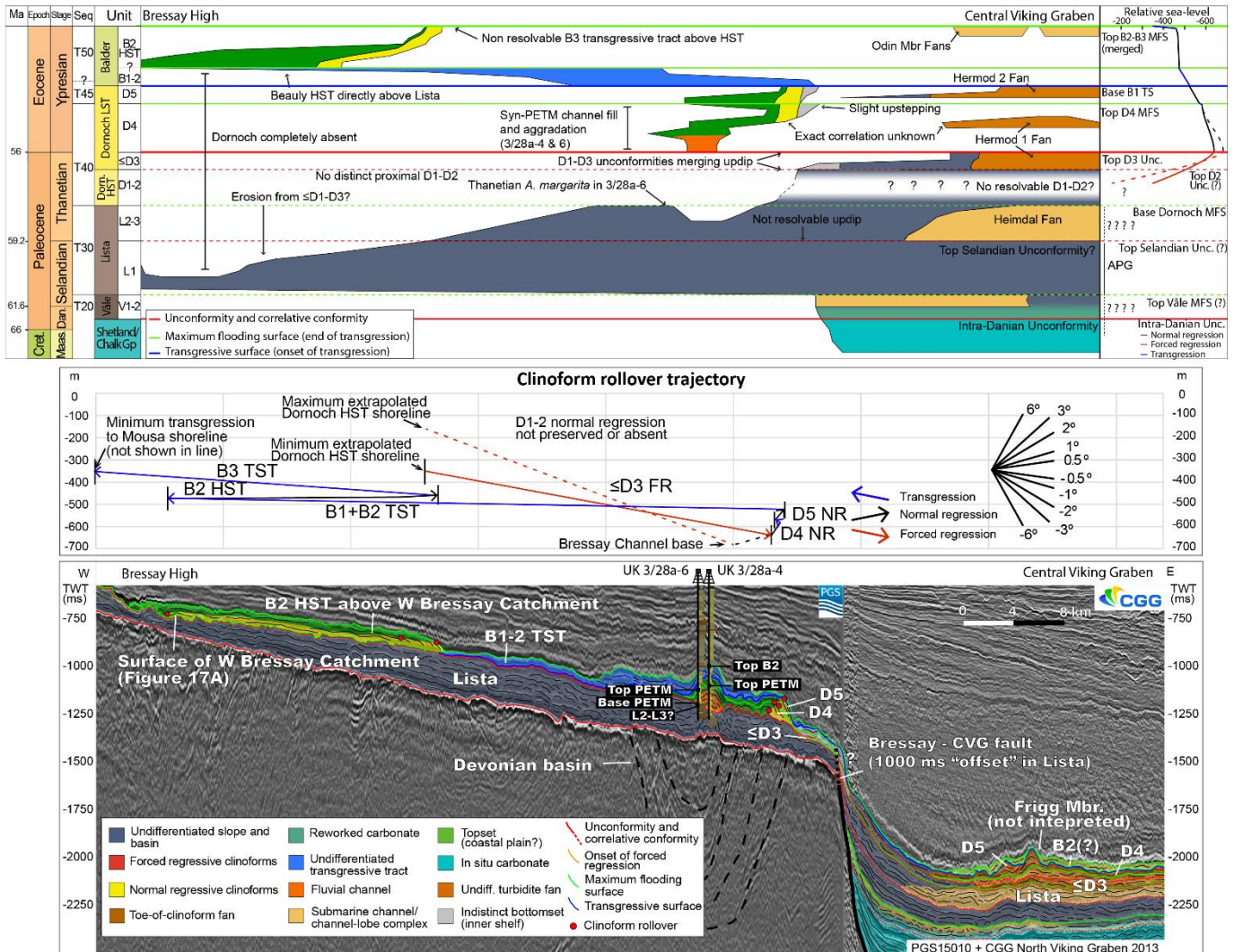
Figure 11: Wheeler chart elaborated in the Bressay High. Initial shoreline rollover before the D2-D3 RSL fall is based on the depth of the W. Bressay Catchment where the Dornoch HST is now eroded (minimum estimate) and a maximum estimate obtained by adding an eroded thickness of ~200 m (based on the thickness of the Dornoch HST elsewhere). Distinction of submarine channel/lobe complexes from «undifferentiated turbidite fans» is based on mapping and seismic attribute analysis (Figures 4-6, 15-16). Presence of a "top Selandian" surface is hinted by the clear distinction between the Heimdal fan and lower Lista Fm. in the Viking Graben. APG – Accommodation in platform and graben.
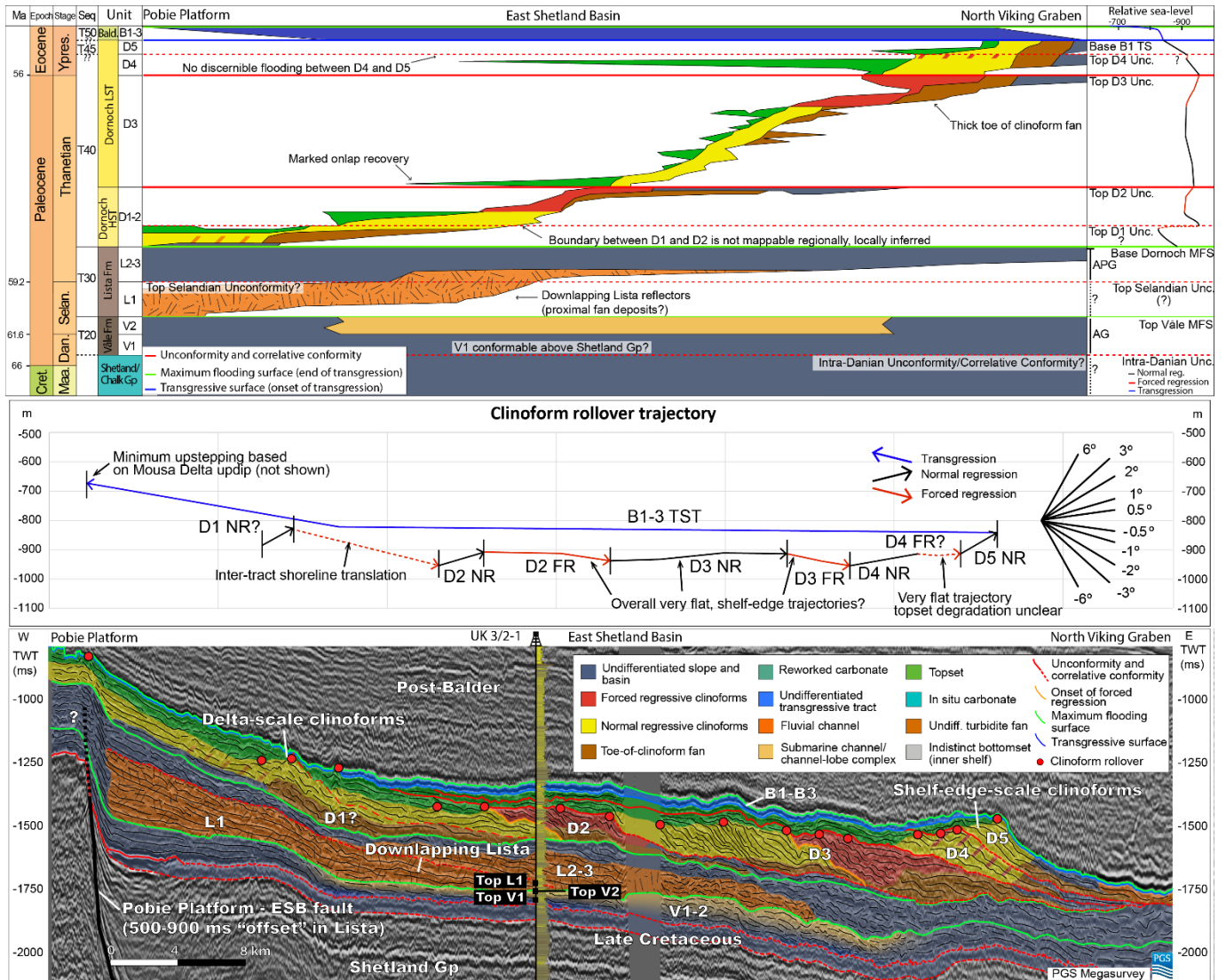
Figure 12: Wheeler chart elaborated in the East Shetland Basin. It was not possible to subdivide D1-D2 systematically in this area, but a tentative division is shown in this figure. Presence of a "top Selandian" unconformity or surface is hinted by the geometry of downlapping L1 reflectors (Selandian), which appear to be truncated or onlapped upon by L2-3 (Thanetian). AG – Accommodation in graben; APG – accommodation in platform and graben.

Along-strike rollover trajectory comparison
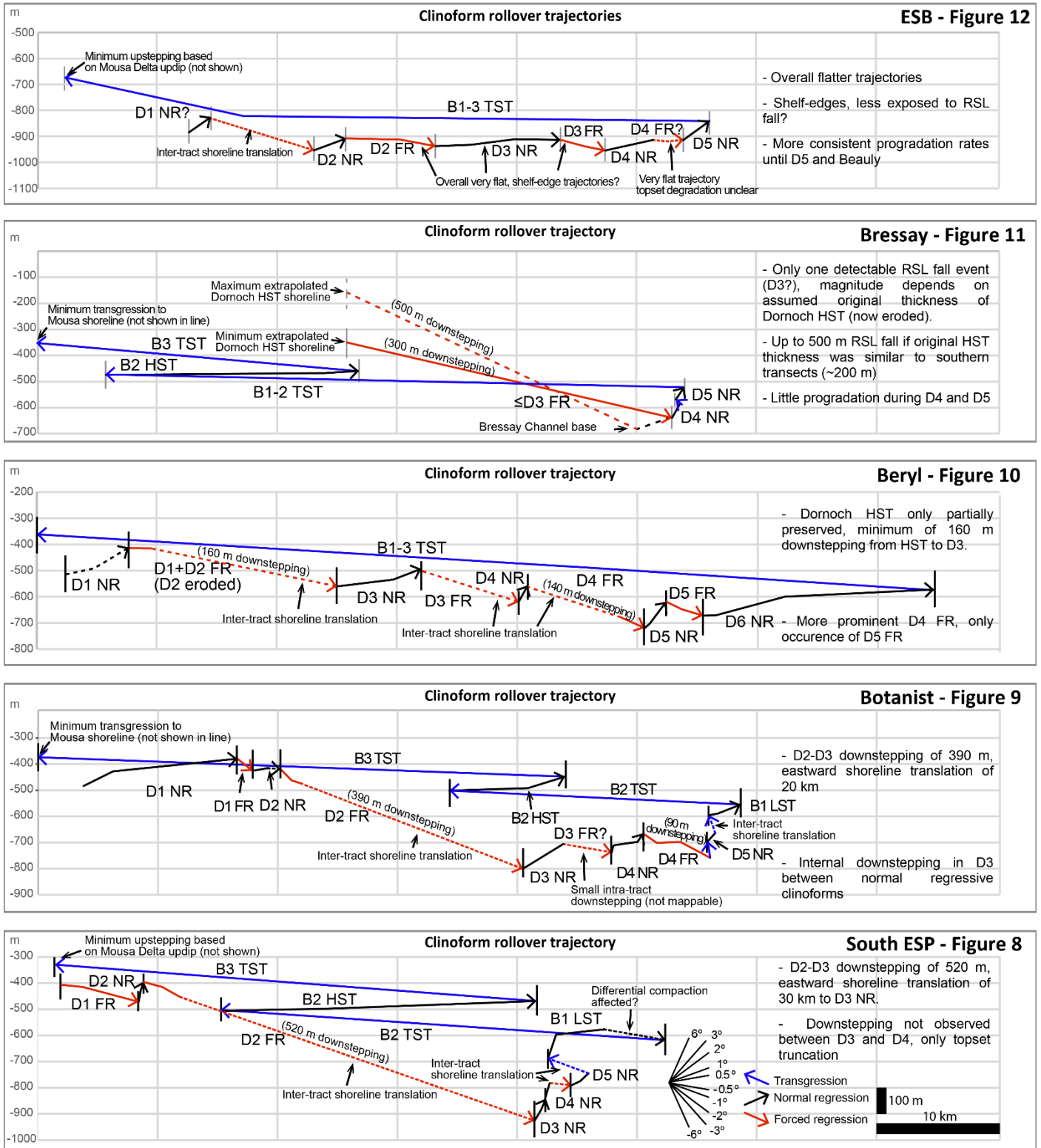
Figure 13: Comparison of shoreline or clinoform rollover trajectories measured for the transects of Figures 8 – 12. All plots have the same scale. Absolute values in meters refer to the uncorrected bathymetries obtained from overburden backstripping (Supp. Material).
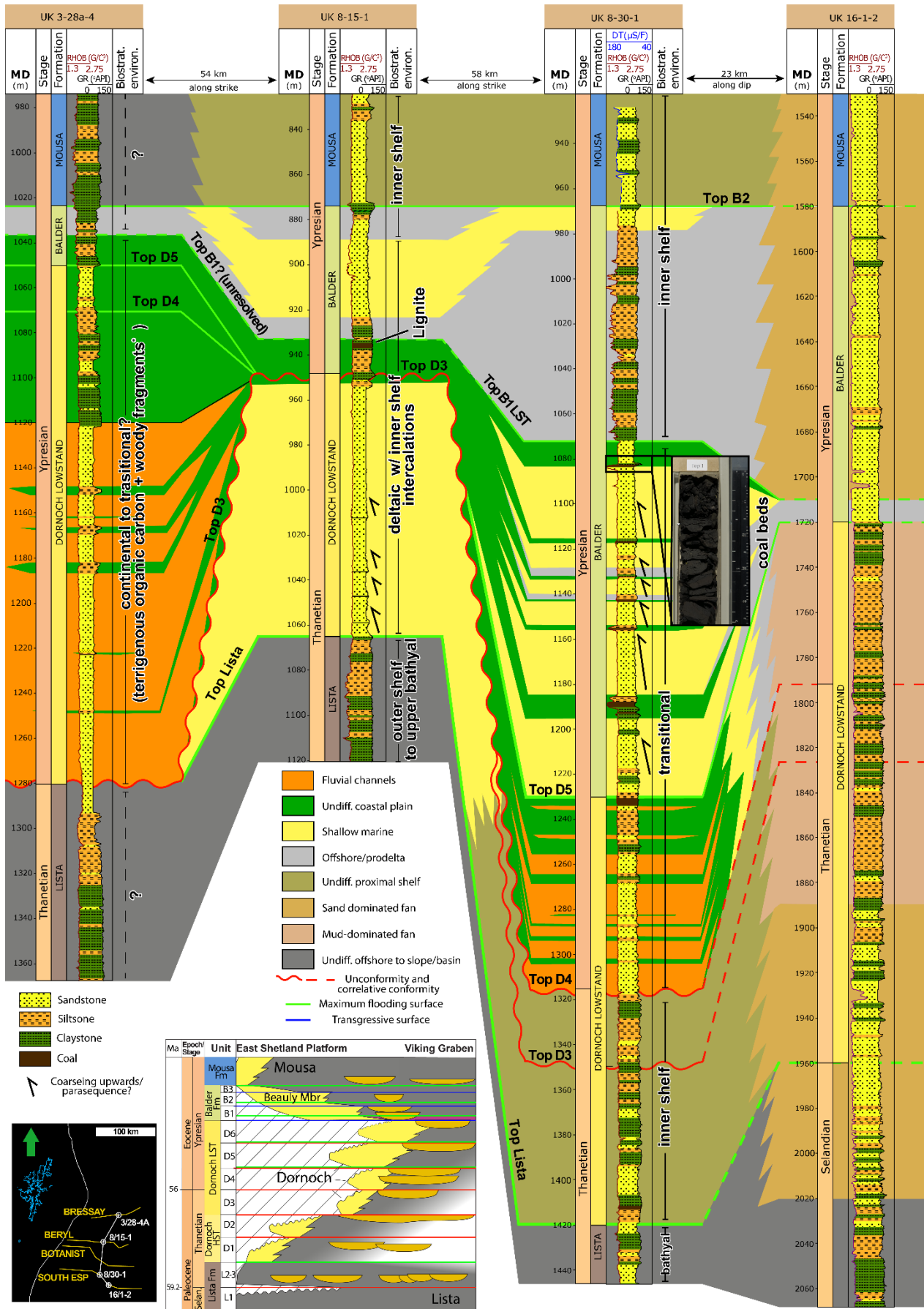
Figure 14: Correlation of key wells and interpretation of depositional environments, which was integrated with data from seismic and well reports. Higher resolution subdivisons are possible when compared to seismic. Paleontological constraints for environments taken from well reports, except for *, which is based on Underhill (2001) and Stucky de Quay et al., (2017).

A

50 km

Magnus Basin

?? ?? ??

Emergent Shetland Platform

D1 and D2 undivided

? (not mapped)

Pobie Platform

ESB transect

East Shetland Basin

D1 time thickness

N

Time thickness (ms)

200
100
10

Pre-D3 Hermod fan? (not imaged)

??
??

D1 and D2 eroded

? (eroded)

? (not mapped)

Bressay transect

C. Viking Graben

??

D1 shelf (and later escarpment)

Bressay High

Beryl transect

Botanist transect

BE

D1 unconformity

CS

South ESP transect

S. Viking Graben

Piper Shelf D1 clinoforms

Utsira High

Piper Shelf

D1 paleogeographic map

CGG

?? ??

N. Viking Graben

? (not mapped)

Pobie Platform

ESB transect

East Shetland Basin

Extrapolated shoreline

??
??

? (eroded)

? (not mapped)

Bressay transect

C. Viking Graben

??

Lateral truncation of HST shelf

Bressay High

Submarine channel

Beryl transect

Botanist transect

BE

Sandwick channel

CS

South ESP transect

S. Viking Graben

Utsira High

Piper Shelf

PGS

Legend:
- Supply from longer-term source area
- Supply from reworked shelf
- Sediment transport direction
- Erosion/bypass
- Erosion/bypass during forced regression
- Topset (coastal plain)
- Fluvial channel
- Tidal canyon
- Normal regressive foreset
- Forced regressive foreset
- Toe-of-clinoform apron
- Undiff. offshore shelf
- Submarine channel/channel-lobe complex
- Undiff. turbidite fan
- Undiff. slope/basin

B

50 km

Magnus Basin

?? ??

Emergent Shetland Platform

D1 and D2 undivided

Pobie Platform

ESB transect

East Shetland Basin

D2 time thickness

N

Time thickness (ms)

200
100
10

D1 and D2 eroded

? (eroded)

? (not mapped)

Pre-D3 Hermod fan? (not imaged)

C. Viking Graben

Bressay transect

? (eroded)

Bressay High

Beryl transect

BE

Botanist transect

D2 unconformity

CS

South ESP transect

S. Viking Graben
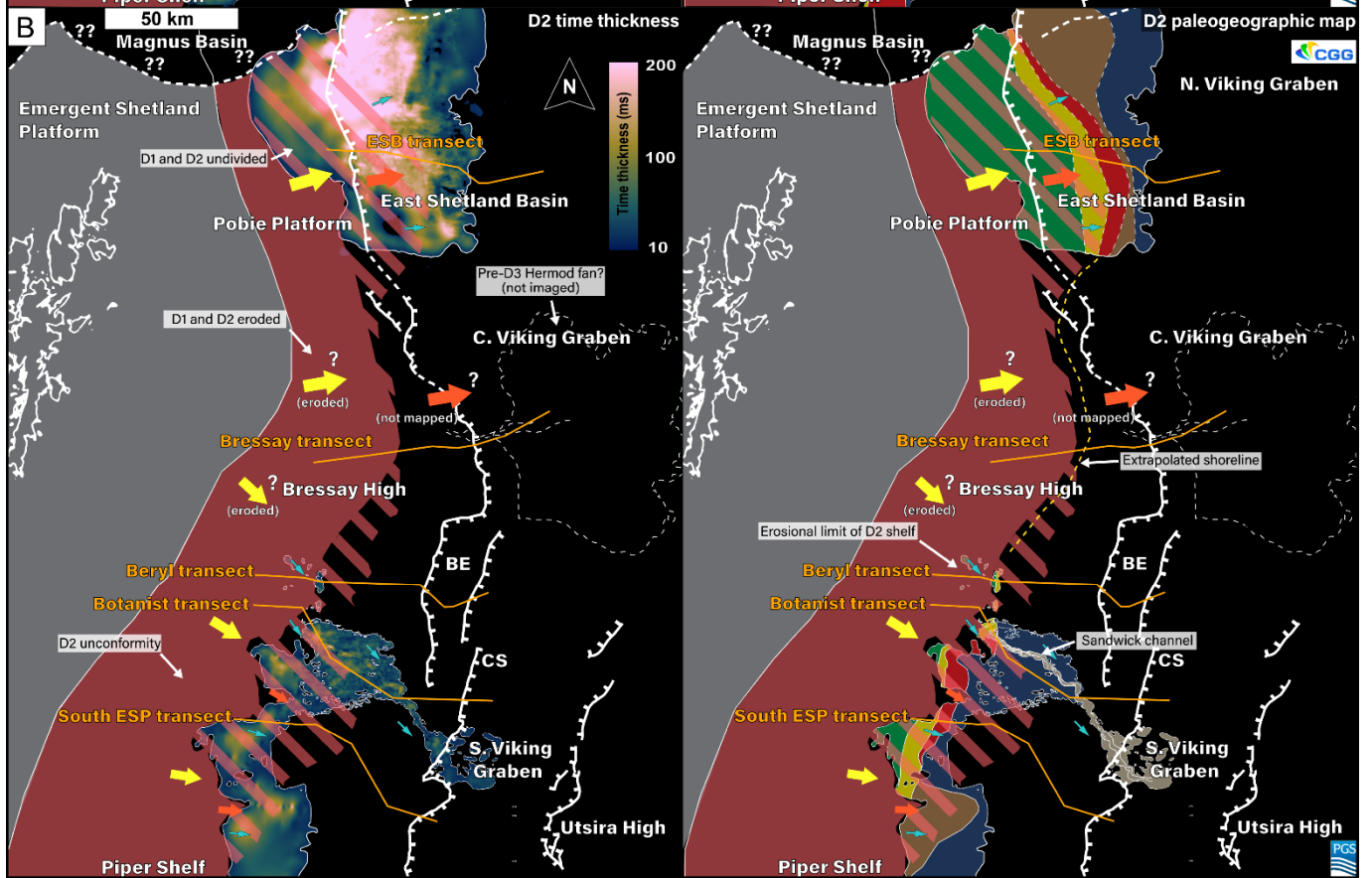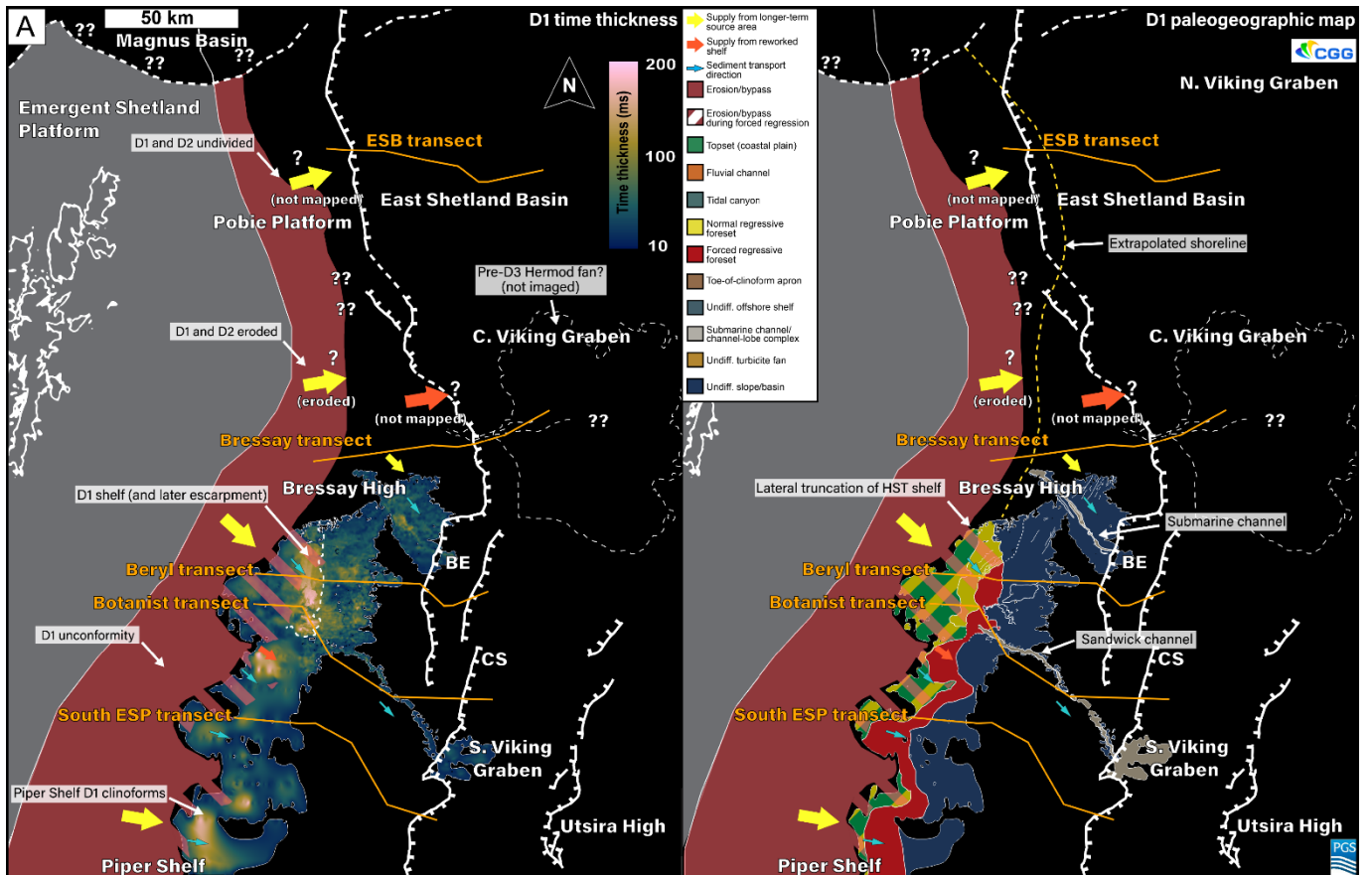
Utsira High

Piper Shelf

D2 paleogeographic map

CGG

?? ??

N. Viking Graben

Emergent Shetland Platform

Pobie Platform

ESB transect

East Shetland Basin

? (eroded)

? (not mapped)

C. Viking Graben

Bressay transect

Extrapolated shoreline

? (eroded)

Bressay High

Erosional limit of D2 shelf

BE

Beryl transect

Botanist transect

Sandwick channel

CS

South ESP transect

S. Viking Graben

Utsira High

Piper Shelf

PGS

C — D3 time thickness

Magnus Basin ?? ??
Emergent Shetland Platform
50 km
D3 time thickness

Legend:
- Supply from longer-term source area
- Supply from reworked shelf
- Sediment transport direction
- Erosion/bypass
- Erosion/bypass during forced regression
- Topset (coastal plain)
- Fluvial channel
- Tidal canyon
- Normal regressive foreset
- Forced regressive foreset
- Toe-of-clinoform apron
- Undiff. offshore shelf
- Submarine channel/channel-lobe complex
- Undiff. turbidite fan
- Undiff. slope/basin

Time thickness (ms) — 200, 100, 10

ESB transect
ESB depocenter
East Shetland Basin
Pobie Platform
C. Viking Graben
Bressay transect
Bressay High
Beryl transect
Botanist transect
Beryl and Botanist depocenters
BE
CS
South ESP transect
D3 unconformity
S. Viking Graben
Utsira High
Piper Shelf

D3 paleogeographic map

Magnus Basin ?? ??
Emergent Shetland Platform
N. Viking Graben
ESB transect
East Shetland Basin
Pobie Platform
Redeposition in wide T40 Hermod fan
C. Viking Graben
Dornoch Fm absent in W Bressay Catchment
D1 – D3 erosion in and near Bressay Channel
Fig 17C
Bressay transect
Bressay High
Beryl delta offlapping on HST shelf
Beryl transect
Sediment starved south of delta
BE
Fig 6A
Botanist transect
Emergent Dornoch HST slope segmenting lowstand
Main fluvial channel and strandplain in Botanist delta
CS
South ESP transect
S. Viking Graben
Utsira High
Skadan Mbr. channel-lobe complex
Piper Shelf
CGG   PGS

D — D4 time thickness

Magnus Basin ?? ??
Emergent Shetland Platform
50 km
D4 time thickness

Time thickness (ms) — 200, 100, 10

ESB transect
ESB depocenter
East Shetland Basin
Pobie Platform
C. Viking Graben
NO 30/7-7
NO 30/11-5
UK 3/28a-6
UK 3/28a-4
Bressay transect
Bressay High
Beryl Embayment depocenter
Beryl transect
Thinning due to FR erosion
Botanist transect
D4 unconformity
BE
CS
UK 9/22-1
South ESP transect
S. Viking Graben
UK 16/1-2
Utsira High
Piper Shelf

D4 paleogeographic map

Magnus Basin ?? ??
Emergent Shetland Platform
N. Viking Graben
ESB transect
East Shetland Basin
Pobie Platform
C. Viking Graben
Onlap recovery and coastal plain aggradation
Bressay transect
Bressay High
Normal regression only
Beryl Embayment incised valley
Beryl transect
Beryl small deltas (Fig 6A)
BE
Fig 6A
Botanist transect
Multiple fluvial channels and drainages
Wider strandplain and forced regressive wedge
CS
Small forced regressive wedge
South ESP transect
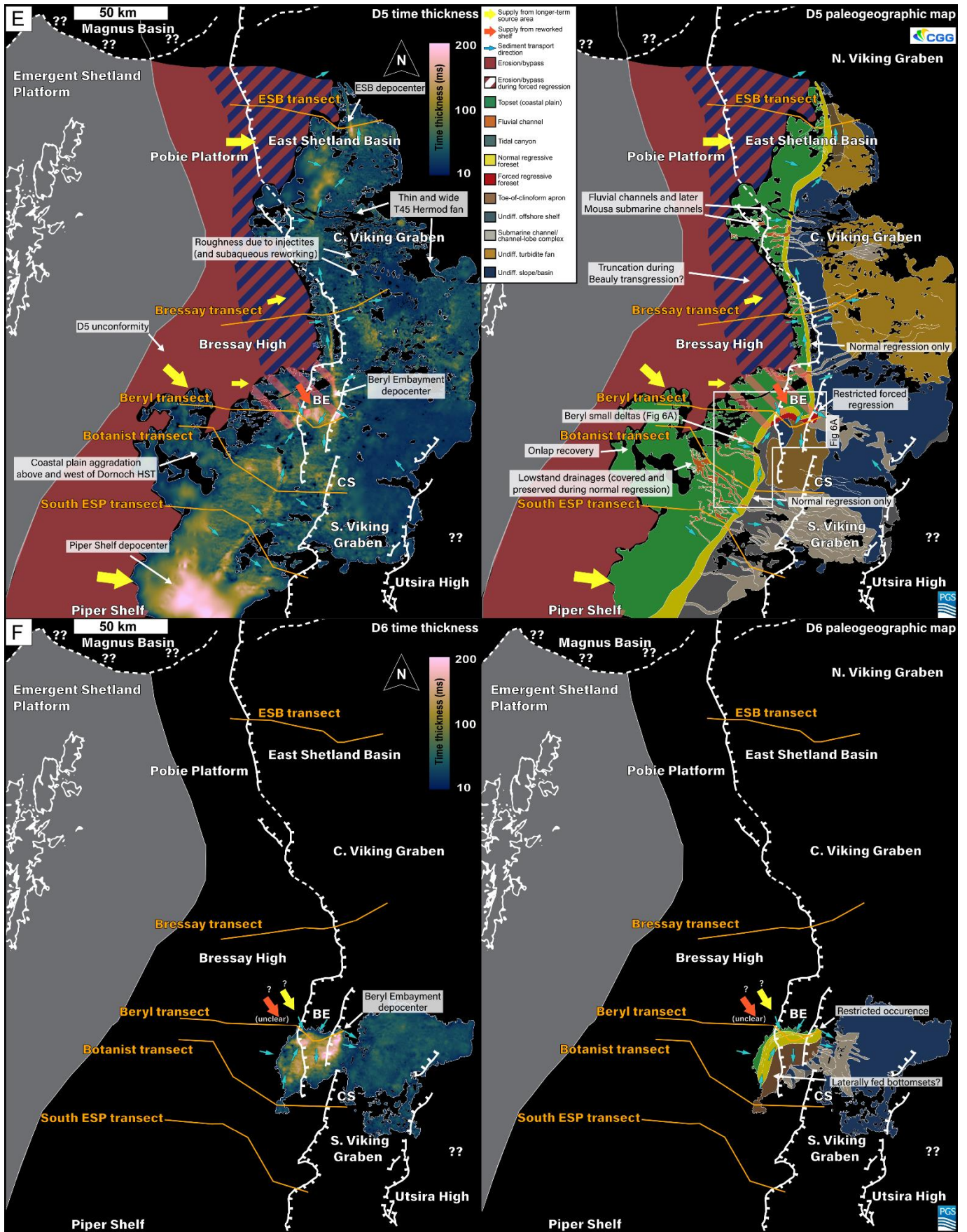S. Viking Graben
Utsira High
Piper Shelf
CGG   PGS

Figure 15: Maps of Dornoch Formation. The grey polygon represents an area emerged during deposition of all the Moray Group, while the red "erosion/bypass" polygons mark the extent of the coastal onlap/offlap mapped for each unit (regardless of normal or forced regression). Hatched red polygons refer to areas of additional erosion updip of forced regressive offlaps (may include upstream-controlled erosion). A) Time thickness and paleogeography of D1. B) Time thickness and paleogeography of D2. D1 and D2 correspond to

a lower-order Dornoch highstand. Mapped portion of the ESB corresponds to undivided, pre-D3 Dornoch. For D2, the hatched erosion polygon represents the total extent of erosion during forced regression, which covers a significant portion of the unit. This was mapped by using the extent of the lowstand D3 shoreline to the east of the D2 shelf and slope. Both D1 and D2 are not preserved in the Bressay high and are likely condensed in most of the Viking Graben. However, in the Central Viking Graben, it is possible that pre-D4 deposits include reworked D1-D2 sediments that were removed from the Bressay High during continuous D1-D3 erosion (not resolvable currently). C) Time thickness and paleogeography of D3, the first lowstand unit. Dornoch deposits are relatively transparent in seismic to the east of the Beryl Embayment, with homogeneous thicknesses across a relatively large area, which means they are not easily subdivided in seismic there. D) Time thickness and paleogeography of D4. This unit is partially or totally coincident with the PETM (key wells where *A. augustum* are detected are shown in the time thickness map). Units D1-D4 correspond to T40 in the BP scheme. E) Time thickness and paleogeography of D5, the last regional lowstand unit, which corresponds to post-PETM Dornoch (~T45 in BP scheme). Hatched blue polygon represents the area where D5 is truncated by transgressive Beauly deposits. F) Local unit D6.
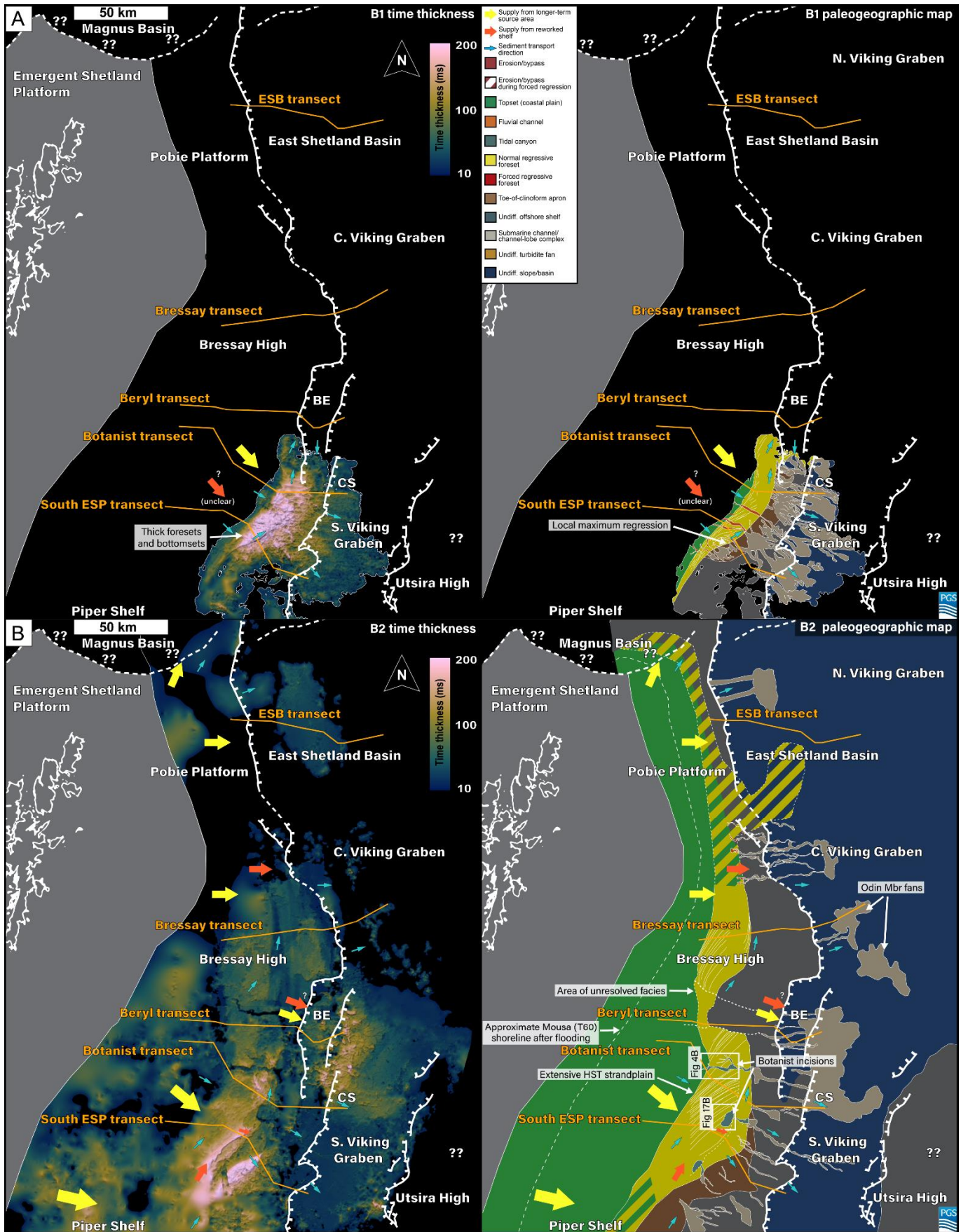
Figure 16: Maps of Balder Formation. A) Time thickness and paleogeography of the B1 lowstand. B) Time thickness of B2 including an undifferentiated thin B3, and paleogeography of B2 HST. Unit is interpreted to be present even in areas with no resolvable seismic thickness. From D6 to B3, depocenters and bottomsets shift towards the south. BE - Beryl Embayment; CS – Crawford Spur.
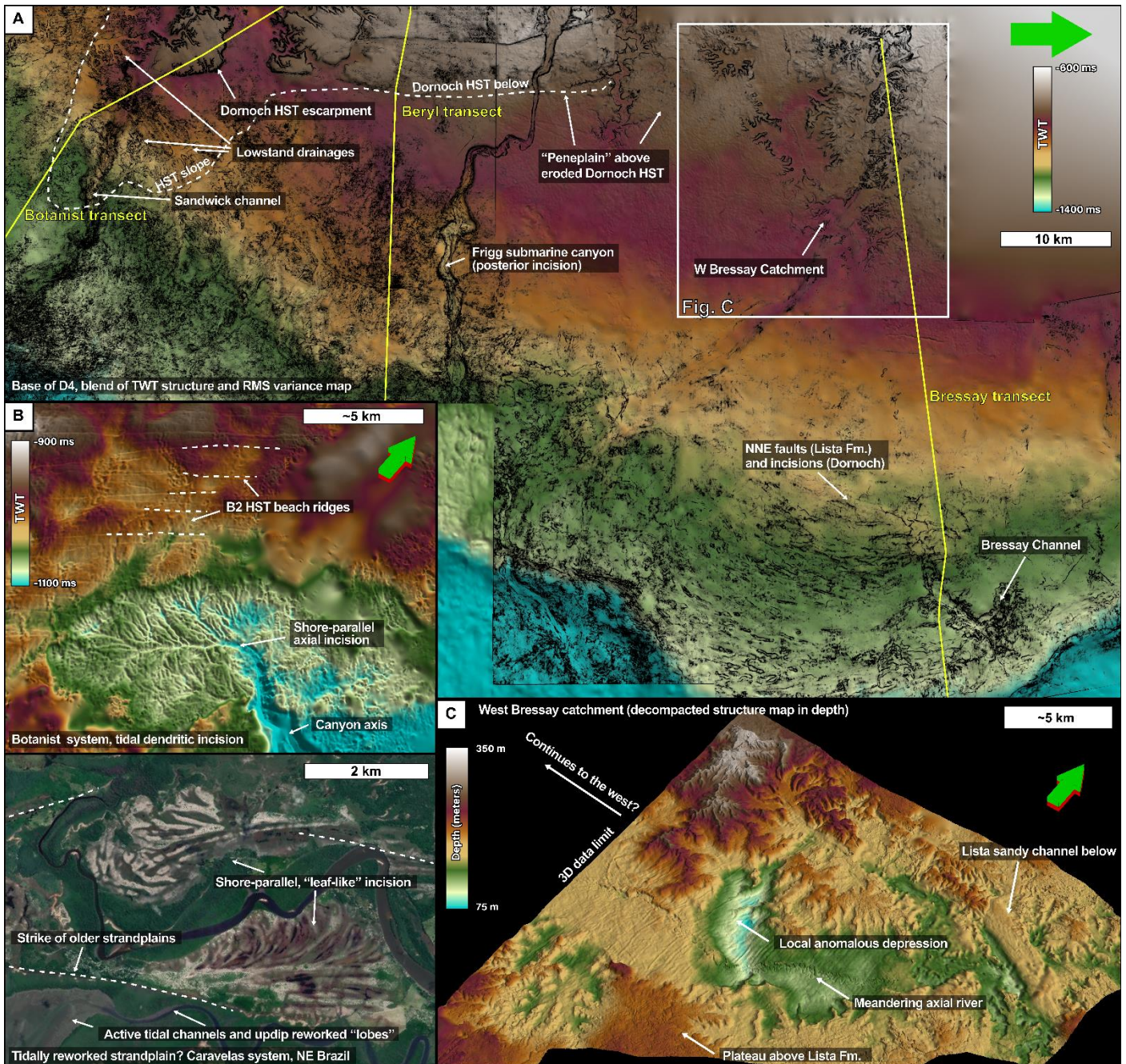
Figure 17: Structure maps showcasing erosional features around the ESP. A) Structure map and variance RMS blend of the base of the D4 merged with the top of underlying units (including the Dornoch HST, and the top of Lista). Location shown in Figure 1A. B) 10 km wide dendritic network in Botanist, interpreted to be tidal in origin. Above Top of Balder Fm. Modern analogue is system of tidal channels in the Caravelas strandplain system, NE Brazil. C) Structure map of the Western Bressay catchment after depth conversion and decompaction. Relief values after the minimum addition of 350 m to correct for subaerial bathymetries in the Upper Dornoch Fm – Beauly Mbr (*e.g.* Milton et al., 1990; Nadin et al., 1997; Roberts, 2019 - see Supplementary Material). Location also shown in Figure 12C.
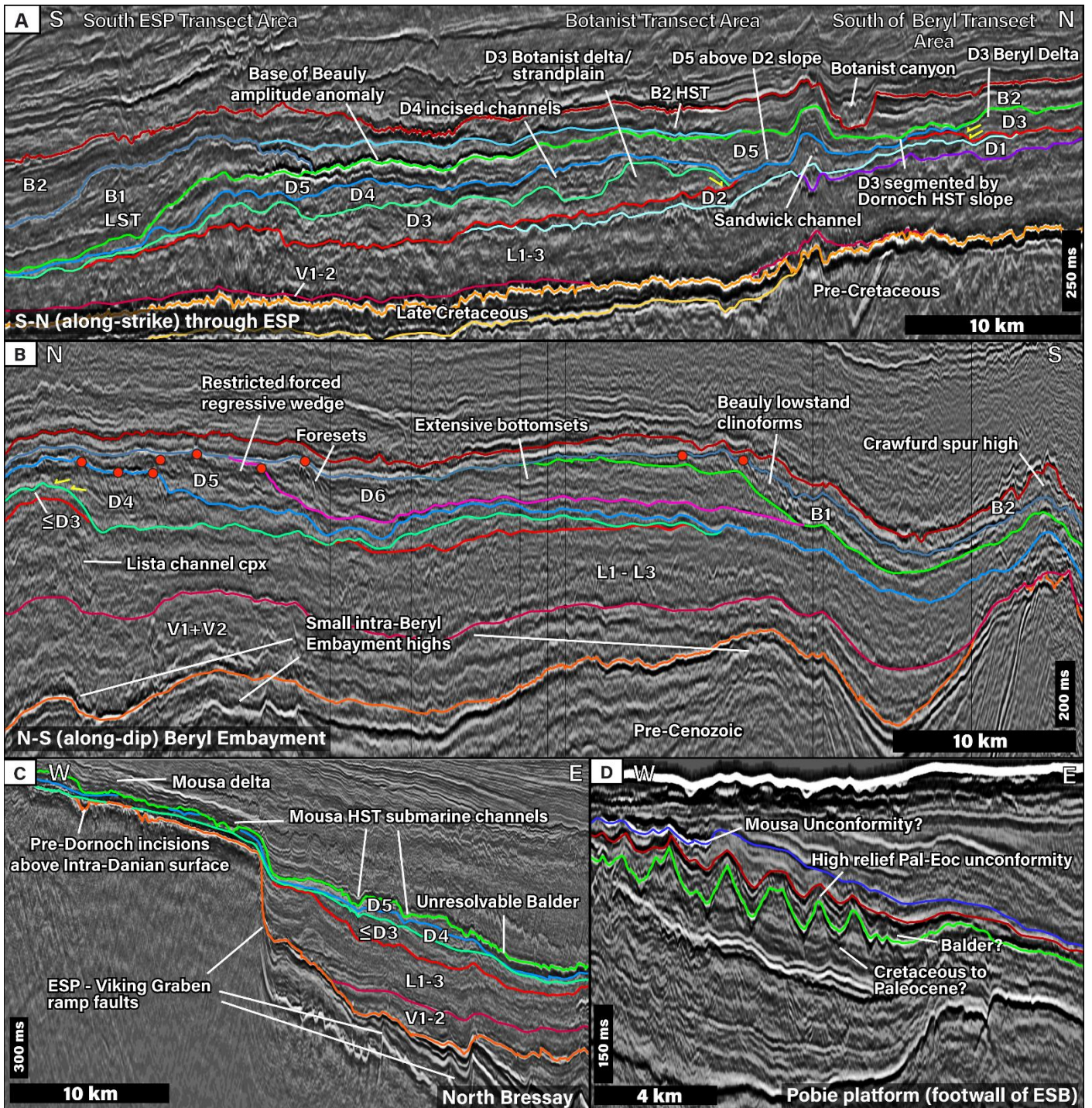
Figure 18: Additional seismic lines, locations in figure 1A. A) Along-strike, south-to-north line from the South ESP (where the locally thick B1 LST can be observed) to the south Beryl transect area. Close to the Sandwick Channel, lateral terminations of the D3 deltas are noticed (yellow arrows), consistent with segmentation of the lowstand shore by an emergent remnant of the highstand slope in this area. B) N-S line (along-dip) in the Beryl embayment, showing the local development of D4 RSL fall (leading to downstepping towards D5. red circles are clinoform rollovers). Smaller scale downstepping during D5 is connected to the local development of D6, which includes extensive bottomsets, succeeded by a B1 lowstand clinoform. C) Northern Bressay, where Eocene Dornoch (D4 and D5) covers thin to absent Paleocene deposits updip of the local ESP fault-boundary. Incision above the Intra-Danian surface match channels observed in Stucky de Quay and Roberts (2022). D) Erosional relief observed in a Paleocene (?) surface in the Pobie Platform, updip of the East Shetland Basin.
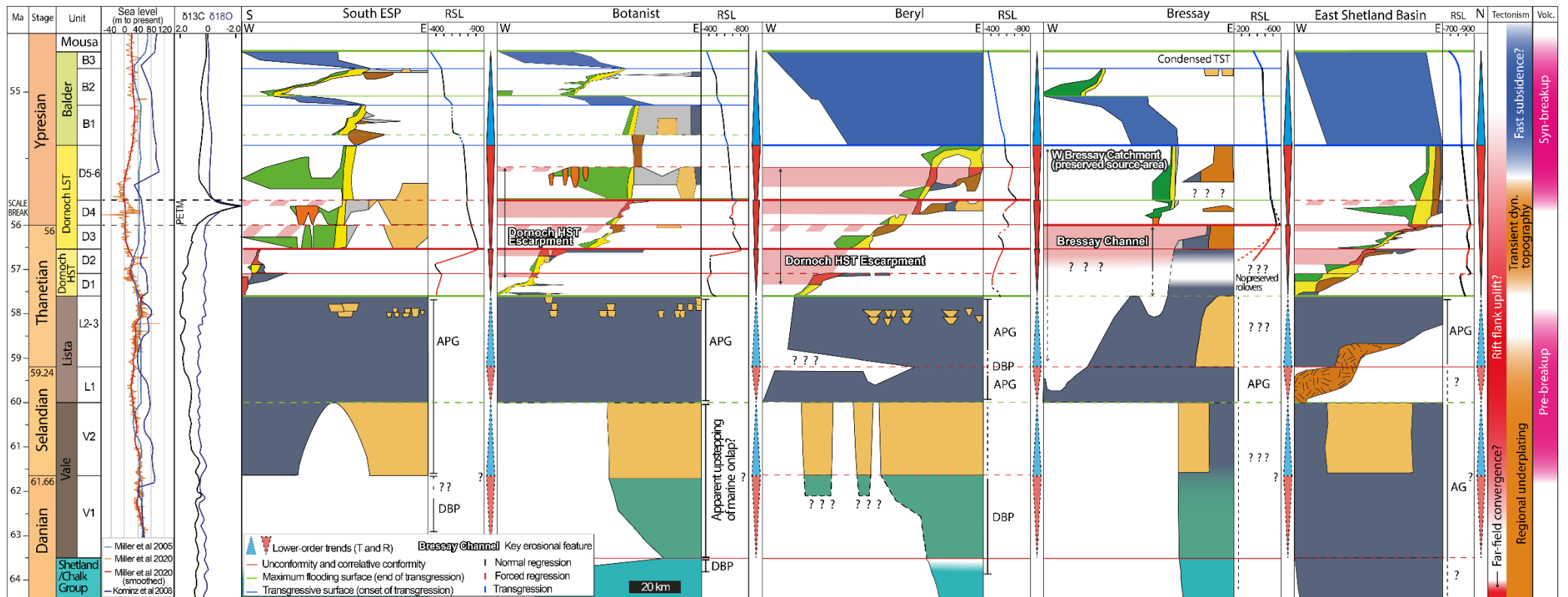
Figure 19: Comparison of Wheeler diagrams and RSL curves from south to north, with vertical scale in Myr. Development of forced regressive wedges, unconformities, transgressive tracts and flooding surfaces is notably varied along-strike. Before the Dornoch progradation, all changes in onlap are interpreted to represent shifts in submarine depositional trends, which cannot be confidently used to track RSL changes and development of subaerial unconformities. In Dornoch, pre-PETM unconformities (D1-D3) appear to increase in expression towards the north. In the south ESP, lowstand unconformities in general are observed, but clear forced regressive wedges are almost absent. The D2-D3 transition is the dominant RSL-fall event, as in Botanist and Beryl. In Beryl, it includes further erosion of D2, and the unit is not resolvable, and in general this episode of RSL fall was fast enough to incur in a significant shoreline translation towards the Dornoch lowstand. Pre-PETM unconformities completely merge in Bressay, where a binary pre-PETM degradation and post-PETM aggradation system is developed. South of Bressay, intermittent forced regression and alternation between topset aggradation and degradation occur. Post-PETM unconformities are more prominent in Beryl. AG – Accommodation in graben; APG – accommodation in platform and graben; DBP – degradation in the platform.
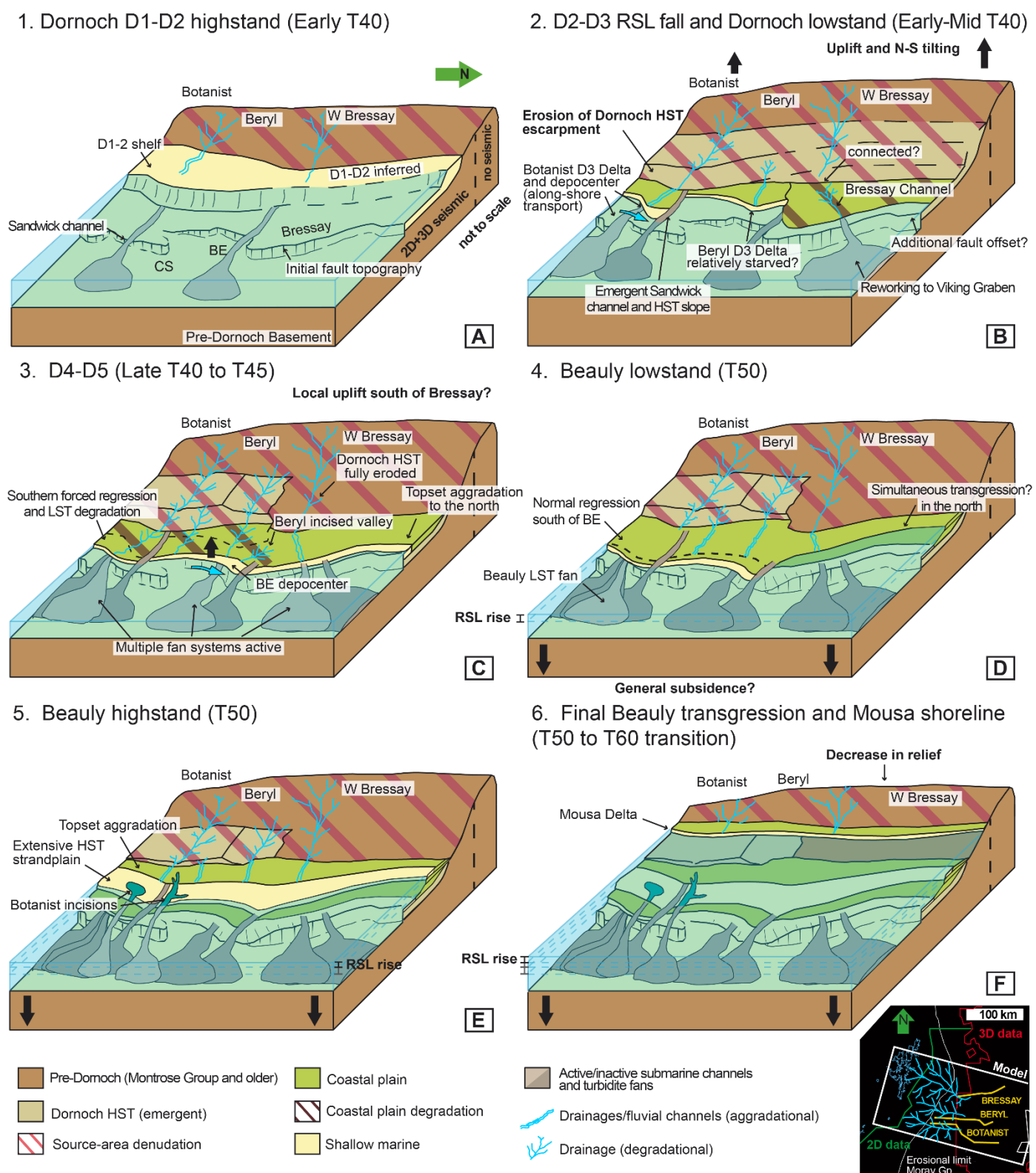
Figure 20: Schematic summarized evolution of study area, focusing on the South ESP to the Bressay High. Stages are explained in the text. Not to scale.

10. Reference list

Abdelmalak, M. M., Planke, S., Faleide, J. I., Jerram, D. A., Zastrozhnov, D., Eide, S., Myklebust, R. (2016). The development of volcanic sequences at rifted margins: New insights from the structure and morphology of the Vøring Escarpment, mid-Norwegian Margin. Journal of Geophysical Research: Solid Earth, 121(7), 5212-5236.

Ahmadi, Z., Sawyers, M., Kenyan-Roberts, S., Stan-Worht, C. W., Kugler, K., Kristensen, J., Fugelli, E. Mg. (2003). Palaeocene. The Millenium Atlas: Petroleum geology of the central and northern North Sea, 235-259.

Al-Hajri, Y., White, N., Fishwick, S. (2009). Scales of transient convective support beneath Africa. Geology, 37(10), 883-886.

Anell, I., Thybo, H., Artemieva, I. M. (2009). Cenozoic uplift and subsidence in the North Atlantic region: Geological evidence revisited. Tectonophysics, 474(1-2), 78-105.

Arnould, M., Coltice, N., Flament, N., Seigneur, V., Müller, R. D. (2018). On the scales of dynamic topography in whole-mantle convection models. Geochemistry, Geophysics, Geosystems, 19(9), 3140-3163.

Baby, G., Guillocheau, F., Braun, J., Robin, C., Dall'Asta, M. (2020). Solid sedimentation rates history of the Southern African continental margins: Implications for the uplift history of the South African Plateau. Terra Nova, 32(1), 53-65.

Baby, G., Guillocheau, F., Morin, J., Ressouche, J., Robin, C., Broucke, O., Dall'Asta, M. (2018). Post-rift stratigraphic evolution of the Atlantic margin of Namibia and South Africa: Implications for the vertical movements of the margin and the uplift history of the South African Plateau. Marine and Petroleum Geology, 97, 169-191.

Barefoot, E. A., Nittrouer, J. A., Foreman, B. Z., Hajek, E. A., Dickens, G. R., Baisden, T., Toms, L. (2022). Evidence for enhanced fluvial channel mobility and fine sediment export due to precipitation seasonality during the Paleocene-Eocene thermal maximum. Geology, 50(1), 116-120.

Barnett-Moore, N., Hassan, R., Flament, N., & Müller, D. (2017). The deep Earth origin of the Iceland plume and its effects on regional surface uplift and subsidence. Solid Earth, 8(1), 235-254.

Berndt, C., Planke, S., Alvarez Zarikian, C. A., Frieling, J., Jones, M. T., Millett, J. M., ... Yager, S. L. (2023). Shallow-water hydrothermal venting linked to the Palaeocene–Eocene Thermal Maximum. Nature Geoscience, 1-7.

Bertram, G. T., Milton, N. J. (1988). Reconstructing basin evolution from sedimentary thickness; the importance of palaeobathymetric control, with reference to the North Sea. Basin Research, 1(4), 247-257.

Bittencourt, A. C. D. S. P., Dominguez, J. M. L., Martin, L., Silva, I. R. (2005). Longshore transport on the northeastern Brazilian coast and implications to the location of large scale accumulative and erosive zones: An overview. Marine Geology, 219(4), 219-234.

Brunstad, H., Gradstein, F., Lie, J. E., Hammer, Ø., Munsterman, D., Ogg, G., Hollerbach, M. (2013). Stratigraphic guide to the rogaland group, Norwegian North Sea. Newsletters on Stratigraphy, 137-286.

Burgess, P. M., Prince, G. D. (2015). Non-unique stratal geometries: Implications for sequence stratigraphic interpretations. Basin Research, 27(3), 351-365.

Burov, E., Gerya, T. (2014). Asymmetric three-dimensional topography over mantle plumes. Nature, 513(7516), 85-89.

Burov, E., Guillou-Frottier, L. (2005). The plume head–continental lithosphere interaction using a tectonically realistic formulation for the lithosphere. Geophysical Journal International, 161(2), 469-490.

Castelltort, S., Van Den Driessche, J. (2003). How plausible are high-frequency sediment supply-driven cycles in the stratigraphic record? Sedimentary geology, 157(1-2), 3-13.

Catuneanu, O. (2019). Model-independent sequence stratigraphy. Earth-science reviews, 188, 312-388.

Catuneanu, O., Zecchin, M. (2016). Unique vs. non-unique stratal geometries: relevance to sequence stratigraphy. Marine and Petroleum Geology, 78, 184-195.

Chiarella, D., Longhitano, S. G., & Tropeano, M. (2019). Different stacking patterns along an active fold-and-thrust belt—Acerenza Bay, Southern Apennines (Italy). Geology, 47(2), 139-142.

Conway-Jones, B. W., White, N. (2022). Paleogene buried landscapes and climatic aberrations triggered by mantle plume activity. Earth and Planetary Science Letters, 593, 117644.

Coward, M.P., Dewey, J.F., Hempton, M. and Holroyd, J. 2003. Tectonic evolution. In: D. Evans, C. Graham, A. Armour and P. Bathurst (eds) The Millennium Atlas: Petroleum Geology of the Central and Northern North Sea, The Geological Society, London, pp. 17–33.

Deegan, C. E., Scull, B. J. (1977). Institute of Geological Sciences Report. A proposed standard lithostratigraphic nomenclature for the Central and Northern North Sea, 77.

Del Río, L., Gracia, F. J., Benavente, J. (2013). Shoreline change patterns in sandy coasts. A case study in SW Spain. Geomorphology, 196, 252-266.

Ding, X., Salles, T., Flament, N., Mallard, C., Rey, P. F. (2019). Drainage and sedimentary responses to dynamic topography. Geophysical Research Letters, 46(24), 14385-14394.

Dixon, R. J., Pearce, J. (1995). Tertiary sequence stratigraphy and play fairway definition, Bruce-Beryl Embayment, Quadrant 9, UKCS. Sequence Stratigraphy on the Northwest European Margin. Norwegian Petroleum Society, Special Publications, 5, 443-469.

Dominguez, J. L., Bittencourt, A. C. D. S. P., Martin, L. (1992). Controls on Quaternary coastal evolution of the east-northeastern coast of Brazil: roles of sea-level history, trade winds and climate. Sedimentary Geology, 80(3-4), 213-232.

Donato, J. A., Tully, M. C. (1982). A proposed granite batholith along the western flank of the North Sea Viking Graben. Geophysical Journal International, 69(1), 187-195.

Dunkley Jones, T., Manners, H. R., Hoggett, M., Kirtland Turner, S., Westerhold, T., Leng, M. J., ... Grimes, S. T. (2018). Dynamics of sediment flux to a bathyal continental margin section through the Paleocene–Eocene Thermal Maximum. Climate of the Past, 14(7), 1035-1049.

Fletcher, R., Kusznir, N., Roberts, A., Hunsdale, R. (2013). The formation of a failed continental breakup basin: the Cenozoic development of the Faroe-Shetland Basin. Basin Research, 25(5), 532-553.

Fossen, H. (2010). Extensional tectonics in the North Atlantic Caledonides: a regional view. Geological Society, London, Special Publications, 335(1), 767-793.

Foulger, G. R., Doré, T., Emeleus, C. H., Franke, D., Geoffroy, L., Gernigon, L., Hey, R., Holdsworth, R.E., Hole, M., Höskuldsson, Á., Julian, B., Kusznir, N., Martinez, F., McCaffrey, K. J.W., Natland, J. H., Peace, A. L., Petersen, K., Schiffer, C., Stephenson. R., Stoker, M. (2020). The Iceland microcontinent and a continental Greenland-Iceland-Faroe ridge. Earth-Science Reviews, 206, 102926.

Friedrich, A. M., Bunge, H. P., Rieger, S. M., Colli, L., Ghelichkhan, S., Nerlich, R. (2018). Stratigraphic framework for the plume mode of mantle convection and the analysis of interregional unconformities on geological maps. Gondwana Research, 53, 159-188.

Færseth, R. B. (1996). Interaction of Permo-Triassic and Jurassic extensional fault-blocks during the development of the northern North Sea. Journal of the Geological Society, 153(6), 931-944.

Gale, A. S., Lovell, B. (2018). The Cretaceous–Paleogene unconformity in England: uplift and erosion related to the Iceland mantle plume. Proceedings of the Geologists' Association, 129(3), 421-435.

Galloway, W. E. (1989). Genetic stratigraphic sequences in basin analysis I: architecture and genesis of flooding-surface bounded depositional units. AAPG bulletin, 73(2), 125-142.

Gernigon, L., Gaina, C., Olesen, O., Ball, P. J., Péron-Pinvidic, G., Yamasaki, T. (2012). The Norway Basin revisited: From continental breakup to spreading ridge extinction. Marine and Petroleum Geology, 35(1), 1-19.

Hall, A. M. (2021). Long-Term Denudation and Geomorphology in Scotland. In Landscapes and Landforms of Scotland (pp. 41-52). Cham: Springer International Publishing.

Hampson, G. J. (2016). Towards a sequence stratigraphic solution set for autogenic processes and allogenic controls: Upper Cretaceous strata, Book Cliffs, Utah, USA. Journal of the Geological Society, 173(5), 817-836.

Hampson, G. J., Howell, J. A. (2005). Sedimentologic and geomorphic characterization of ancient wave-dominated deltaic shorelines: Upper Cretaceous Blackhawk Formation, Book Cliffs, Utah, USA. In: Giosan, L., Bhattacharya, J. P. River deltas–Concepts, models, and examples. SEPM Society for Sedimentary Geology.

Hardman, J. P., Schofield, N., Jolley, D. W., Holford, S. P., Hartley, A. J., Morse, S., ... Zimmer, E. H. (2018). Prolonged dynamic support from the Icelandic plume of the NE Atlantic margin. Journal of the Geological Society, 175(3), 396-410.

Hartley, R. A., Roberts, G. G., White, N., Richardson, C. (2011). Transient convective uplift of an ancient buried landscape. Nature Geoscience, 4(8), 562-565.

Helland-Hansen, W., Gjelberg, J. G. (1994). Conceptual basis and variability in sequence stratigraphy: a different perspective. Sedimentary Geology, 92(1-2), 31-52.

Helland-Hansen, W., Hampson, G. J. (2009). Trajectory analysis: concepts and applications. Basin Research, 21(5), 454-483.

Heller, P. L., Burns, B. A., Marzo, M. (1993). Stratigraphic solution sets for determining the roles of sediment supply, subsidence, and sea level on transgressions and regressions. Geology, 21(8), 747-750.

Hoggard, M. J., White, N., Al-Attar, D. (2016). Global dynamic topography observations reveal limited influence of large-scale mantle flow. Nature Geoscience, 9(6), 456-463.

Holloway, S., Reay, D. M., Donato, J. A., Beddoe-Stephens, B. (1991). Distribution of granite and possible Devonian sediments in part of the East Shetland Platform, North Sea. Journal of the Geological Society, 148(4), 635-638.

Hunt, D., Tucker, M. E. (1992). Stranded parasequences and the forced regressive wedge systems tract: deposition during base-level'fall. Sedimentary Geology, 81(1-2), 1-9.Jin, S., Kemp, D. B., Jolley, D. W., Vieira, M., Zachos, J. C., Huang, C., ... Chen, W. (2022). Large-scale, astronomically paced sediment input to the North Sea Basin during the Paleocene Eocene Thermal Maximum. Earth and Planetary Science Letters, 579, 117340.

Jolley, D. W., Millett, J. M., Schofield, N., Broadley, L. (2021). Stratigraphy of volcanic rock successions of the North Atlantic rifted margin: the offshore record of the Faroe–Shetland and Rockall basins. Earth and Environmental Science Transactions of the Royal Society of Edinburgh, 112(2), 61-88.

Jolley, D., Vieira, M., Jin, S., Kemp, D. B. (2023). Palynofloras, palaeoenvironmental change and the inception of the Paleocene Eocene Thermal Maximum; the record of the Forties Fan, Sele Formation, North Sea Basin. Journal of the Geological Society, 180(1), jgs2021-131.

Jones, R. W., Milton, N. J. (1994). Sequence development during uplift: Palaeogene stratigraphy and relative sea-level history of the Outer Moray Firth, UK North Sea. Marine and Petroleum Geology, 11(2), 157-165.

Jones, S. M., White, N. (2003). Shape and size of the starting Iceland plume swell. Earth and Planetary Science Letters, 216(3), 271-282.

Jones, S. M., White, N., Clarke, B. J., Rowley, E., Gallagher, K. (2002). Present and past influence of the Iceland Plume on sedimentation. Geological Society, London, Special Publications, 196(1), 13-25.

Jones, T. D., Lunt, D. J., Schmidt, D. N., Ridgwell, A., Sluijs, A., Valdes, P. J., Maslin, M. (2013). Climate model and proxy data constraints on ocean warming across the Paleocene–Eocene Thermal Maximum. Earth-Science Reviews, 125, 123-145.

Karstens, J., Müller, P., Berndt, C., Patruno, S. (2022). Deep-seated focused fluid migration as indicator for hydrocarbon leads in the East Shetland Platform, North Sea Province.

Kilhams, B., Hartley, A., Huuse, M., Davis, C. (2015). Characterizing the Paleocene turbidites of the North Sea: Maureen Formation, UK Central Graben. Geological Society, London, Special Publications, 403(1), 43-62.

Knox, R. W. O. B. (1996). Tectonic controls on sequence development in the Palaeocene and earliest Eocene of southeast England: implications for North Sea stratigraphy. Geological Society, London, Special Publications, 103(1), 209-230.

Knox, R. W. O. B., Holloway, S. (1992). Paleogene of the central and northern North Sea. Lithostratigraphic nomenclature of the UK North Sea, 1, 72-73.

Krob, F. C., Glasmacher, U. A., Bunge, H. P., Friedrich, A. M., Hackspacher, P. C. (2020). Application of stratigraphic frameworks and thermochronological data on the Mesozoic SW Gondwana intraplate environment to retrieve the Paraná-Etendeka plume movement. Gondwana Research, 84, 81-110.

Lovell, B. (2010). A pulse in the planet: regional control of high-frequency changes in relative sea level by mantle convection. Journal of the Geological Society, 167(4), 637-648.

Martinsen, O. J., Helland-Hansen, W. (1995). Strike variability of clastic depositional systems: Does it matter for sequence-stratigraphic analysis?. Geology, 23(5), 439-442.

Miller, K. G., Browning, J. V., Schmelz, W. J., Kopp, R. E., Mountain, G. S., Wright, J. D. (2020). Cenozoic sea-level and cryospheric evolution from deep-sea geochemical and continental margin records. Science advances, 6(20), eaaz1346.

Miller, K. G., Kominz, M. A., Browning, J. V., Wright, J. D., Mountain, G. S., Katz, M. E., ... Pekar, S. F. (2005). The Phanerozoic record of global sea-level change. science, 310(5752), 1293-1298.

Milton, N. J., Bertram, G. T., Vann, I. R. (1990). Early Palaeogene tectonics and sedimentation in the Central North Sea. Geological Society, London, Special Publications, 55(1), 339-351.

Milton, N., Dyce, M. (1995). Systems tract geometries associated with Early Eocene lowstands, imaged on a 3D seismic dataset from the Bruce area, UK North Sea. In Norwegian Petroleum Society Special Publications (Vol. 5, pp. 429-442). Elsevier.

Mudge, D. C. (2015). Regional controls on Lower Tertiary sandstone distribution in the North Sea and NE Atlantic margin basins. London: The Geological Society of London.

Mudge, D. C., Bujak, J. P. (1996). An integrated stratigraphy for the Paleocene and Eocene of the North Sea. Geological Society, London, Special Publications, 101(1), 91-113.

Mudge, D. C., Bujak, J. P. (2001). Biostratigraphic evidence for evolving palaeoenvironments in the Lower Paleogene of the Faeroe–Shetland Basin. Marine and Petroleum Geology, 18(5), 577-590.

Mudge, D. C., Jones, S. M. (2004). Palaeocene uplift and subsidence events in the Scotland–Shetland and North Sea region and their relationship to the Iceland Plume. Journal of the Geological Society, 161(3), 381-386.

Muto, T. (2001). Shoreline autoretreat substantiated in flume experiments. Journal of Sedimentary Research, 71(2), 246-254.

Muto, T., Steel, R. J., Swenson, J. B. (2007). Autostratigraphy: a framework norm for genetic stratigraphy. Journal of Sedimentary Research, 77(1), 2-12.

Nadin, P. A., Kusznir, N. J., Cheadle, M. J. (1997). Early Tertiary plume uplift of the North Sea and Faeroe-Shetland basins. Earth and Planetary Science Letters, 148(1-2), 109-127.

Neal, J. E. (1996). A summary of Paleogene sequence stratigraphy in northwest Europe and the North Sea. Geological Society, London, Special Publications, 101(1), 15-42.

Parkes, L., Wood, P., Macdonald, C. (2020). The Kraken and Kraken North fields, Block 9/2b, UK North Sea. Geological Society, London, Memoirs, 52(1), 863-874.

Patruno, S., Helland-Hansen, W. (2018). Clinoforms and clinoform systems: Review and dynamic classification scheme for shorelines, subaqueous deltas, shelf edges and continental margins. Earth-Science Reviews, 185, 202-233.

Patruno, S., Kombrink, H., Archer, S. G. (2022). Cross-border stratigraphy of the Northern, Central and Southern North Sea: a comparative tectono-stratigraphic megasequence synthesis.

Patruno, S., Reid, W. (2016). Chronostratigraphic panel for the PESGB structural framework of the North Sea and Atlantic margin map, 2017 version. Poster published by the Petroleum Exploration Society of Great Britain.

Patruno, S., Reid, W., Berndt, C., Feuilleaubois, L. (2019). Polyphase tectonic inversion and its role in controlling hydrocarbon prospectivity in the Greater East Shetland Platform and Mid North Sea High, UK. Geological Society, London, Special Publications, 471(1), 177-235.

Petersen, K. D., Nielsen, S. B., Clausen, O. R., Stephenson, R., & Gerya, T. (2010). Small-scale mantle convection produces stratigraphic sequences in sedimentary basins. Science, 329(5993), 827-830.

Phillips, T. B., Fazlikhani, H., Gawthorpe, R. L., Fossen, H., Jackson, C. A. L., Bell, R. E., ... Rotevatn, A. (2019). The influence of structural inheritance and multiphase extension on rift development, the NorthernNorth Sea. Tectonics, 38(12), 4099-4126.

Pogge von Strandmann, P. A., Jones, M. T., West, A. J., Murphy, M. J., Stokke, E. W., Tarbuck, G., ... Schmidt, D. N. (2021). Lithium isotope evidence for enhanced weathering and erosion during the Paleocene-Eocene Thermal Maximum. Science Advances, 7(42), eabh4224.

Posamentier, H. W., Allen, G. P. (1993). Variability of the sequence stratigraphic model: effects of local basin factors. Sedimentary geology, 86(1-2), 91-109.

Platt, N. H., Cartwright, J. A. (1998). Structure of the east Shetland platform, northern North Sea. Petroleum Geoscience, 4(4), 353-362.

Prieur, M., Nuriel, P., Whittaker, A.C., Schlunegger, F., Somme, T.O., Braun, J., Fillon, C., Castelltort, S. 2023. Enhanced channel mobility assessed from the preservation of floodplain elements in fluvial to coastal sandstones: An example from the Paleocene Eocene Thermal Maximum (PETM) in the Southern Pyrenees (Spain). No. EGU23-15839. Copernicus Meetings.

Pujalte, V., Schmitz, B., Baceta, J. I. (2014). Sea-level changes across the Paleocene–Eocene interval in the Spanish Pyrenees, and their possible relationship with North Atlantic magmatism. Palaeogeography, Palaeoclimatology, Palaeoecology, 393, 45-60.

Rainbird, R. H., Ernst, R. E., & Buchan, K. L. (2001). The sedimentary record of mantle-plume uplift. Special Papers-Geological Society of America, 227-246.

Rasmussen, E. S., Heilmann-Clausen, C., Waagstein, R., & Eidvin, T. (2008). The tertiary of Norden. Episodes Journal of International Geoscience, 31(1), 66-72.

Rotevatn, A., Kristensen, T. B., Ksienzyk, A. K., Wemmer, K., Henstra, G. A., Midtkandal, I., ... Andresen, A. (2018). Structural inheritance and rapid rift-length establishment in a multiphase rift: The East Greenland rift system and its Caledonian orogenic ancestry. Tectonics, 37(6), 1858-1875.

Rudge, J. F., Champion, M. E. S., White, N., McKenzie, D., Lovell, B. (2008). A plume model of transient diachronous uplift at the Earth's surface. Earth and Planetary Science Letters, 267(1-2), 146-160.

Sanderson, P. G., Eliot, I. (1999). Compartmentalisation of beachface sediments along the southwestern coast of Australia. Marine Geology, 162(1), 145-164.

Shaw Champion, M.E, White, N. J., Jones, S. M., Lovell, J. P. B. (2008). Quantifying transient mantle convective uplift: An example from the Faroe-Shetland basin. Tectonics, 27(1).

Silcock, S. Y., Baptie, R. J., Iheobi, A., Frost, S., Simms, A., Brettle, M. (2020). The Mariner Field, Block 9/11a, UK North Sea. Geological Society, London, Memoirs, 52(1), 886-896.

Soutter, E. L., Kane, I. A., Huuse, M. (2018). Giant submarine landslide triggered by Paleocene mantle plume activity in the North Atlantic. Geology, 46(6), 511-514.

Speijer, R. P., Pälike, H., Hollis, C. J., Hooker, J. J., Ogg, J. G. (2020). The paleogene period. In: Geologic time scale 2020 (pp. 1087-1140). Elsevier.

Stewart I.J., 1987. A revised stratigraphic interpretation of the early Paleogene of the Central North Sea. In: Brooks J. & Glennie K.W. (eds.) Petroleum Geology of NW Europe. Graham & Trotman, London p 557-576.

Stoker, M. S., Holford, S. P., Hillis, R. R. (2018). A rift-to-drift record of vertical crustal motions in the Faroe–Shetland Basin, NW European margin: establishing constraints on NE Atlantic evolution. Journal of the Geological Society, 175(2), 263-274.

Stucky de Quay, G., Roberts, G. G. (2022). Geodynamic generation of a Paleocene–Eocene landscape buried beneath North Bressay, North Sea. Journal of the Geological Society, 180(1), jgs2022-063.

Stucky de Quay, G., Roberts, G. G., Watson, J. S., Jackson, C. L. (2017). Incipient mantle plume evolution: Constraints from ancient landscapes buried beneath the N orth S ea. Geochemistry, Geophysics, Geosystems, 18(3), 973-993.

Surlyk, F., Dons, T., Clausen, C. K., Higham, J., Evans, D., Graham, C., ... Bathurst, P. (2003). Upper cretaceous. The Millennium Atlas: petroleum geology of the central and northern North Sea, 1, 213-233.

Svensen, H., Planke, S., Malthe-Sørenssen, A., Jamtveit, B., Myklebust, R., Rasmussen Eidem, T., Rey, S. S. (2004). Release of methane from a volcanic basin as a mechanism for initial Eocene global warming. Nature, 429(6991), 542-545.

Sømme, T. O., Huwe, S. I., Martinsen, O. J., Sandbakken, P. T., Skogseid, J., Valore, L. A. (2023). Stratigraphic expression of the Paleocene-Eocene Thermal Maximum climate event during long-lived transient uplift—An example from a shallow to deep-marine clastic system in the Norwegian Sea. Frontiers in Earth Science, 11, 1082203.

Sømme, T. O., Skogseid, J., Embry, P., Løseth, H. (2019). Manifestation of tectonic and climatic perturbations in deep-time stratigraphy–an example from the Paleocene succession offshore western Norway. Frontiers in Earth Science, 7, 303.

Underhill, J. R. (2001). Controls on the genesis and prospectivity of Paleogene palaeogeomorphic traps, East Shetland Platform, UK North Sea. Marine and Petroleum Geology, 18(2), 259-281.

Underhill, J. R., Richardson, N. (2022). Geological controls on petroleum plays and future opportunities in the North Sea Rift Super Basin. AAPG Bulletin, 106(3), 573-631.

Van Wagoner JC, Posamentier HW, Mitchum RM, Vail PR, Sarg JF, Loutit TS, Hardenbol J. An overview of the fundamentals of sequence stratigraphy and key definitions. Van Wagoner JC, Posamentier HW, Mitchum RM. An overview of sequence stratigraphy and key definitions. Wilgus, C.K., Hastings, B.S., Van Wagoner,

J.C., Posamentier H. W., Ross, C.A., Kendall, C. G. C. Sea level changes: An integrated approach. 1988;42:39-45.

Vandenberghe, N., Hilgen, F. J., Speijer, R., Gradstein, F. M., Ogg, J. G., Schmitz, M. D., Ogg, G. J. (2012). The paleogene period. In: Gradstein, F.M., Ogg, J.G., Schmitz, M.D., Ogg, G.M. (eds), The Geologic time scale 2012. Elsevier, 855–921.

Vimpere, L., Spangenberg, J. E., Roige, M., Adatte, T., De Kaenel, E., Fildani, A., ... Castelltort, S. (2023). Carbon isotope and biostratigraphic evidence for an expanded Paleocene–Eocene Thermal Maximum sedimentary record in the deep Gulf of Mexico. Geology, 51(4), 334-339.

Walker, F., Schofield, N., Millett, J., Jolley, D., Planke, S., Holford, S. (2022). Paleogene drainage system evolution in the NE Faroe–Shetland Basin. Journal of the Geological Society, 179(5), jgs2021-121.

Watson, D., Schofield, N., Jolley, D., Archer, S., Finlay, A. J., Mark, N., ... Watton, T. (2017). Stratigraphic overview of Palaeogene tuffs in the Faroe–Shetland Basin, NE Atlantic margin. Journal of the Geological Society, 174(4), 627-645.

White, N., Lovell, B. (1997). Measuring the pulse of a plume with the sedimentary record. Nature, 387(6636), 888-891.

White, R., McKenzie, D. (1989). Magmatism at rift zones: the generation of volcanic continental margins and flood basalts. Journal of Geophysical Research: Solid Earth, 94(B6), 7685-7729.

Wilkinson, M. (2017). Cenozoic erosion of the Scottish Highlands–Orkney–Shetland area: implications for uplift and previous sediment cover. Journal of the Geological Society, 174(2), 209-216.

Zecchin, M., Catuneanu, O. (2020). High-resolution sequence stratigraphy of clastic shelves VII: 3D variability of stacking patterns. Marine and Petroleum Geology, 121, 104582.

Zhang, J., Burgess, P. M., Granjeon, D., Steel, R. (2019). Can sediment supply variations create sequences? Insights from stratigraphic forward modelling. *Basin Research*, *31*(2), 274-289.

Ziegler, P. A. (1992). North Sea rift system. Tectonophysics, 208(1-3), 55-75.

Supplementary Material

Bio- and chronostratigraphic considerations

First, it is important to remember that the usage of regional biostratigraphic datums for comparison between schemes requires some simplification of quantitative biomarker analysis and biozonations, favoring the selection of more easily correlated key datums. This approach is obviously not devoid of possible errors. However, the quantitative analysis of biomarkers and biozonations may be difficult to compare between schemes or even sometimes between wells being interpreted in the same scheme. This is due to two main issues:

- Differential preservation or sampling of biomarkers controlled by local biogeographic and lithological factors. This may impact absolute and relative count signatures, leading to inconsistencies in the use of quantitative or qualitative bioevents;

- Large differences in the lateral continuity of time-constrained units such as clinoform packages, submarine fan units and channels in general, which results in significant non-depositional or erosional hiatuses and pinch-outs;

On that note, references to acmes, common occurrences and other semi-quantitative terms are kept from the originals, and may not be comparable across schemes. Additional caveats and uncertainties for each classification can be referred to in the original papers.

Further explanations of the schemes included in Figure 3

Some recent proposed schemes start from better defined biozones as broader time intervals of more or less constrained duration and then use those to position key stratigraphic surfaces such as unconformities and flooding surfaces (Brunstad et al., 2013; Mudge, 2015). In other words, these frameworks are heavily based on lithological well-log interpretation (primarily) and seismic data (secondarily), rather than being only biostratigraphic zonations.

Mudge (2015) is one of the most recent well-based studies on regional stratigraphy of the Paleocene, including a comprehensive and revised litho- and chronostratigraphic overview of the North Sea and Faroe-Shetland basins based on the author's previous work (amongst others, Mudge and Copestake, 1992; Mudge and Bujak, 1996, 2001; Mudge and Jones 2004). In it, the author uses biostratigraphic and well-log data to interpret MFSs and unconformities observed inside specific biozones and not necessarily at their boundaries. We include it here because of its comprehensive nature.

A similar approach is taken by the Norwegian Offshore Stratigraphic Lexicon (NORLEX) in Brunstad et al. (2013), which showcases a revised implementation of Knox and Holloway's (1992) scheme, in addition to extensive seismic and well - based mapping in all the North Sea, being here included for this reason. In Figure 3, a representation of their stratigraphic chart for the East Shetland Platform/Viking Graben and the Horda platform is displayed, with the inclusion of the Forties member of Dornoch Formation and Maureen Member of Våle Formation in the South Viking Graben (Brunstad et al., 2013; Mudge, 2015). Brunstad et al. (2013) mostly follow the subdivision of the Moray Gp proposed in Knox and Holloway (1992), which includes subunits that are marked by contrasts in lithology and stratal architecture rather than definite sequence stratigraphic surfaces (marked in dashed black-lines in figure 3).

The widely used T sequences of British Petroleum are referred to here as presented in the seismic stratigraphic framework of Jones and Milton (1994), building on Stewart (1987) and Anderton (1993). Our chart adds the refined biostratigraphic tie published in Dixon and Pearce (1995). Several different versions of this chart and related biostratigraphic zonations have been reproduced in literature over time, some of them including further subdivisions of these sequences based on clinoform-based sequence stratigraphy (Milton and Dyce, 1995) and well data interpretation (as also seen in Dixon and Pearce, 1995, not included in figure 3). When compared to other schemes in our chart, a key difference can be pinpointed. Dixon and Pearce (1995) include two last stratigraphic occurrences (LSOs) of Apectodinium Augustum, with the LSO of common A. Augustum being used to distinguish the boundary between T40 and T45. Another LSO of A. Augustum is positioned inside T45, marking the top of their palynozone PT8. While these two datums have been observed in other works (Neal 1996) their exact significance for cross-scheme comparisons is unclear, especially because many only refer to the first and last occurrences of A. Augustum (Mudge and Bujak, 1996).

We also included a recently proposed stratigraphic scheme in the Faroe-Shetland Basin for the sake of comparison (Jolley et al., 2021). Differently from some of the other schemes, Jolley et al., (2021) do not use A. Gippingensis or P. Pyrophorum for their 100 and 125 flooding surfaces. As indicated in Figure 3, correlation to similar surfaces in other schemes is not defined, although they have similar reported ages (e.g. a top Selandian age to both MFS 100 and the "Mid Paleocene Unconformity" in Mudge, 2015).

Additionally, it is important to keep in mind that these schemes are variable in terms of their approach towards sequence stratigraphy. Some of the units can be obviously be classified as MFS-bounded genetic sequences, such as the T sequences in both Faroe-Shetland and the North Sea (Dixon and Pearce, 1995; Ebdon et al., 1995; Jolley et al., 2021). Other schemes use a mixed approach that

considers maximum flooding surfaces and unconformities as unit boundaries (Brunstad et al., 2013; Mudge, 2015). This is consistent with the view that individual system tracts or depositional trends should be used as fundamental and self-sufficient building blocks for sequence stratigraphic schemes (Helland-Hansen, 2009), seeing that system tracts may not be repeated in a cyclic fashion throughout a stratigraphic succession. We follow a similar philosophy in our division, since a switch from an interval dominated by unconformities (D1-D5) to an interval marked by transgressive+maximum flooding surfaces (D6-B3) is clear.

Relative sea-level curves

In general, many works from the 1990s describe several different episodes of RSL fall inserted in a context of variably sinusoidal sea-level curves during the Paleocene, such as Den Hartog Jager et al. (1993, 9 episodes), Dixon and Pearce (1995) Jones and Milton (1994) and Neal (1996, total of 10 RSL fall episodes, excluding sequences recognized only in outcrops), most of them during the Late Paleocene progradation. These were overall comparable in number to the total of 7 eustatic sea-level falls that had then been suggested by Haq et al. (1988). However, a particular challenge since that time has been to relate these episodes to a cohesive paleogeographical history, especially in what concerns shorter cycle RSL changes.

In Milton and Dyce (1995) and Dixon and Pearce (1995), interpretation is based on well and seismic-based mapping in the Bruce and Beryl area, something that results in some differences when compared to the framework of Jones and Milton (1994) for the Outer Moray Firth/Piper Shelf. Jones and Milton (1994) recognize proximal late T30 – early T40 clinoforms and observe thicker T40 fan deposits associated to more prominent RSL fall, which is followed by relatively more stable T45 onlap. This is accompanied by several minor cycles of RSL change during T40-T50 overall.

Near the Beryl and Bruce fields, Milton and Dyce (1995) and Dixon and Pearce (1995) recognize less contribution of T40 deposition and interpret that the wide Hermod fans in the Viking Graben are associated to late T45 incision, with potentially more significant RSL fall than in Jones and Milton (1994), which is associated to specific erosion in the Bressay area. Additionally, Milton and Dyce (1995) observe a T50 age highstand and a lowstand systems tract, the latter being related to Odin Mbr fans (as defined Mudge and Copestake, 1992), while Dixon and Pearce (1995) individualize in their sequence T49 (late T45) a prominent backstepping succession that predates the Balder ash layers and the more often observed T50 transgression. This T49 sequence is similar to the lowermost transgressive unit we observe in our interpretation of Balder Fm. deposits (B1 TST in Figs 8-9), although in Dixon and Pearce (1995) they were included in Sele/Dornoch Fm.

Overall, these works correspond to some of the earliest descriptions of the north-to-south variability in RSL fall and timing of fan deposition that prevail in the ESP. In essence, however, all of these recognize considerable short-cycle fluctuations in shoreline and coastal onlap behavior during that time. This occurs within a generally prograding trend, with transient flooding at the T40-T45 boundary and increased aggradation to the end of T45, eventually transitioning to full transgression during T50.

Depth conversion and decompaction

We conducted both 2D and 3D backstripping in this study. 2D backstripping consisted in simple overburden removal of the seismic transects in Figures 8-12 to better constraint clinoform rollover trajectories and RSL fluctuations derived from them. This was done by first depth-converting the seismic sections using a basin-wide time-depth curve based on checkshot data (Figure S1).
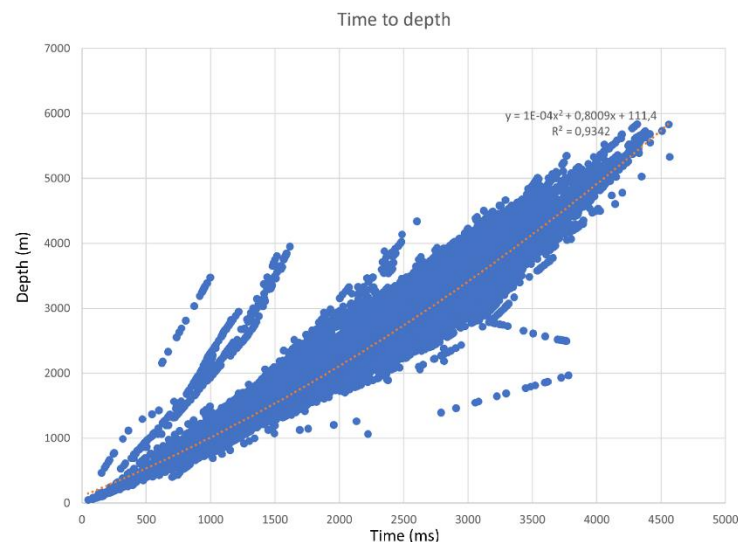

Figure S1 – Time-depth curve based on checkshot data from 250 wells penetrating Paleocene sediments in the North Sea. From polynomial regression, we obtain the equation $y = 0.0004x^2 + 0.8009x + 111.4$, where y is depth in meters and x is time in milliseconds.

We then removed the thermal subsidence and overburden above the Moray Group using flexural isostasy. For this, we used a stretching factor map extrapolated from Roberts et al., (2019), with β values ranging between 1.1 - 1.3. Values for elastic thickness in the North Sea are generally considered to be low (1.5-4 km, Nadin et al., 1997; Roberts et al., 2019) – we used a constant value of 1.5 km following Roberts et al. (2019). Late Jurassic rifting was considered to last between 155 and 140 Ma. Lastly, lithological parameters used to calculate compaction (*e.g* Sclater and Christie, 1980) are outlined in table S1. The decompacted sections can be seen in Figures S2-S6. 3D backstripping

used the same parameters, but involved further decompaction until the level of the West Bressay catchment (complete removal of the Moray Group), as seen in Figure 17B. The relief values shown in Figure 17B are obtained from adjusting the decompacted paleobathymetries by 350 m to compensate for excessive burial during the Upper Dornoch Fm – Beauly Member (Bertram and Milton, 1988; Milton et al., 1990; Nadin et al., 1997; Łuszczak et al., 2018; Roberts et al., 2019). This could be related to transient dynamic support which is no longer present in the area.

Table S1 – Lithological parameters used for decompaction

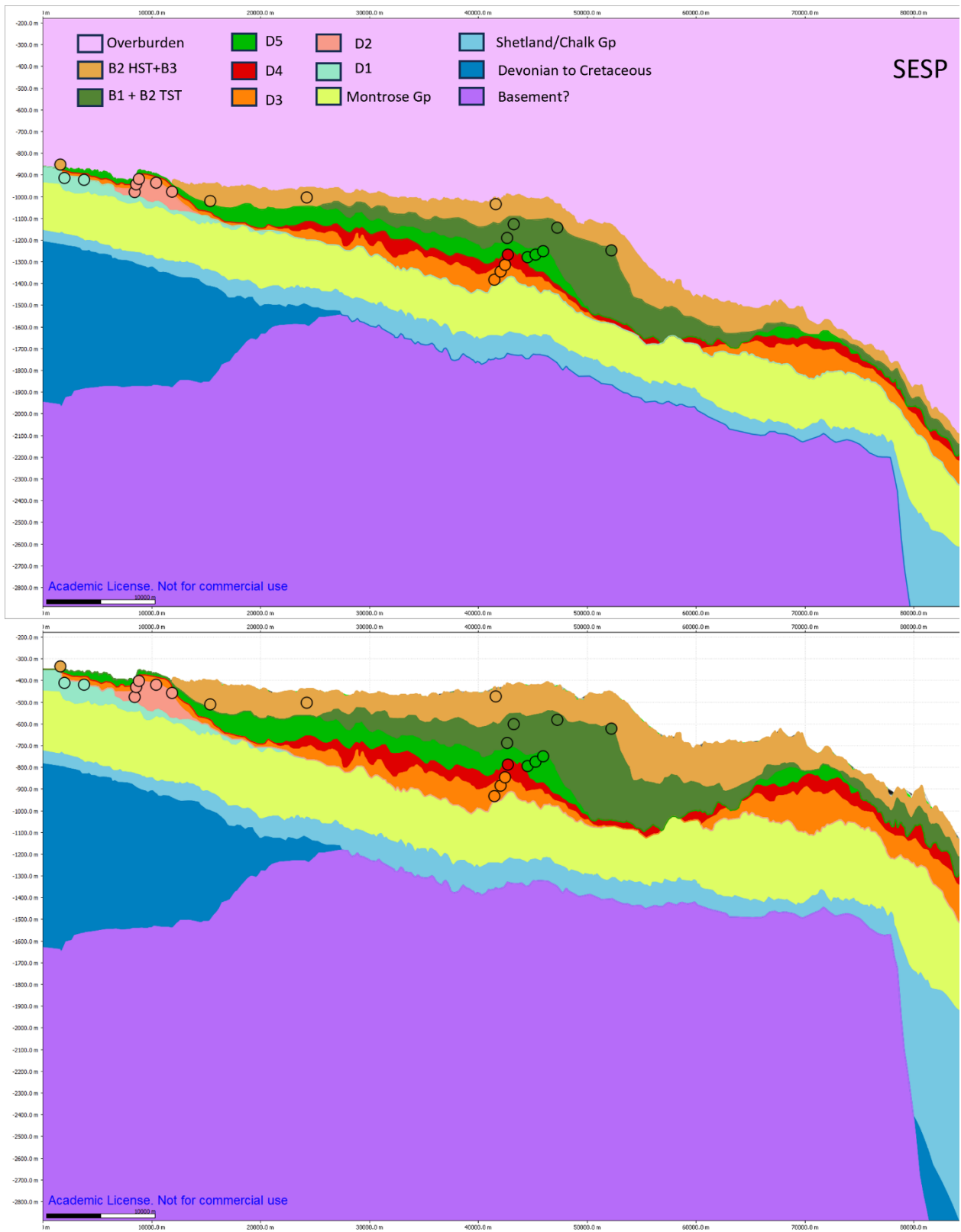| Unit	Sand (%)	Shale (%)	Limestone (%)	Original porosity	Depth coefficient	Age at top
Post-Beauly	10	90	0	0.616	0.486	0.0
Beauly	20	80	0	0.602	0.462	54.7
Dornoch LST	35	65	0	0.581	0.426	55.4
Dornoch HST	30	70	0	0.588	0.438	56.6
Montrose Group	25	65	10	0.573	0.439	57.6
Shetland Group	10	30	60	0.484	0.42	63
Pre-Shetland Group	20	70	10	0.58	0.451	100

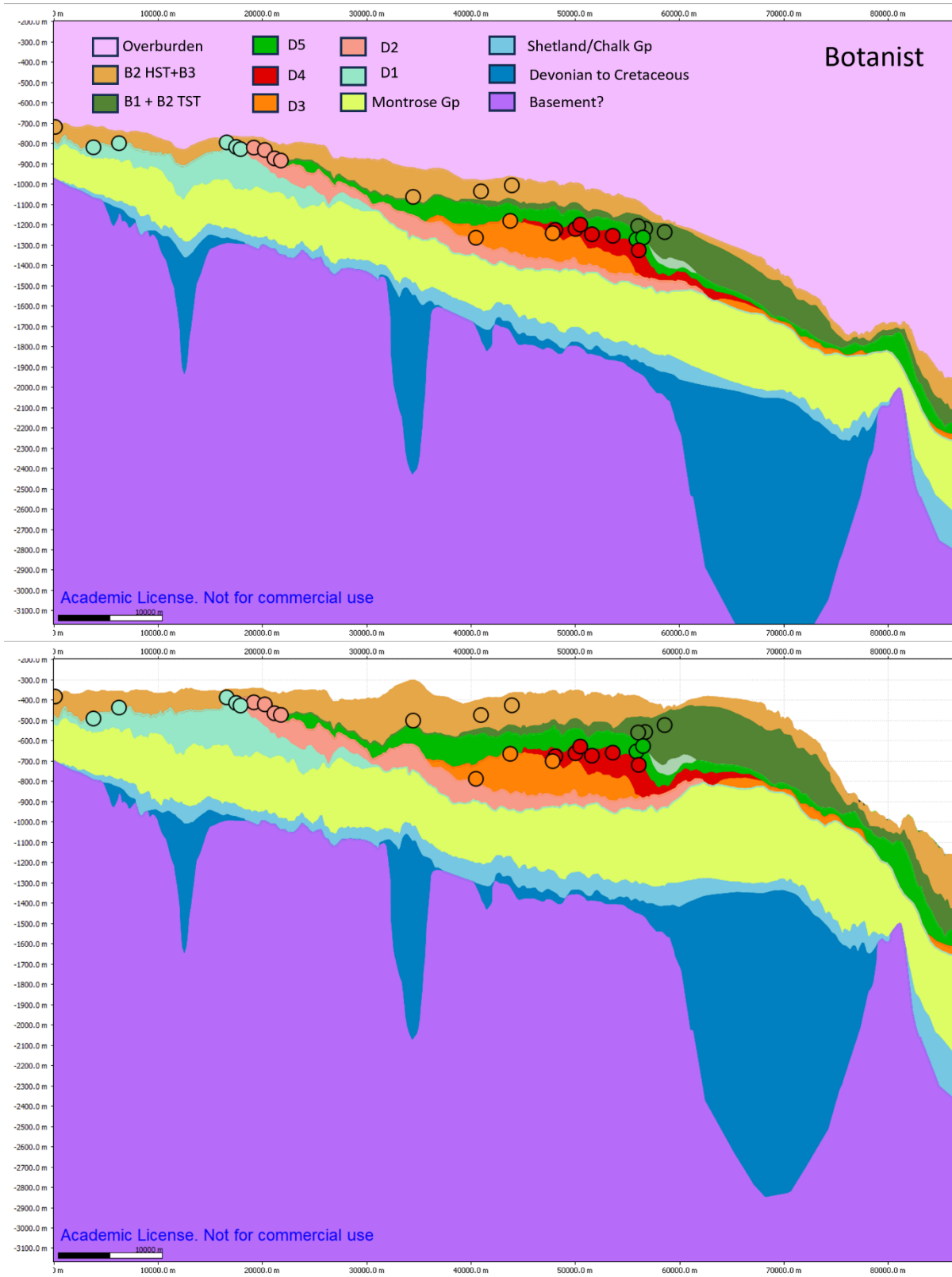Figure S2 – Overburden-removed transect in the South ESP (Figure 8 in main text).

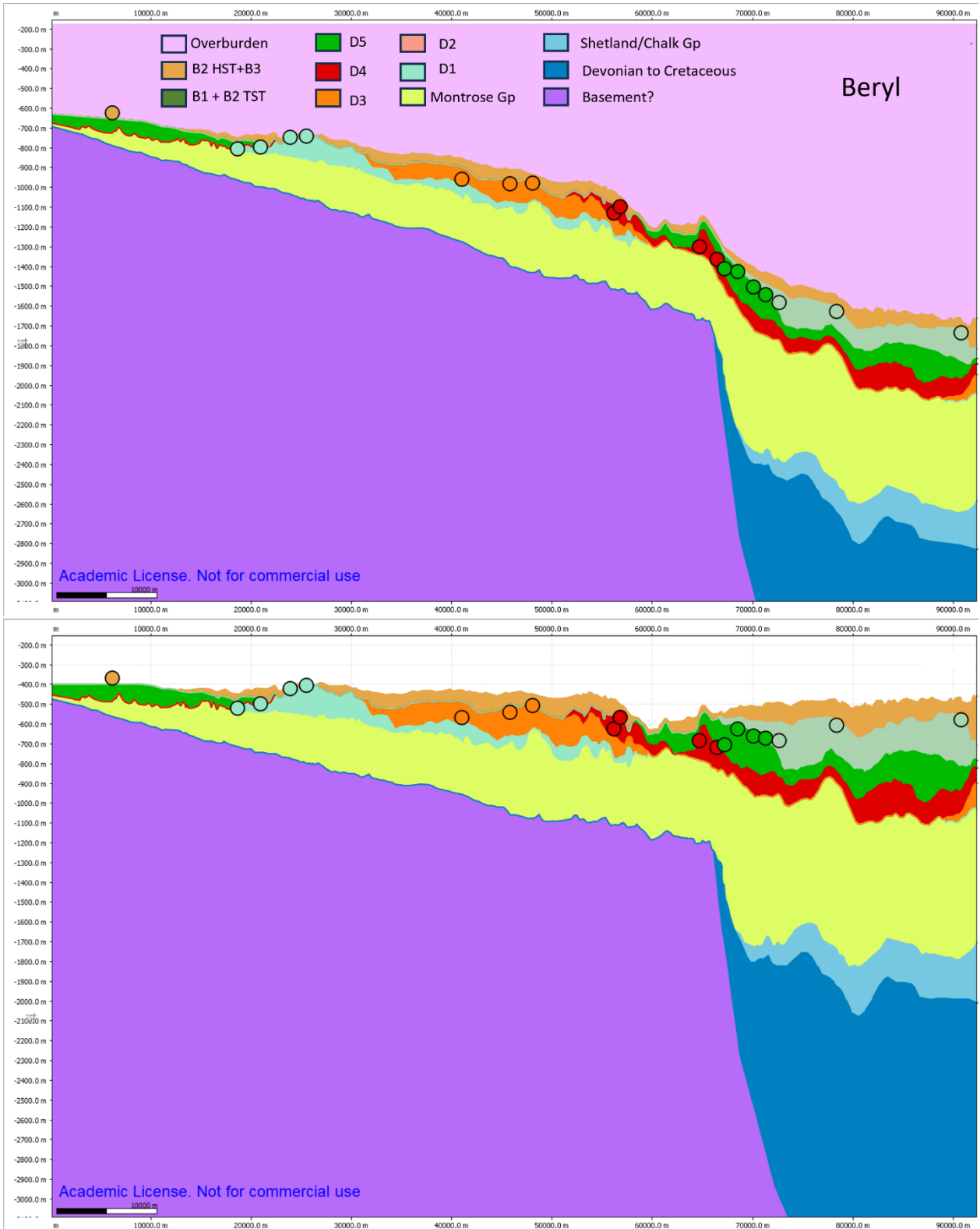Figure S3 – Overburden-removed transect in the Botanist area (Figure 9 in main text).

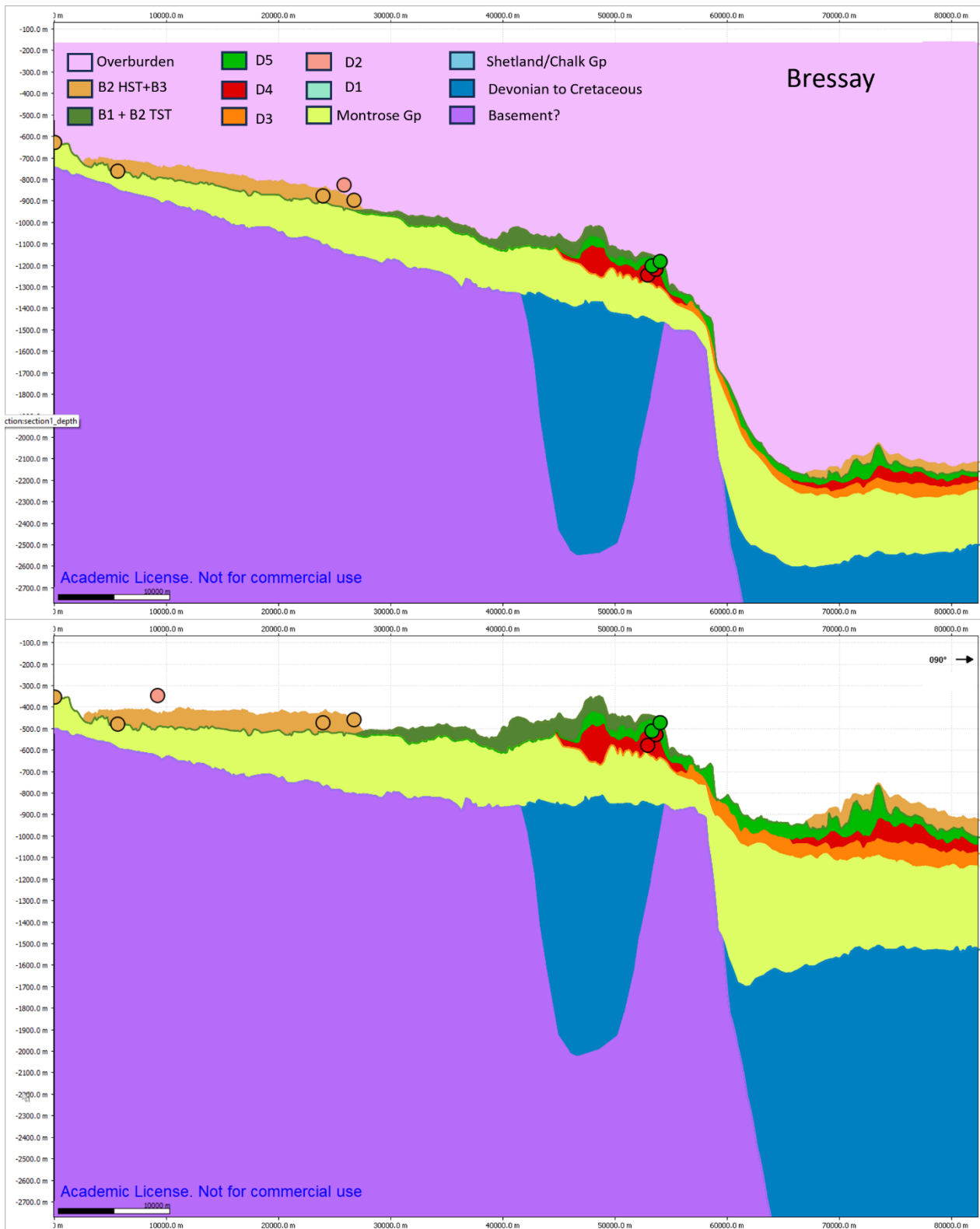Figure S4 – Overburden-removed transect in the Beryl area (Figure 10 in main text).

Figure S5 – Overburden-removed transect in the Bressay area (Figure 11 in main text).
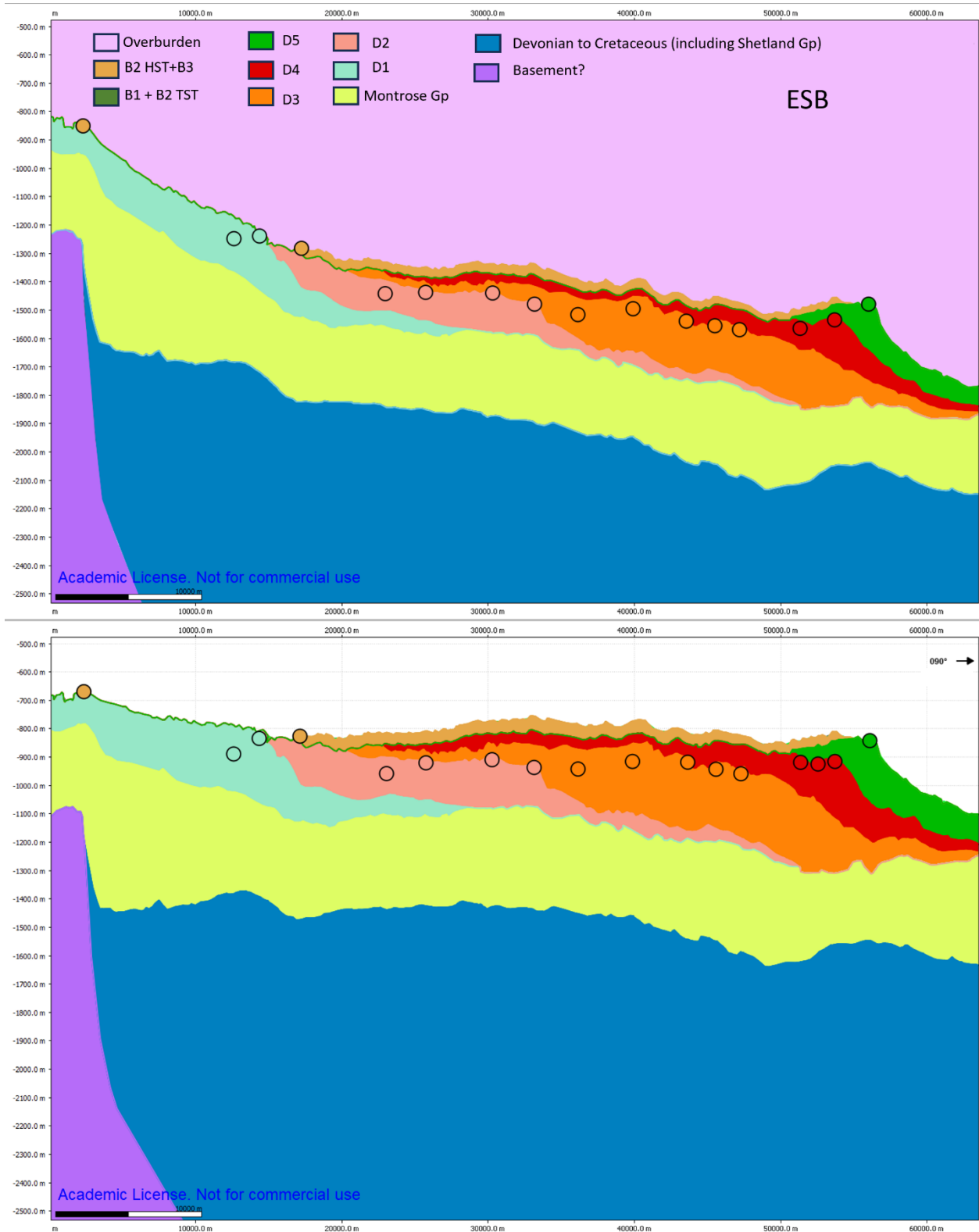
Figure S6 – Overburden-removed transect in the ESB (Figure 12 in main text).

**Non-unique stratigraphic responses and possible controlling parameters –
transgression and autoretreat**

Multiple individual controls can be superimposed during the development of flooding surfaces and transgression. For instance, longer-term flooding and landward shoreline retreat during Beauly can be correlated to eustatic and subsidence related RSL-rise (Pujalte et al., 2014; Stucky de Quay et al., 2017; Hardman et al., 2018). However, in areas of more complex deposition during Beauly, individual, internal flooding surfaces may have been triggered by superimposed controls. This is the case of the South ESP and Botanist, where progradational sequences within longer-term backstepping are better developed (B1 and B2). If accommodation rates are assumed to be relatively stable during this time, as suggested by comparable topset thicknesses between B1 and B2, internal Beauly flooding surfaces may have been caused either by decrease in supply (allogenic or autogenic) or autoretreat. Autoretreat can be constrained by understanding the characteristic depositional length of a system (D, Muto, 2001; Muto et al., 2007):

$$D = S/A,$$

where S is a two dimensional measurement of sediment supplied for a specific unit of time and A is a constant rate of accommodation increase or decrease. D represents the maximum length of a sediment routing system that can be established before supply becomes insufficient to compensate for topset areal growth and maintain progradation.

Simple estimates of D can be seen in Table S2. Values calculated here suggest that D exceeded the maximum depositional distance observed in the Beauly LST and HST in almost all areas, with the exception of B2 HST in the South ESP. Hence, in most areas, autoretreat was precluded, potentially due to high supply rates during progradation. Moreover, autoretreat above the B2 HST would still be followed by the significant basin-wide flooding that is observed in all of the area. In summary, in this scenario, internal flooding during Beauly is more likely caused by fast episodes of flooding (subsidence related?) or a shift to sediment starvation (wave-climate or source-driven) rather than self-limited progradation.

Table S2 – Calculated parameters for Beauly units.

Unit	Duration (yr)	Total accommodation (m)	A (m.yr^{-1})	Total 2D supply (m^2)	S (m^2.yr^{-1})	D (m)	Depositional length of coastal system (m)
B2 HST Botanist	500000	68	0.000136	3500000	7.0000	51470.59	37500
B1 LST Botanist	500000	30.6	0.0000612	3108000	6.2160	101568.6	23900
B2 HST South ESP	500000	115	0.00023	4631000	9.2620	40269.57	55000
B1 LST South ESP	500000	95	0.00019	4880000	9.7600	51368.42	24400
B2 HST Bressay	500000	37.7	0.0000754	1508000	3.0160	40000	23980

References

Anderton, R. (1993). Sedimentation and basin evolution in the Paleogene of the Northern North Sea and Faeroe–Shetland basins. In Geological Society, London, Petroleum Geology Conference Series (Vol. 4, No. 1, pp. 31-31). The Geological Society of London.

Bertram, G. T., & Milton, N. J. (1988). Reconstructing basin evolution from sedimentary thickness; the importance of palaeobathymetric control, with reference to the North Sea. Basin Research, 1(4), 247-257.

Brunstad, H., Gradstein, F., Lie, J. E., Hammer, Ø., Munsterman, D., Ogg, G., & Hollerbach, M. (2013). Stratigraphic guide to the rogaland group, Norwegian North Sea. Newsletters on Stratigraphy, 137-286.

Den Hartog Jager, D. D., Giles, M. R., & Griffiths, G. R. (1993). Evolution of Paleogene submarine fans of the North Sea in space and time. In Geological Society, London, Petroleum Geology Conference Series (Vol. 4, No. 1, pp. 59-71). The Geological Society of London.

Ebdon, C. C., Granger, P. J., Johnson, H. D., & Evans, A. M. (1995). Early Tertiary evolution and sequence stratigraphy of the Faeroe-Shetland Basin: implications for hydrocarbon prospectivity. Geological Society, London, Special Publications, 90(1), 51-69.

Hampson, G. J. (2016). Towards a sequence stratigraphic solution set for autogenic processes and allogenic controls: Upper Cretaceous strata, Book Cliffs, Utah, USA. Journal of the Geological Society, 173(5), 817-836.

Haq, B. U., Hardenbol, J., & Vail, P. R. (1988). Mesozoic and Cenozoic chronostratigraphy and cycles of sea-level change.

Hardman, J. P., Schofield, N., Jolley, D. W., Holford, S. P., Hartley, A. J., Morse, S., ... & Zimmer, E. H. (2018). Prolonged dynamic support from the Icelandic plume of the NE Atlantic margin. Journal of the Geological Society, 175(3), 396-410.

Helland-Hansen, W. (2009). Towards the standardization of sequence stratigraphy. Earth-Science Reviews, 1(94), 95-97.

Jolley, D. W., Millett, J. M., Schofield, N., & Broadley, L. (2021). Stratigraphy of volcanic rock successions of the North Atlantic rifted margin: the offshore record of the Faroe–Shetland and Rockall basins. Earth and Environmental Science Transactions of the Royal Society of Edinburgh, 112(2), 61-88.

Jones, R. W., & Milton, N. J. (1994). Sequence development during uplift: Palaeogene stratigraphy and relative sea-level history of the Outer Moray Firth, UK North Sea. Marine and Petroleum Geology, 11(2), 157-165.

Knox, R. W. O. B., & Holloway, S. (1992). Paleogene of the central and northern North Sea. Lithostratigraphic nomenclature of the UK North Sea, 1, 72-73.

Łuszczak, K., Persano, C., & Stuart, F. M. (2018). Early Cenozoic denudation of central west Britain in response to transient and permanent uplift above a mantle plume. Tectonics, 37(3), 914-934.

Milton, N. J., Bertram, G. T., & Vann, I. R. (1990). Early Palaeogene tectonics and sedimentation in the Central North Sea. Geological Society, London, Special Publications, 55(1), 339-351.

Milton, N., & Dyce, M. (1995). Systems tract geometries associated with Early Eocene lowstands, imaged on a 3D seismic dataset from the Bruce area, UK North Sea. In Norwegian Petroleum Society Special Publications (Vol. 5, pp. 429-442). Elsevier.

Mudge, D. C. (2015). Regional controls on Lower Tertiary sandstone distribution in the North Sea and NE Atlantic margin basins. London: The Geological Society of London.

Mudge, D. C., & Bujak, J. P. (1996). An integrated stratigraphy for the Paleocene and Eocene of the North Sea. Geological Society, London, Special Publications, 101(1), 91-113.

Mudge, D. C., & Bujak, J. P. (2001). Biostratigraphic evidence for evolving palaeoenvironments in the Lower Paleogene of the Faeroe–Shetland Basin. Marine and Petroleum Geology, 18(5), 577-590.

Mudge, D. C., & Jones, S. M. (2004). Palaeocene uplift and subsidence events in the Scotland–Shetland and North Sea region and their relationship to the Iceland Plume. Journal of the Geological Society, 161(3), 381-386.

Muto, T. (2001). Shoreline autoretreat substantiated in flume experiments. Journal of Sedimentary Research, 71(2), 246-254.

Muto, T., Steel, R. J., & Swenson, J. B. (2007). Autostratigraphy: a framework norm for genetic stratigraphy. Journal of Sedimentary Research, 77(1), 2-12.

Nadin, P. A., Kusznir, N. J., & Cheadle, M. J. (1997). Early Tertiary plume uplift of the North Sea and Faeroe-Shetland basins. Earth and Planetary Science Letters, 148(1-2), 109-127.

Neal, J. E. (1996). A summary of Paleogene sequence stratigraphy in northwest Europe and the North Sea. Geological Society, London, Special Publications, 101(1), 15-42.

Pujalte, V., Schmitz, B., & Baceta, J. I. (2014). Sea-level changes across the Paleocene–Eocene interval in the Spanish Pyrenees, and their possible relationship with North Atlantic magmatism.

Roberts, A. M., Kusznir, N. J., Yielding, G., & Beeley, H. (2019). Mapping the bathymetric evolution of the Northern North Sea: from Jurassic synrift archipelago through Cretaceous–Tertiary post-rift subsidence. Petroleum Geoscience, 25(3), 306-321.

Sclater, J. G., & Christie, P. A. (1980). Continental stretching: An explanation of the post-mid-Cretaceous subsidence of the central North Sea basin. Journal of Geophysical Research: Solid Earth, 85(B7), 3711-3739.

Stewart I.J., 1987. A revised stratigraphic interpretation of the early Paleogene of the Central North Sea. In: Brooks J. & Glennie K.W. (eds.) Petroleum Geology of NW Europe. Graham & Trotman, London p 557-576.

Stucky de Quay, G., Roberts, G. G., Watson, J. S., & Jackson, C. L. (2017). Incipient mantle plume evolution: Constraints from ancient landscapes buried beneath the N orth S ea. Geochemistry, Geophysics, Geosystems, 18(3), 973-993.